UNIVERSIDAD NACIONAL AUTÓNOMA DE MÉXICO

POSGRADO EN CIENCIAS FÍSICAS

ULTRACOLD ATOMS IN QUANTUM OPTICAL LATTICES AND ARTIFICIAL GAUGE FIELDS.

TESIS

QUE PARA OPTAR POR EL GRADO DE

MAESTRO EN CIENCIAS (FÍSICA)

PRESENTA:

ADOLFO ALEJANDRO HERNÁNDEZ CÁSARES

TUTOR PRINCIPAL
DR. SANTIAGO FRANCISCO CABALLERO BENÍTEZ
Instituto de Fisica

MIEMBROS DEL COMITÉ TUTOR
DR. ISAAC PÉREZ CASTILLO (UAM-IZTAPALAPA)
DR. PABLO BARBERIS BLOSTEIN (IIMAS)

MÉXICO, CIUDAD DE MÉXICO, JUNIO 2022

Agradecimientos.

Agradezco al programa de becas del Consejo Nacional de Ciencia y Tecnología (CONACYT) a través del Posgrado en Ciencias Físicas de la UNAM por el apoyo económico brindado durante todo el programa de maestría. Así mismo, agradezco a los proyectos DGAPA-PAPIIT de la UNAM número IN109619 y CONACYT: A1-S-30934 de donde se obtuvo apoyo para partcipaciones en eventos académicos y equipo de cómputo para el grupo de investigación.

De los colegios: a Juan S. y Erik M., que la vida nos puso una pregunta en la secundaria y después nos puso en Física para conocer la respuesta. Gracias por compartir origen y porque al final nos acoplamos y supimos estar 'aquí nomás'. A Karina P., compañera, por el vínculo tan *sui géneris* y sus temporadas (con excelente soundtrack, sobre todo ésta última, la favorita). Gracias por todo. A los mejores amigos de los hot dogs de los jueves, José Carlos, Rafael y Lygia, porque ustedes siempre supieron que así iríamos y vendríamos con este paso alegre por el mundo y por la vida. Corrales y Gil, los dos amigos intelectuales internacionales Maestros Aire, gracias por el calor de hogar que me instalaron en Puebla y en donde sea que coincidimos.

Mis amigos/hermanos del Voluntariado, comunidad desperdigada por todo el norte, de anécdotas interminables, que no necesita lugres y que la mueve el Espíritu. Gracias por el acompañamiento permanente.

A los físicos Jorge y Kevin, las personas más brillantes que conozco, cálidos, comprensivos y sensibles a las cosas bellas de la vida; de amistad relajada y saludable. Gracias por creer que yo también soy eso. Gracias por sostener la realidad y por los momentos de genuina felicidad mientras paseábamos en lugares especiales de CU, la ciudad y otros fuera de ella. Porque juntos cargamos la vida a punta de risas y algo de filosofía. Por las muchas ideas, las emociones y los abrazos bien sentidos. Por la aceptación inmediata y el apoyo a nuestras trayectorias. Su amistad es de lo más valioso que he encontrado.

Gracias también al grupo de amigos/estudio permanente que duró desde el inicio de la carrera hasta el final de la maestría y que vio pasar entre varios a Jama H., Luis E., Fernando J., Marcela O., Miguel H., Humberto, Princess y Charlie O. Hicieron disfrutable el manicomio. Gracias al Buen JCO, por las preguntas y su presencia pacífica, y al Buen Brahyam, hermano académico gemelo, auténtico *tru* colombiano que le dio el toque a esta experiencia de la maestría.

A todos aquellos profesores/gurús de la vida que llegaron (o a los que llegué) de formas inesperadas durante mis estudios: Alfredo Mtz., Oscar R., Javier F., Lioudmila B.,

Zamfir M., los amigos fugaces del Prometeo, y otras varias manifestaciones bellas de sabiduría. Destaco aquí a mi asesor Santiago Caballero de infinita paciencia, quien me formó en esta área desde cero, compartiendo sus amplísimos conocimientos, y me impulsó hasta el final sin dudar nunca de mis capacidades. Gracias, profe, por la constante orientación que me dio, por su empatía y su interés en el futuro de mi carrera que terminó por catapultarme a seguir mis estudios en el extranjero.

Agradezco a mi mamá, quien me encaminó a soñar desde el principio. Fue el soporte necesario para conlcuir, y en quien volví a encontrar durante el proceso una guía (incluso desconociendo), compañía excepcional (a veces la única) y una fuente infinita de motivación (que brota desde el amor). También agradezco a mi papá por la patada inicial, por creer en mí y por revelarme que ir riendo en el camino es más importante que la meta. Gracias, hermanos Peito y Gabi, por que sentí su apoyo, generosidad y cariño en bonitos y nobles gestos, conocidos y no conocidos.

Resumen.

Los átomos ultrafríos en redes ópticas han demostrado ser un excelente candidato a simulador cuántico por el nivel de control experimental que actualmente se ha logrado y por la gran plasticidad que un sistema así posee. En esta tesis partimos de la posibilidad de incorporar teorías de norma en el sistema y el acceso que esto representa a propiedades topológicas importantes, para presentar un estudio de la respuesta en el espacio de fases de la red óptica cuántica que incluyen el Aislante de Mott (MI), la fase Superfluida (SF) y Ondas de Densidad de Carga (DW) en presencia de un campo magnético artificial, y de la robustez de la conductancia de Hall cuando las interacciones mediadas por la cavidad de alta reflectancia se vuelven importantes para el límite de bosones duros. Adicionalmente, se estudia el efecto retroactivo por medición que se tiene en las fases preexistentes en el Hamiltoniano de Bose-Hubbard en presencia de la misma cavidad, cuantificando las variaciones de las fluctuaciones por sitio que definen a las fases MI y SF.

Abstract.

Ultracold Atoms in Optical Lattices have demonstrated to be an excelent candidate to quantum simulator due to the experimental control level achieved and the remarkable plasticity that such a system poses. In this thesis, we start from the real posibility of incorporate Gauge Theories to the system that give access to important topological properties, to present a study of the response in the phase space of the Quantum Optical Lattice that includes the Mott Insulator (MI), the Superfluid (SF), and the Density Wave (DW) phases in the presence of an artificial magnetic field, and also of the robustness of the Hall conductance when the high-Q-cavity-mediated interactions become important in the hard-core bosons limit. Addicionally, we study the effects of the measurement back action on the pre-existing phases of the Bose-Hubbard Hamiltonian with the presence of the cavity too, quantifying the variation of the number of particles per site, which define the the MI and SF phases.

Contents

Introduction.

Ultracold neutral atoms loaded in optical lattices constitute an exceptional platform to the study of a broad range of analog physical effects from Condensed Matter models and even High Energy Physics due to their unique flexibility and the high control level displayed in the state-of-the-art experiments [1] [2]. From synthetic dimensions based on inner degrees of freedom (for example, [3]), to Yang-Mills lattice gauge theories (for example see [4]) and $SU(N)$ gauge fields [5], the target of the proposals for quantum simulations are dabbling into the more exotic ideas and pushing the frontiers of applicability of this system.

Another area of study that can be explored is Topology in Condensed Matter. The quantum Hall effect (observed in 1980 [63]) represents the access door to the exploration of Chern numbers with Ultracold atoms, meaning analogue 2D systems as the Harper model [44] are now viewed as a quantum simulation target since they host interesting topological phenomena that could be accessed exploiting the Berry phase as the cornerstone [51]. Nowadays, these Berry phases can be added to the system using various methods [6], [7], [8]. In 2014, the Chern numbers of the energy spectrum were experimentally measured [9], and it represents one of the biggest incursions of the Ultracold atoms in topology.

Going further the simulation capabilities, once the system actually hosts and mimics physical properties from other system, it displays new physical dynamics and characteristics that in combination with the level of control over interactions and parameters not available otherwise, make it an interesing system by its own. An example of this is the light-matter interaction features and collective phenomena that can also be addressed with detail and control through this kind of systems by placing the system inside an optical cavity [11]; the experimental realization details can be found in [76]. We can also find novel phenomena regarding measurement back-action effects on the system [78]. Exotic phenomena can arise from such system, just as a new control over critical exponents of phase transitions [10].

In this thesis we take part of this efforts studying the situation of Ultracold Neutral Atoms in a 2D lattice in the presence of an Artificial Magnetic Field inside a High Reflectance (high-Q) Cavity distinguishing the fermionic, bosonic and hard-core bosons limit cases; we examine the physics of each ingredient to better understand the competition between them. The robustness of the topological quantity the Hall conductance is also studied. Given the state-of-the-art in Ultracold atoms we consider this work is timely and highly achievable. It is divided as follows. Chapter 1 presents the Bose-Hubbard model for ultracold atoms, the Mott Insulator and Superfluid phases,

the reproduction of theoretical and numerical solutions, and the limit of hard-core bosons [13], [32]. Chapter 2 introduces the Haprer model and its quantum simulation using ultracold atoms, as well as the minimal topological tools required to understand the Hall conductance [44], [47], [57]. Chapter 3 presents the high-Q cavity and its effects on the system, specially the new Density Wave phase, and extends it to the case in which an artificial magnetic field is present in the system [78], finding a stabilization of the Density Wave phase as one of its consequences and the study of the Hall conductances in the presence of the cavity-mediated on-site interactions. Lastly, Chapter 4 presents the measurement backaction consequences on the already known phases of the system, reproducing the results in [78] passing through long-range tunneling and Zeno effects, to later add the cavity.mediated interactions.

Chapter 1: The Bose Hubbard Hamiltonian.

The main subject of this chapter is to introduce the Bose Hubbard Hamiltonian (BHH). This Hamiltonian model is the cornerstone of the study of bosons moving in a discrete space subject to on-site interactions at a zero temperature, including competition between kinetic and interaction energy of the system. In particular, a system of ultracold bosons confined in an optical lattice potential is usually considered as one that meets the later description, and thus could be described by this model [12]. The particles vibrational motion within a fixed well and tunneling to its neighbor wells create an energy spectrum describable as band structure [14]. For big filling factors and a far-detuned lattice it has been observed scattering times in the order of minutes that creates a conservative potential capable of being loaded with tens of atoms per site [15].

In this chapter, we briefly review where the BHH comes from, its main features, and the phases we can find in it. We also determine the associated phase diagram, the general behavior of the system for specific limits of the parameters, and delve deeper into Mean Field (MF) and Bogoliubov approaches to solve it as well as the implementation of Numerical Exact Diagonalization (NED) on it. The BHH constitutes the principal ingredient for the present work. From now we will restrict our work to a system consisting of a single species of spin-polarized neutral bosons loaded in an optical lattice.

1.1 Derivation of BHH from the Many-Body Quantum Field Hamiltonian.

Following the original derivation of this Hamiltonian [12], we consider the Many-Body quantum field Hamiltonian for atoms subjected to external potentials including interactions given by:

$$\begin{aligned}\hat{H} = &\int d^3x \Psi^\dagger(\mathbf{x}) \left(-\frac{\hbar^2 \nabla^2}{2m} + V_0(\mathbf{x}) + V_T(\mathbf{x}) \right) \Psi(\mathbf{x}) \\ &+ \int d^3x d^3x' \Psi^\dagger(\mathbf{x}) \Psi^\dagger(\mathbf{x}') V(\mathbf{x} - \mathbf{x}') \Psi(\mathbf{x}) \Psi(\mathbf{x}'),\end{aligned} \tag{1.1}$$

where $\Psi^{(\dagger)}(\mathbf{x})$ is the boson creation (annihilation) field operator, $V_0(\mathbf{x})$ is an external but localized potential (the optical lattice potential), $V_T(\mathbf{x})$ stands for an additional outer (slowly varying) potential (e. g. a magnetic trap), and $V(\mathbf{x}-\mathbf{x}')$ accounts for the interaction potential, which assumes an explicit dependence on the distance vector between two particles of the system. According to [16], for alkali-gases (as those typically used to create ultracold gases experimentally) atom-atom scattering is well described by a short-range (s-wave) contact-potential that considers two-body collisions as the only possibility due to the very low kinetic energy of the elements of the system when they are at an almost zero temperature. Thus, the potential acquires the form

$$V(\mathbf{x}-\mathbf{x}') \approx \frac{4\pi a_s \hbar^2}{m}\delta(\mathbf{x}-\mathbf{x}') \tag{1.2}$$

with m the mass of one boson, and a_s the low-temperature s-wave scattering length, which encodes the direct consequences for the scattering amplitude function of considering the very low kinetic energy bosons have at an almost zero temperature. Inserting this in the second integral in eq. (1.1) leads to

$$\begin{aligned}\hat{H} = &\int d^3x \Psi^\dagger(\mathbf{x}) \left(-\frac{\hbar^2\nabla^2}{2m} + V_0(\mathbf{x}) + V_T(\mathbf{x})\right)\Psi(\mathbf{x}) \\ &+ \frac{4\pi a_s \hbar^2}{m}\int d^3x \Psi^\dagger(\mathbf{x})\Psi^\dagger(\mathbf{x})\Psi(\mathbf{x})\Psi(\mathbf{x}).\end{aligned} \tag{1.3}$$

A typical optical lattice consists of two counterpropagating lasers that interfere outcomming in a periodical arrange. For example $V_0(\mathbf{x}) = \sum_{i=1}^{3} V_{0i}\sin^2(kx_j)$ with wave vectors $k = 2\pi/\lambda$ and being λ the wavelength of the laser and $a = \lambda/2$ corresponds to the lattice period. This implies that $V_0(\mathbf{x}) = V_0(\mathbf{x}+\mathbf{d})$ with d a lattice vector, and this is the hypothesis for the Bloch theorem so we are allowed to propose a Bloch functions basis to describe the eigenfunctions of the Hamiltonian. These functions are of the form $\psi_{\mathbf{k},n}(\mathbf{x}) = e^{i\mathbf{k}\cdot\mathbf{x}}u_{\mathbf{k},n}(\mathbf{x})$ with $u_{\mathbf{k},n}(\mathbf{x})$ being real functions that approximately satisfy the Schrödinger equation for $V(\mathbf{x})$ at its minimums having the same periodicity of the potential consequently (also known as the atomic orbitals), and $\mathbf{k}$ being the quasimomentum. The energy spectrum created by the periodic potential is discrete and collectively conform the so-called Bloch energy bands labeled by index n.

In the experiment, the lattices must be deep enough to confine particles which, in other terms means that the chemical potential is too small to excite particles to other than the first Bloch energy band. The confinement of the particles suggests a localized form of the wave function, with the peaks centered around the sites of the lattice. It is natural, then, to look for localized linear combinations of the Bloch waves to work with. We will take the next subsection to introduce these functions and to establish the limits for their application.

1.1.1 Wannier Functions and final BHH.

Now we introduce the Wannier functions denoted by $w_n(\mathbf{x}-\mathbf{x}_i)$ where $\mathbf{x}_i$ is a fixed lattice site, and are mathematically defined as the next particular linear combination

$$w_n(\mathbf{x}-\mathbf{x}_i) = \frac{1}{\sqrt{N}} \sum_{k\in \mathrm{BZ}} e^{-i\mathbf{k}\cdot\mathbf{x}_i} \psi_{\mathbf{k},n}(\mathbf{x}), \tag{1.4}$$

a superposition of the Bloch functions where N is the total number of sites of the lattice, and $\mathbf{k}$ running over all the first Brillouin Zone. Occasionally, this is called the linear combination of atomic orbitals and is the basis for tight-binding models [17]. In fact, the Wannier functions and the Bloch functions are related by a Fourier transform and as such, they inherit some of their properties, the most important: they conform a complete orthonormal basis for the Hilbert space spanned by the Bloch functions obeying the relation

$$\int d^3x w_n^*(\mathbf{x}-\mathbf{x}_i) w_m(\mathbf{x}-\mathbf{x}_j) = \delta_{ij}\delta_{nm}, \tag{1.5}$$

including all the Bloch bands.

The localization of the functions is not an easy thing to find and may occur only for a specific physical condition. A complete analytical analysis of the Wannier displayed in [18] shows that for each Bloch band there is a unique way to choose the phases of the Bloch functions such that the Wannier function is real, symmetric and exponentially localized, which means an asymptotic exponential behavior of the function going to zero in the surroundings of $x = 0$. For the lowest band $n = 0$ and also the quasimomentum $\mathbf{k} = 0$ where the Wannier function acquires a finite value the asymptotic behavior of the localization manifest in the way [19]

$$|w_0(\mathbf{x})| \sim |\mathbf{x}|^{-3/4} \exp(-h_n|\mathbf{x}|), \tag{1.6}$$

where h_n is a constant decay and also a decreasing function of the index n. This is typically what we will understand as the localization of the Wannier functions. In the following we may provide another way to describe their localization with the occupation number basis.

The creation and anihilation field operators in the original Hamiltonian (1.3) now can be expanded in the complete Wannier basis in such a manner that anihilation (creation) process of a single particle (labeled by typical second quantization operators $\hat{b}_i^{(\dagger)}$ for the lattice site i) is localized at a potential minimum:

$$\Psi(\mathbf{x}) = \sum_i w_0(\mathbf{x}-\mathbf{x}_i)\hat{b}_i \tag{1.7}$$

inserting this field operator into (1.3) we note that the integrals will involve only the potentials, the differential operator, and the Wannier functions since the operators $\hat{b}_i^{(\dagger)}$ do not depend explicitly on the position. The potentials $V_0(\mathbf{x})$ and $V_T(\mathbf{x})$ are completely defined and using the property (1.5) it is straightforward that the four sums in the second double integral reduce to a single one by (1.5). Finally

$$\hat{H} = -\sum_{ij} t_{ij}\hat{b}_i^\dagger \hat{b}_j + \sum_{ij} \epsilon_{ij}\hat{b}_i^\dagger \hat{b}_j + \frac{1}{2}\sum_{ijkl} U_{ijkl}\hat{b}_i^\dagger \hat{b}_j^\dagger \hat{b}_k \hat{b}_l. \tag{1.8}$$

The parameters in (1.8) are given by

$$t_{ij} = \int d^3x w_0^*(\mathbf{x}-\mathbf{x}_i)\left(-\frac{\hbar^2\nabla^2}{2m}+V_0(\mathbf{x})\right)w_0(\mathbf{x}-\mathbf{x}_j) \tag{1.9}$$

$$\mu_{ij} = \int d^3x V_T(\mathbf{x}) w_0^*(\mathbf{x}-\mathbf{x}_i) w_0(\mathbf{x}-\mathbf{x}_j) \tag{1.10}$$

$$U_{ijkl} = \frac{4\pi a_s \hbar^2}{m}\sum_{ijkl}\int d^3x w_0^*(\mathbf{x}-\mathbf{x}_i)w_0^*(\mathbf{x}-\mathbf{x}_j)w_0(\mathbf{x}-\mathbf{x}_k)w_0(\mathbf{x}-\mathbf{x}_l). \tag{1.11}$$

Now we take advantage of the physical meaning of the equation (1.9) which is the probability that one state highly localized in x_j evolve and change its center to x_i, i. e. a hoping from site j to site i. The simplest way this could be nontrivial is considering hopings from one site to the immediately next sites and nothing else, which agrees with a lattice of deep wells. Being the case, we keep only the J_{ij}'s corresponding to pairs of nearest neighbors (NN) and neglect the other cases. The only way (1.10) and (1.11) are non-zero is to take all the labels to be the same; in other cases, the integrand is an almost zero and considered negligible. Following this reasoning the new parameters are

$$\mu_i = \int d^3x V_T(\mathbf{x})|w_0(\mathbf{x}-\mathbf{x}_i)|^2 \approx V_T(\mathbf{x}_i) \tag{1.12}$$

$$U_i = \frac{4\pi a_s \hbar^2}{m}\sum_i \int d^3x |w_0(\mathbf{x}-\mathbf{x}_i)|^4. \tag{1.13}$$

In equation (1.12) we also employ the smoothness of the trapping potential $V_T(\mathbf{x})$ and treat it as a constant whose value is best approximated by the centered potential $V_T(\mathbf{x}_i)$. Assuming the system is homogenous and the kinetic energy has no privileged directions, the latter equations holds for each of the sites and two pairs of NN, thus, $t_{ij} = t$ (for all pairs of NN) and $\mu_i = \mu$ and $U_i = U$ (for each lattice site), finding the Bose Hubbard Hamiltonian

$$\begin{aligned}\hat{H}_{\text{BH}} &= -t\sum_{\langle i,j\rangle}\hat{b}_i^\dagger\hat{b}_j + \frac{U}{2}\sum_i \hat{b}_i^\dagger\hat{b}_i^\dagger\hat{b}_i\hat{b}_i + \mu\sum_i \hat{b}_i^\dagger\hat{b}_i \\ &= -t\sum_{\langle i,j\rangle}\hat{b}_i^\dagger\hat{b}_j + \frac{U}{2}\sum_i \hat{n}_i\left(\hat{n}_i-1\right) + \mu\sum_i \hat{n}_i\end{aligned} \tag{1.14}$$

where we used the definition for the number operator $\hat{n}_i = \hat{b}_i^\dagger\hat{b}_i$ and the (bosonic) commutation rule $\left[\hat{b}_i, \hat{b}_i^\dagger\right] = 1$, and the notation $\langle\cdot\rangle$ refers to pairs of nearest neighbours. Note that $\mu\sum_i \hat{n}_i$, wehere μ is the chemical potential, is just an overall constant added to the Hamiltonian if the total number N of particles is fixed.

The BHH has its origins in the serching for a model of superconductivity in restricted geometries [20], [21] such as granular films (e.g. Vycor) and for porous media where the

Cooper pairs behave approximately as bosons. It was until 1989 that this model arrive to its modern form, derived by M. Fisher [22] (see [23]). In 1998, Jaksch et. al. [12] proposed to use the Bose-Hubbard Hamiltonian to describe a BEC in an optical lattice. Both works were focused on finding quantum phase transitions in the system. The main two types of phases distinguished for the limits $U/J \to \infty, 0$, and filling of the lattice n are the various Mott Insulator phases (MI-n) and the Superfluid (SF) respectively. Localization is the main distinctive factor of these two phases, the Mott insulator is characterized by highly localized bosons in the sites of the lattices (zero fluctuations of every site number operator) and the superfluid phase is characterized by the delocalization of all the particles of the system; physically one may understand this as the hopping process being intensely promoted. This will be explored in detail through the next sections and the two phases and the theoretical and numerical methods used in the analysis will also be explained.

1.2 Understanding the BHH.

Now with the final BHH, we go deeper into the physics hosted by it, in particular, we are interested in showing the intrinsic phases of the model and their characterization through calculations for observables of the system, and we will do it as van Oosten, et. al. in [13]. Following the operational part of quantum mechanics, this means to diagonalize the Hamiltonian and study the spectrum and the eigenfunctions because everything may be derived from there, but the problem here is the part of the Hamiltonian that involves products of four operators, which are very difficult to deal with in order to perform a diagonalization. The absence of a mathematical method typically puts us in the necessity of address this problem by proposing reasonable physical approximations to develop a more friendly Hamiltonian that hopefully encodes the most important physics of the system. Another option is to try numerical methods. Here we show effectively three ways in which one may try to do it for the BHH. The first is the Bogoliuvob approach followed by the Mean-Field Decoupling to explore the phase space of the system. Then, we move to numerical methods to perform an Exact Diagonalization to find the ground state and its energy. This will be one of the pillars for the rest of this thesis. All the hidden steps may be found in Appendix A.

1.2.1 Bogoliubov approach.

Starting with the Hamiltonian operator 1.14, and considering first a finite volume V, we apply a transformation to the momentum space of the site operators given by

$$\begin{aligned} \hat{b}_i &= \frac{1}{\sqrt{N_s}} \sum_{\mathbf{k}} \hat{a}_{\mathbf{k}} e^{-i\mathbf{k}\cdot\mathbf{r}_i} \\ \hat{b}_i^\dagger &= \frac{1}{\sqrt{N_s}} \sum_{\mathbf{k}} \hat{a}_{\mathbf{k}}^\dagger e^{i\mathbf{k}\cdot\mathbf{r}_i}, \end{aligned} \tag{1.15}$$

obtaining discrete values of momenta $\hbar\mathbf{k}$ running over the first Brillouin Zone (BZ). Later, the usual limit for $V \to \infty$ will allow us to change the sums by integrals using the fact that $\sum_i e^{i(\mathbf{k}-\mathbf{k}')\cdot r_i} = M\delta_{\mathbf{k}\mathbf{k}'}$ for M the total number of sites. Calling $H_{1,2,3}$ each

of the sums in 1.14 respectively, we insert the definitions (and drop the hats above the operators from now on) to find

$$H_1 = -t \sum_{\mathbf{k}} \sum_{\mathbf{k'}} \sum_{\langle i,j \rangle} a^\dagger_{\mathbf{k}} a_{\mathbf{k'}} e^{i(\mathbf{k}-\mathbf{k'})\cdot\mathbf{r}_i} e^{-i\mathbf{k'}\cdot(\mathbf{r}_j-\mathbf{r}_i)}. \tag{1.16}$$

Note that the sum over $\langle i,j \rangle$ involve only the vector $\mathbf{r}_j - \mathbf{r}_i$, with magnitud a, the lattice spacing. Each r_i has $2d$ neighbors at a distance a (being d the spacial dimension of the lattice). Fixing $\mathbf{r}_i$ and moving $\mathbf{r}_j$ then

$$\sum_{\langle i,j \rangle} e^{i(\mathbf{k}-\mathbf{k'})\cdot\mathbf{r}_i} e^{-i\mathbf{k'}\cdot(\mathbf{r}_j-\mathbf{r}_i)} = \sum_i e^{i(\mathbf{k}-\mathbf{k'})\cdot\mathbf{r}_i} \left(2 \sum_j^d \cos(k'_j a) \right) = N_s \delta_{\mathbf{k},\mathbf{k'}} \left(2 \sum_j^d \cos(k'_j a) \right). \tag{1.17}$$

This leaves the first part of the Hamiltonian as

$$H_1 = -\sum_{\mathbf{k}} \bar{\epsilon}_{\mathbf{k}} a^\dagger_{\mathbf{k}} a_{\mathbf{k}} \tag{1.18}$$

with $\bar{\epsilon}_{\mathbf{k}} = 2t \sum_{j=1}^d \cos(k'_j a)$. For the second and third part of the Hamiltonian the calculation is easier, and the result is

$$H_2 + H_3 = \frac{1}{2} \frac{U}{N_s} \sum_{\mathbf{k}} \sum_{\mathbf{k'}} \sum_{\mathbf{k''}} \sum_{\mathbf{k'''}} a^\dagger_{\mathbf{k}} a^\dagger_{\mathbf{k'}} a_{\mathbf{k''}} a_{\mathbf{k'''}} \delta_{\mathbf{k}+\mathbf{k'},\mathbf{k''}+\mathbf{k'''}} - \mu \sum_{\mathbf{k}} a^\dagger_{\mathbf{k}} a_{\mathbf{k}}. \tag{1.19}$$

Being the total Hamiltonian $H = H_1 + H_2 + H_3$, its final expression is as

$$H = \sum_{\mathbf{k}} (-\bar{\epsilon}_{\mathbf{k}} - \mu) a^\dagger_{\mathbf{k}} a_{\mathbf{k}} + \frac{1}{2} \frac{U}{N_s} \sum_{\mathbf{k}} \sum_{\mathbf{k'}} \sum_{\mathbf{k''}} \sum_{\mathbf{k'''}} a^\dagger_{\mathbf{k}} a^\dagger_{\mathbf{k'}} a_{\mathbf{k''}} a_{\mathbf{k'''}} \delta_{\mathbf{k}+\mathbf{k'},\mathbf{k''}+\mathbf{k'''}}. \tag{1.20}$$

In a BEC the average number of atoms in the system N_0 (in the least energetical state) is much greater than 1, so if $N_0 = \langle a^\dagger_0 a_0 \rangle$ and $\langle a_0 a^\dagger_0 \rangle - \langle a_0 a^\dagger_0 \rangle = 1$, then $\langle a_0 a^\dagger_0 \rangle \approx \langle a^\dagger_0 a_0 \rangle$ and this allow us to see the agreement with a commutation of both operators and conclude $N_0 = \langle a^\dagger_0 \rangle \langle a_0 \rangle$. Since $\langle a_0 \rangle$ and $\langle a^\dagger_0 \rangle$ are complex conjugates then $\langle a_0 \rangle = \langle a^\dagger_0 \rangle = \sqrt{N_0}$.

The heart of Bogoliubov approach is that the creation and annihilation operators now should be replaced by its average value plus a fluctuation

$$\begin{aligned} a^\dagger_0 &\to \sqrt{N_0} + a^\dagger_0 \\ a_0 &\to \sqrt{N_0} + a_0. \end{aligned} \tag{1.21}$$

At the minimum of the energy, the linear terms of the fluctuations must be zero. Keeping only with the first order terms (denoted by superscript (1))

$$H^{(1)} = \left(-\bar{\epsilon}_0 - \mu + \frac{U}{N_s}N_0\right)(\sqrt{N_0}(a_0^\dagger + a_0)). \tag{1.22}$$

Since this term must be 0 for all $a_0^\dagger$ and a_0 then:

$$-\bar{\epsilon}_0 - \mu + \frac{U}{N_s}N_0 = -2td - \mu + \frac{U}{N_s}N_0 = 0 \tag{1.23}$$

where $\bar{\epsilon}_0 = 2t\sum_{j=1}^{d} 1 = 2td$ and we conclude that for the lower-order approximation

$$\mu = Un_0 - zt \tag{1.24}$$

with $n_0 = N_0/N_s$ the density of states in the first band and $z = 2d$ the number of neighbors of each site.

Continuing with the approximation to find zero and second order approximations

$$\begin{aligned} H^{(0)} &= (-\bar{\epsilon}_0 - \mu)N_0 + \frac{1}{2}\frac{U}{N_s}N_0N_0 = (-2td - \mu + \frac{1}{2}Un_0)N_0 \\ H^{(3)} &= \frac{1}{2}Un_0(\sum_{\mathbf{k}} a_{\mathbf{k}}a_{\text{-}\mathbf{k}} + \sum_{\mathbf{k}} 4a_{\mathbf{k}}^\dagger a_{\mathbf{k}} + \sum_{\mathbf{k}} a_{\mathbf{k}}^\dagger a_{\text{-}\mathbf{k}}^\dagger). \end{aligned} \tag{1.25}$$

Finally the effective Hamiltonian acquires the form

$$H_{\text{eff}} = -\frac{1}{2}Un_0N_0 - \frac{1}{2}\sum_{\mathbf{k}}(\epsilon_{\mathbf{k}}+Un_0) + \frac{1}{2}\sum_{\mathbf{k}}\begin{pmatrix} a_{\mathbf{k}}^\dagger & a_{\text{-}\mathbf{k}} \end{pmatrix}\begin{bmatrix} \epsilon_{\mathbf{k}}+Un_0 & Un_0 \\ Un_0 & \epsilon_{\mathbf{k}}+Un_0 \end{bmatrix}\begin{pmatrix} a_{\mathbf{k}} \\ a_{\text{-}\mathbf{k}}^\dagger \end{pmatrix} \tag{1.26}$$

using the definition of $\epsilon_{\mathbf{k}} = zt - \bar{\epsilon}_{\mathbf{k}}$ and having using the facts that $\epsilon_{\mathbf{k}} = \sum_{j=1}^{d}\cos(k_j a) = \sum_{j=1}^{d}\cos(-k_j a) = \epsilon_{\text{-}\mathbf{k}}$, $\sum_{\mathbf{k}} a_{\mathbf{k}}a_{\mathbf{k}}^\dagger(\epsilon_{\mathbf{k}} + Un_0) = \sum_{\text{-}\mathbf{k}} a_{\text{-}\mathbf{k}}a_{-\mathbf{k}}^\dagger(\epsilon_{\mathbf{k}} + Un_0)$ and that we may change the sign of the label due to the symmetric region of the Fourier space we are dealing with.

Looking for a diagonal way to write this Hamiltonian, the Bogoliubov transformation requires the new bosonic operators $b_k^\dagger$ and b_k, designed to be an abstract rotation of the originals $b_k^\dagger$ and b_k. They must fulfill the algebraic relations for bosonic operators too. The transformation relating the two pairs of operators is

$$\begin{pmatrix} b_{\mathbf{k}} \\ b_{\text{-}\mathbf{k}}^\dagger \end{pmatrix} = \begin{bmatrix} u_{\text{k}} & v_{\text{k}} \\ u_{\text{k}}^* & v_{\text{k}}^* \end{bmatrix}\begin{pmatrix} a_{\mathbf{k}} \\ a_{\text{-}\mathbf{k}}^\dagger \end{pmatrix} \tag{1.27}$$

with u's and v's being unknown complex scalars that awaiting to be determined. From there, since $b_{-\mathbf{k}} = \left(b_{\pm\mathbf{k}}^\dagger\right)^\dagger$ and $b_{-(-\mathbf{k})}^\dagger = b_{\mathbf{k}}^\dagger$ must hold, then the coefficients satisfy $u_{\mathbf{k}} = u_{\text{-}\mathbf{k}}$, $u_{\mathbf{k}}^* = u_{\text{-}\mathbf{k}}^*$, $v_{\mathbf{k}} = v_{\text{-}\mathbf{k}}$, and $v_{\mathbf{k}}^* = v_{\text{-}\mathbf{k}}^*$. To make sure the new operators obey the bosonic commutation rules we expand the commutation relation and request the result to be equal to 1:

$$[b_{\mathbf{k}}, b_{\mathbf{k}}^{\dagger}] = |u_{\mathbf{k}}|^2 - |v_{\mathbf{k}}|^2 \to 1 \tag{1.28}$$

which tell us the matrix has inverse and it is such that

$$\begin{pmatrix} a_{\mathbf{k}} \\ a_{\text{-}\mathbf{k}}^{\dagger} \end{pmatrix} = \begin{bmatrix} u_{\mathbf{k}}^{*} & -v_{\mathbf{k}} \\ -v_{\mathbf{k}}^{*} & u_{\mathbf{k}} \end{bmatrix} \begin{pmatrix} b_{\mathbf{k}} \\ b_{\text{-}\mathbf{k}}^{\dagger} \end{pmatrix}. \tag{1.29}$$

Inserting 1.29 in 1.26 yields to

$$\begin{aligned} H_{\text{eff}} = &-\frac{1}{2}Un_0N_0 - \\ &\frac{1}{2}\sum_{\mathbf{k}}\left[(\epsilon_{\mathbf{k}} + Un_0)(|v_{\mathbf{k}}|^2 + |u_{\mathbf{k}}|^2) - Un_0(u_{\mathbf{k}}v_{\mathbf{k}}^{*} + v_{\mathbf{k}}u_{\mathbf{k}}^{*}) - (\epsilon_{\mathbf{k}} + Un_0)\right] \\ &-\frac{1}{2}\sum_{\mathbf{k}}[-2(\epsilon_{\mathbf{k}} + Un_0)u_{\mathbf{k}}v_{\mathbf{k}} + Un_0(u_{\mathbf{k}}^2 + v_{\mathbf{k}}^2)]b_{\mathbf{k}}^{\dagger}b_{\text{-}\mathbf{k}}^{\dagger} + \text{h. c.} \\ &+\sum_{\mathbf{k}}[(\epsilon_{\mathbf{k}} + Un_0)(|u_{\mathbf{k}}|^2 + |v_{\mathbf{k}}|^2) - Un_0(u_{\mathbf{k}}v_{\mathbf{k}}^{*} + v_{\mathbf{k}}u_{\mathbf{k}}^{*})].b_{\mathbf{k}}^{\dagger}b_{\mathbf{k}} \end{aligned} . \tag{1.30}$$

We request this to take the next diagonal form

$$H_{\text{eff}} = -\frac{1}{2}Un_0N_0 - \frac{1}{2}\sum_{\mathbf{k}}[\hbar\omega_{\mathbf{k}} - (\epsilon_{\mathbf{k}} + Un_0)] + \sum_{\mathbf{k}}\hbar\omega_{\mathbf{k}}b_{\mathbf{k}}^{\dagger}b_{\mathbf{k}}, \tag{1.31}$$

so we identify the respective coefficients, and it follows that

$$\begin{cases} 0 = -2(\epsilon_{\mathbf{k}} + Un_0)u_{\mathbf{k}}v_{\mathbf{k}} + Un_0\left[v_{\mathbf{k}}^2 + u_{\mathbf{k}}^2\right] \\ \hbar\omega_{\mathbf{k}} = (\epsilon_{\mathbf{k}} + Un_0)(|u_{\mathbf{k}}|^2 + |v_{\mathbf{k}}|^2) - Un_0(u_{\mathbf{k}}v_{\mathbf{k}}^{*} + v_{\mathbf{k}}u_{\mathbf{k}}^{*}). \end{cases} \tag{1.32}$$

Solving these equations leads to

$$\hbar\omega_{\mathbf{k}} = \sqrt{\epsilon_{\mathbf{k}}^2 + 2\epsilon_{\mathbf{k}}Un_0} \tag{1.33}$$

$$|v_{\mathbf{k}}|^2 = |u_{\mathbf{k}}|^2 - 1 = \frac{1}{2}\left(\frac{\epsilon_{\mathbf{k}} + Un_0}{\hbar\omega_{\mathbf{k}}} - 1\right). \tag{1.34}$$

Following with the general calculation, we focus in to know the density of the condensate n_0, which requires to know the total density n in terms of the effective Hamiltonian,

$$n = \frac{1}{M}\sum_{\mathbf{k}}\langle a_{\mathbf{k}}^{\dagger}a_{\mathbf{k}}\rangle_{H^{\text{eff}}}, \tag{1.35}$$

we separate the density of the lowest energy level n_0 from the rest of the spectrum populations since the beginning,

$$n = n_0 + \frac{1}{M}\sum_{\mathbf{k}\neq 0}\langle a_{\mathbf{k}}^{\dagger}a_{\mathbf{k}}\rangle_{H^{\text{eff}}} \tag{1.36}$$

and writing this in terms of (1.27) changing the sign of $\mathbf{k}$ appropiately and noting that the operators $b_{\text{-}\mathbf{k}}b_{\mathbf{k}}$ and $b^\dagger_{\mathbf{k}}b^\dagger_{\text{-}\mathbf{k}}$ are always 0, since they represent products of orthogonal number states for all $\mathbf{k} \neq 0$, we arrive to

$$\begin{aligned} n &= n_0 + \frac{1}{M}\sum_{\mathbf{k}\neq 0}\left[(|v_{\mathbf{k}}|^2 + |u_{\mathbf{k}}|^2)\langle b^\dagger_{\mathbf{k}}b_{\mathbf{k}}\rangle_{H^{\text{eff}}} + |v_{\mathbf{k}}|^2\right] \\ &= n_0 + \frac{1}{M}\sum_{\mathbf{k}\neq 0}\left[\frac{\epsilon_{\mathbf{k}}+Un_0}{\hbar\omega_{\mathbf{k}}}\langle b^\dagger_{\mathbf{k}}b_{\mathbf{k}}\rangle_{H^{\text{eff}}} + \frac{\epsilon_{\mathbf{k}}+Un_0-\hbar\omega_{\mathbf{k}}}{2\hbar\omega_{\mathbf{k}}}\right], \end{aligned} \tag{1.37}$$

and inserting $\langle b^\dagger_{\mathbf{k}}b_{\mathbf{k}}\rangle_{H^{\text{eff}}}$, the Bose distribution evaluated in $\hbar\omega_{\mathbf{k}}$ it follows that

$$n = n_0 + \frac{1}{M}\sum_{\mathbf{k}\neq 0}\left[\frac{\epsilon_{\mathbf{k}}+Un_0}{\hbar\omega_{\mathbf{k}}}\frac{1}{e^{\beta\hbar\omega_{\mathbf{k}}}-1} + \frac{\epsilon_{\mathbf{k}}+Un_0-\hbar\omega_{\mathbf{k}}}{2\hbar\omega_{\mathbf{k}}}\right]. \tag{1.38}$$

In the limit where $T = 0$ we have $\beta \to \infty$, therefore $\frac{1}{e^{\beta\hbar\omega_{\mathbf{k}}}-1} \to 0$ for all $\mathbf{k} \neq 0$, finding the density

$$n = n_0 + \frac{1}{M}\sum_{\mathbf{k}\neq 0}\left[\frac{\epsilon_{\mathbf{k}}+Un_0-\hbar\omega_{\mathbf{k}}}{2\hbar\omega_{\mathbf{k}}}\right]. \tag{1.39}$$

To take the continuous limit in $\mathbf{k}$ we must do $\sum_{\mathbf{k}} \to V\int_{-\frac{\pi}{a}}^{\frac{\pi}{a}} d\mathbf{k}/(2\pi)^d$, then

$$n = n_0 + V\int_{-\frac{\pi}{a}}^{\frac{\pi}{a}} \frac{\epsilon_{\mathbf{k}}+Un_0-\hbar\omega_{\mathbf{k}}}{2\hbar\omega_{\mathbf{k}}}\frac{d\mathbf{k}}{(2\pi)^d} \tag{1.40}$$

taking the variable change $\mathbf{k} = \frac{2\pi}{a}\mathbf{q}$ we find for $\bar{\epsilon}_{\mathbf{k}} = 2t\sum_{j=1}^{d}\cos(k_j a) \to \bar{\epsilon}_{\mathbf{q}} = 2t\sum_{j=1}^{d}\cos(2\pi q_j)$, therefore, $\epsilon_{\mathbf{k}} = zt - \bar{\epsilon}_{\mathbf{k}} \to \epsilon_{\mathbf{q}} = zt - \bar{\epsilon}_{\mathbf{q}}$ and it's clear that $\hbar\omega_{\mathbf{k}} = \sqrt{\epsilon_{\mathbf{k}^2}+2\epsilon_{\mathbf{k}}Un_0} \to \hbar\omega_{\mathbf{q}} = \sqrt{\epsilon_{\mathbf{q}^2}+2\epsilon_{\mathbf{q}}Un_0}$ remains unchanged and the integral is now

$$n = n_0 + V\int_{-\frac{1}{2}}^{\frac{1}{2}} \frac{\epsilon_{\mathbf{q}}+Un_0-\hbar\omega_{\mathbf{q}}}{2\hbar\omega_{\mathbf{q}}}d\mathbf{q}\left(\frac{2\pi}{a}\right)^d\frac{1}{(2\pi)^d} \tag{1.41}$$

modifying the integration limits in such a manner that $k_j = \pm\pi/a$ and then $q_j = \pm 1/2$. Knowing that $M = V/(a^d)$ then in the end the density will be

$$n = n_0 + \frac{1}{2}\int_{-\frac{1}{2}}^{\frac{1}{2}}\left(\frac{\epsilon_{\mathbf{q}}+Un_0}{\hbar\omega_{\mathbf{q}}} - 1\right)d\mathbf{q}. \tag{1.42}$$

Finally, in order to discover whether the new model captures the phase transition SF to MI for large U/t, we should be able to find a finite critical value for which the fraction of condensate n_0/n has no solution, or, in other words, goes to zero. It is desirable too that the model display different results when n is or not an integer value since the localizations in the Mott Insulator phase physically imply that the number of atoms is an integer multiple of M, otherwise, a fraction of the atoms will remain spread over the filled lattice sites and thus there could not be possible to achieve the

insulating property. In the following we explore the behavior of n_0 which will provide us a sense of whether the system is in the SF phase or not, this idea is based on the fact that the kinetic part of the BH become the most representative and thus ground state of the system should be Gross-Pitaevskii-type corresponding to a condensate fraction $n_0/n = 1$.

Given that $\epsilon_{\mathbf{q}} = 2t\sum_{j=1}^{d}[1-\cos(2\pi q_j)]$ and, in general, $1-\cos(x) \leq \frac{x^2}{2}$ then $1-\cos(2\pi q_j) \leq \frac{4\pi^2 q_j^2}{2}$, and

$$\epsilon_{\mathbf{q}} \leq 4\pi^2|\mathbf{q}|^2 t \tag{1.43}$$

$$\frac{\epsilon_{\mathbf{q}}+Un_0}{\sqrt{\hbar\omega_{\mathbf{k}}+2\epsilon_{\mathbf{q}}Un_0}} \to_{\frac{U}{t}\to\infty} \frac{Un_0}{\sqrt{2\epsilon_{\mathbf{q}}Un_0}} = \sqrt{\frac{Un_0}{2\epsilon_{\mathbf{q}}}} \tag{1.44}$$

and by 1.43 then

$$\frac{1}{2\pi}\sqrt{\frac{Un_0}{2t}}\int_{-\frac{1}{2}}^{\frac{1}{2}}\frac{d\mathbf{q}}{|\mathbf{q}|} \leq \int_{-\frac{1}{2}}^{\frac{1}{2}} d\mathbf{q}\frac{\epsilon_{\mathbf{q}}+Un_0}{\sqrt{\hbar\omega_{\mathbf{k}}+2\epsilon_{\mathbf{q}}Un_0}} \tag{1.45}$$

for these values of U/t. Calling I_d to the result of the d-dimensional integral in the left (that can be performed theoretically for $d = 2$ and numerically for higher dimensions) and $\int_{-1/2}^{1/2} d\mathbf{q} = \prod_{j=1}^{d}\int_{-1/2}^{1/2} dq_j = \prod_{j=1}^{d}(1/2+1/2) = 1$ the tendence is (from above)

$$n \to n_0 + \frac{1}{2}\frac{1}{2\pi}\sqrt{\frac{Un_0}{2t}}I_d - \frac{1}{2} = n_0 + \frac{1}{4\pi}\sqrt{\frac{Un_0}{2t}}I_d - \frac{1}{2} \tag{1.46}$$

and if we assume we are in a regime where this tendence is a good approximation then a new quadratic equation for $\sqrt{n_0}$ arises:

$$n_0 + \frac{1}{2}\frac{1}{2\pi}\sqrt{\frac{Un_0}{2t}}I_d - \frac{1}{2} - n = 0, \tag{1.47}$$

and solving for n_0 from its positive solution then

$$n_0 = \left(\frac{1}{2}\sqrt{\frac{I_d^2}{16\pi^2}\frac{U}{2t}+4n+2} - \frac{I_d}{8\pi}\sqrt{\frac{U}{2t}}\right)^2 \tag{1.48}$$

Knowing the behavior of the system in this limit, physically we expect that the condensate fraction n_0/n goes to zero for some finite critial value of U/t, and note from the last equation that $n_0 \to 0$ if $U/t \to \infty$ which is almost the expected behavior but we may conclude there is not a critical value with the help of (1.46, we may conclude that Bogoliubov approach looses this information. In addition, the results do not change regarding if the n is an integer or not.

It is very rational to question why we conclude this approach is blind to phase transitions of the system, of course, it is obvious that we have assumed before the calculation

the existence of such phases and also the kind of transition, but in fact, there is enough numerical supporting evidence through many methods such as Monte Carlo simulations ([24], [25], [26], [27]) and Density Matrix Renormalization Group ([28]). Moreover, the experimental observation of this transition (performed by Greiner, M. , et. al. [29]) is a solid proof In the next subsection, we will try another method to build a better-simplified model that captures the BHH information about the SF and MI phases, being congruent with the cited numerical results too.

1.2.2 Decoupling Approximation.

When dealing with quantum Many-Body systems there is a very useful tool called the Mean Field approximation (MF), which is one of the most common methods used when trying to find a more mathematically treatable model but preserving the physics of the system. Essentially, MF's initial proposal to minimize the free energy of the system ends up leaving the Hamiltonian with the weakest possible coupled dynamics of the system (mathematically, the physical result of the action of a quadratic operator will be simplified to a superposition of their effects each one weighted by the scalar expectation value of the other). This could lead to a loss of information of the system but is not the general case and for those successful cases, both the phases and critical curves have been well determined and coincide with results from other methods. Being aware of this we apply MF to the BHH in order to create a simplified model able to capture the important physics of the system.

We first introduce the superfluid parameter order $\psi = \langle \hat{b}_i^\dagger \rangle = \langle \hat{b}_i \rangle \approx \sqrt{n_i}$. Secondly, we use the MF decoupling for the quadratic operators given by

$$\langle \hat{b}_i^\dagger \hat{b}_j \rangle = \langle \hat{b}_i^\dagger \rangle \hat{b}_j + \hat{b}_i^\dagger \langle \hat{b}_j \rangle - \langle \hat{b}_i^\dagger \rangle \langle \hat{b}_i \rangle = \psi(\hat{b}_i^\dagger + \hat{b}_j) - \psi^2 \tag{1.49}$$

and insert both in 1.14 to obtain

$$\begin{aligned} H_{\text{eff}} &= -t \sum_{\langle i,j \rangle} \psi \hat{b}_i^\dagger - t \sum_{\langle i,j \rangle} \psi \hat{b}_j - t \sum_{\langle i,j \rangle} \psi^2 + \frac{U}{2} \sum_i \hat{n}_i(\hat{n}_i - 1) - \mu \sum_i \hat{n}_i \\ &= -zt \sum_i \psi \hat{b}_i^\dagger - zt \sum_j \psi \hat{b}_j - zt \sum_i \psi^2 + \frac{U}{2} \sum_i \hat{n}_i(\hat{n}_i - 1) - \mu \sum_i \hat{n}_i \end{aligned} \tag{1.50}$$

since the sums running over $\langle ij \rangle$ maintain one index fixed and the other is one for each NN and there are $z = 2d$ of them when the lattice we are dealing with is cubic and its dimensionality is d. If we consider the N total number of sites and changing $j \to i$ then

$$\hat{H}_{\text{eff}} = -zt \sum_i \psi(\hat{b}_i^\dagger + \hat{b}_i) - ztN_s\psi^2 + \frac{U}{2} \sum_i \hat{n}_i(\hat{n}_i - 1) - \mu \sum_i \hat{n}_i \tag{1.51}$$

and introducing $\bar{U} = \frac{U}{zt}$ y $\bar{\mu} = \frac{\mu}{zt}$ and noting that the Hamiltonian is now composed of N identical expresions for each site then we may find

$$\frac{H_{\text{eff}}}{Mzt} = H^i_{\text{eff}} = \psi(\hat{b}^\dagger_i + \hat{b}_i) - \psi^2 + \frac{\bar{U}}{2}\hat{n}_i(\hat{n}_i - 1) - \bar{\mu}\hat{n}_i \tag{1.52}$$

for any of the M components (sites), so this Hamiltonian per site will be enough to understand the physics of the whole system.

To determine whether the state is in SF phase or a MI phase one must find when ψ is or not equal to 0, that physically means the expectation value of a creation or annihilation operator is or not zero, and it is when there is no hoping at all: insulating phase. we then consider a few changes of the Hamiltonian

$$H = xH^i_{\text{eff}} = \frac{1}{2}\hat{n}_i(\hat{n}_i - \hat{1}) - \mu\hat{n}_i - x\psi(\hat{b}^\dagger + \hat{b}) + \psi^2 \tag{1.53}$$

for $x = 1/\bar{U}$ and consider the matrix representation of all the operators in the Hamiltonian as

$$n_i = \begin{pmatrix} 1 & 0 & \dots & 0 \\ 0 & 2 & \dots & 0 \\ \vdots & \vdots & \ddots & 0 \\ 0 & 0 & 0 & n \end{pmatrix}, \hat{b}_i = \begin{pmatrix} 0 & \sqrt{1} & \dots & 0 \\ 0 & 0 & \dots & 0 \\ \vdots & \vdots & \ddots & \sqrt{n-1} \\ 0 & 0 & 0 & 0 \end{pmatrix}, \text{ and } \hat{b}^\dagger_i = \begin{pmatrix} 0 & 0 & \dots & 0 \\ \sqrt{1} & 0 & \dots & 0 \\ \vdots & \vdots & \ddots & 0 \\ 0 & 0 & \sqrt{n-1} & 0 \end{pmatrix}$$

which allows to write $\hat{H}^i_{\text{eff}}$ as a matrix too. Next, we'll search by self-consistency for an adequate ψ that satisfy simultanoeusly 1.53 and $\psi = \langle G|\hat{b}_i|G\rangle$ for G the ground eigenstate of the site Hamiltonian. We may find useful to see $H^i_{\text{eff}} = H^i_{\text{eff}}(\psi)$, and name its ground state as $|G(\psi)\rangle$. To start the process give an adequate ψ_0 (near zero by the characterization of the phases) to later create the hopefully convergent sequence

$$\{\psi_n\}_{n\in\mathbf{N}} \to \psi \tag{1.54}$$

$$\psi_{n+1} = \langle G(\psi_n)|\hat{b}_i|G(\psi_n)\rangle \tag{1.55}$$

a suitable way to cut the process close to the limit value uses the Cauchy property of convergent sequences which states that a sequence converge if and only if $\forall\epsilon > 0$, $\exists N \in \mathbf{N}$ such that $|\psi_m - \psi_n| < \epsilon\ \forall n, m > N$; based on it choose an ϵ small enough and stop when $|\psi_n - \psi_{n+1}| < \epsilon$. Results from this analysis are shown in figure 1.1 where the two phases clearly distinguished, as well as the critical curve, is sharp are presented in the function of parameters U and t, and chemical potential (which controls the filling n). When $t/U \to \infty$, the situation should look more like in the trivial limit $U = 0$ where the superfluid phase take place because the kinetic energy domains all over the system, and its state is now made of linear combinations of spread Bloch states since the Hamiltonian is now diagonal in this basis; the parameter ψ is positive accordingly. The fact that every atom wants to hope from site to site is equivalent to an increased possibility of finding more than one atom in the same site at the same moment [30]. This starts to change if $U > 0$ because a new gap appears for a specific value of U in the spectrum defining two new bands being the more energetic the conductive one. To understand the opposite situation we begin noting that the limit $t/U \to 0$ considered effectively equivalent to take $t = 0$ leaves the Hamiltonian already diagonal in the number basis. The state that minimizes the energy will be $|G_{t=0}\rangle = \prod_i |\min\rangle_i$

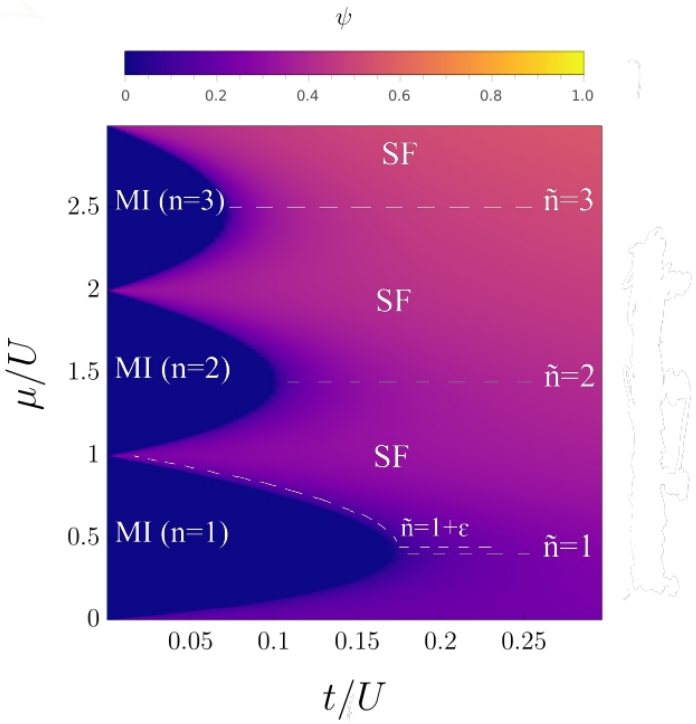

Figure (1.1) The phase diagram of the BHH has a SF for large t/U and several MI phases depending on the filling of the lattice which change with chemical potential. We have a schematic phase transition indicating the corresponding lobes to the values of the filling [30]. This is the numerical calculation of the phase space using self-consisting numerical approach performed by the author.

where the label *min* stands for the requirement that all the sites are filled with the least possible particle number per site. The latter is a good reason to think of the interaction as effectively repulsive since the system will always be trying to minimize the number of particles in each site. When the filling is integer multiple of M then this minimum is equal for all sites and it is exactly the Mott Insulator of order $n = N/M$, but if it is not the case then we may have a superposition of all possible combinations of a minimal number of particles per site. What happens in that case is illustrated in figure 1.1 by the dashed line for a filling $\bar{n} = 1 + \epsilon$ that is slightly greater than the case $n = 1$. Given the physically inaccessibility MI phase we expect that for $t/U \to 0$ the system follows the dashed curve above the first MI lobe [30].

In between the two limit behavior of the system (and for integer fillings), we find the competition between both phases that is not a simple mixture, in fact, there is a specific critical value $(t/U)_c$ that determine if the parameters of the system correspond to SF or MI when comparing to it. The analysis to find the critical value and the expression for the critical line starts with MF Hamiltonian and continues applying second-order perturbation theory. The next section addresses this task.

1.2.3 Critical Values.

Looking carefully at the Hamiltonian 1.53, since the interaction term alone is diagonal in the number basis and we may identify the kinetic term as a perturbation of the system modulated by the parameter ψ, it is easy to write it as $H^{\text{eff}} = H^{(0)} + \psi V$ where

$$H^{(0)} = \frac{1}{2}\bar{U}\hat{n}(\hat{n}-1) - \mu\hat{n} - \psi^2 \tag{1.56}$$

$$V = -(b^\dagger + b_i). \tag{1.57}$$

Calling $E_n^{(0)}$ to the non perturbed system energies for the occupation number of the state $|n\rangle$ and $E_g^{(0)}$ to the energy of the ground state then

$$E_g^{(0)} = \min\{E_i^{(0)} | n = 0, 1, 2, 3...\}. \tag{1.58}$$

if $E_g^{(0)}$ is considered to be the minimum energy then it should satisfy $E_g^{(0)} - E_{g+1}^{(0)} < 0$ and $E_g^{(0)} - E_{g-1}^{(0)} < 0$. For the energy of the eigentates we got $E_n^{(0)} = \frac{1}{2}\bar{U}n(n-1) - \bar{\mu}n - \psi^2$. Now, it is clear from here that if $\bar{\mu} > 0$ then $E_g^{(0)}$ should be zero. In other case, if $\bar{\mu} > 0$ then from the above conditions one obtains that

$$E_g^{(0)} = \begin{cases} 0, & \text{if } \bar{\mu} < 0 \\ \frac{1}{2}\bar{U}g(g-1) - \bar{\mu}g + \psi^2, & \text{if } \bar{U}(g-1) < \bar{\mu} < \bar{U}g. \end{cases} \tag{1.59}$$

For the first order of the energy $E_n^{(1)} = \langle n| - (b^\dagger + b)|n\rangle$ must be calculated but just to find it is zero, which is not the case of the second order corretion:

$$E_n^{(2)} = \sum_{n \neq m} \frac{|\langle n|\psi(b^\dagger + b)|m\rangle|^2}{E_n^{(0)} - E_m^{(0)}} = \frac{n}{\bar{U}(n-1) - \bar{\mu}} + \frac{n+1}{\bar{\mu} - \bar{U}n} \tag{1.60}$$

and considering this two terms of the approximation, we finally arrive for the particular case of the ground state ($n = g$) to

$$E_g \approx E_g^{(0)} + E_g^{(2)} = \frac{1}{2}\bar{U}g(g-1) - \bar{\mu}g + \left[\frac{g}{\bar{U}(g-1) - \bar{\mu}} + \frac{g+1}{\bar{\mu} - \bar{U}g} + 1\right]\psi^2 \tag{1.61}$$

Following the usual Landau's second order phase transitions analysis we expand energy in even potents of ψ to write

$$E_n = a_0(g, \bar{U}, \bar{\mu}) + a_2(g, \bar{U}, \bar{\mu})\psi^2 + O(\psi^4) \tag{1.62}$$

It is clear that whenever a_2 is positive then E_n is a parabola that opens upward and thus the minimum is located at its center, i. e. when $\psi = 0$ which corresponds to an insulating phase. On the other hand, if a_2 is negative then $\psi \neq 0$ since it will be the maximum otherwise, and therefore in this regime, the superfluid takes place. These facts imply that the change from $a_2 > 0 \to a_2 < 0$ is equivalent to $\psi = 0 \to \psi \neq 0$, in other words, the phase transition MI-SF is now found when $a_2 = 0$. We proceed now to find the conditions for it doing

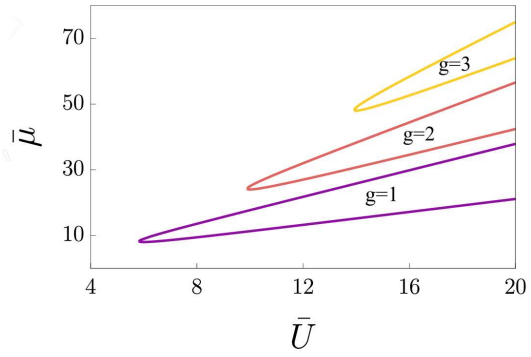

Figure (1.2) Garphics of the regions belonging to the different MI phases enclosed by $\bar{\mu}$ critical curves. If we inverted the axis doing $x \to 1/x$ we obtain the lobes in Fig. 1.1. The graphic is a reproduction of the results in [13].

$$a_2(g, \bar{U}, \bar{\mu}) = \frac{g}{\bar{U}(g-1) - \bar{\mu}} + \frac{g+1}{\bar{\mu} - \bar{U}g} + 1 = 0, \tag{1.63}$$

and from here we solve for

$$\bar{\mu}_{\pm} = \frac{1}{2}\left[\bar{U}(2g-1) - 1\right] \pm \frac{1}{2}\sqrt{\bar{U}^2 - 2\bar{U}(2g+1) + 1}, \tag{1.64}$$

which is essentially a mathematical expression for the boundary between phases in the space $\bar{\mu}$ vs $\bar{U}$. The superscript $\pm$ stands for the upper and lower border of the lobes for each $g = 1, 2...$, corresponding to the lobes in 1.1 but shown under the variable changes made in the beginning in figure 1.2.

Finally, solving for $\bar{\mu}_+ = \bar{\mu}_-$ will determmine the critical value $\bar{U}_c$ we were originally calculating. This gives:

$$\bar{U}_c = 2g + 1 + \sqrt{(2g+1)^2 - 1} \tag{1.65}$$

that for $g = 1$, the Mott Insulator-1 is approximately $\bar{U}_c \approx 5.83$ that is also found in [31].

1.3 Numerical Exploration: Exact Diagonalization of the BHH.

From a few decades ago the introduction of numerical methods in physics has increased the number of results regarding extremely difficult problems and also expanded the physical insight in many cases, they have served as a guide in purely theoretical approaches and in some others as an alternate route to check findings or discover new interesting aspects and research routes. In this case, we will start a numerical analysis parallel to all the theories presented in past sections. Once both phases have been determined as well as their boundaries in the phase diagram through MF theory, the next step is to quantify observable properties of the system as a function of the two parameters and compare the extracted physical information with our knowledge of the

BHH. We will follow the Numerical Exact Diagonalization as presented by [32] and results from [33]. Final conclusions in each calculation will validate the code developed by the author and constitute the solid basis to continue adding new options to go further and continue our research program.

1.3.1 The Computationl Method.

Numerical Exact Diagonalization requires the construction of the complete matrix representation of the Hamiltonian operator to later attempt to diagonalize it through any known numerical method. Given the size of a typical matrix involved in many-body problems, one often calculate the ground state and the spectrum, but also more sophisticated methods are needed, such as Lanczos Algorithm or a more general Arnoldi Iteration which at their core try to take a general matrix to a more tractable Hessenberg matrix form preserving the original eigenvalues [34]. The matrix representation of the Hamiltonian operator in a given orthonormal basis $\{|1\rangle, |2\rangle \dots\}$ is

$$H_{mn} = \langle m|H_{\text{BHH}}|n\rangle. \tag{1.66}$$

The first task in this calculation is to determine the Number basis given by all the configurations in which N particles can be accommodated in M sites which sums

$$D = \frac{(N+M-1)!}{N!(M-1)!} \tag{1.67}$$

elements. The size of the basis grows dramatically when increasing a fixed $N/M = 1$. To get a feeling of how big the basis become, the size of this basis for $N = 9$ is $D = 24310$, for $N = 12$ it increases to $D = 1352078$ and for $N = 13$ it reaches $D = 5200300$. (Is important to mention that the state-of-the-art allows experimentalists to build and control systems with no less than $N = 100$ particles and the dimension of the corresponding Fock basis have a number of elements that is intractable by practically any computer in the world, so the people always try to come up with an idea to get around this problem.)

To build the basis we first define a partial order in the configurations set. Let $|n_1, ..., n_M\rangle$ and $|\bar{n}_1, ..., \bar{n}_M\rangle$ be basis states, if they are not the same then there must exist an integer $k \in \mathbb{N} \cup \{0\}$ for which $n_k = \bar{n}_k$ and $n_{k+1} \neq \bar{n}_{k+1}$, then we shall say that the second is greater if and only if $n_{k+1} < \bar{n}_{k+1}$. Expanding this relation to an structure that takes into account the value of the k too allow us to create an algorithm to find "the next" configuration for any given state except. Moreover, the set now has a minimm and maximum, they are $|N, 0, ..., 0\rangle$ and $|0, ..., 0, N\rangle$ respectively. Given the state $|n_1, ..., n_M\rangle$ we may find the next one $|\bar{n}_1, ..., \bar{n}_M\rangle$ by following:

- $\bar{n}_i = n_i$ for $i \leq k-1$
- $\bar{n}_k = n_k - 1$
- $\bar{n}_{k+1} = N - \sum_{i=1}^{k} \bar{n}_i$
- $\bar{n}_i = 0$ for $i \geq k+2$

Having built the basis and store it in a list we call B, the next step is to find the matrix elements H_{mn} of the programmable operator H_{BH} (and for any other operator) trying to avoid an excessive number of steps. The idea is to compute the vector $H_{\text{BH}}|m\rangle \equiv |v\rangle$ and see if there is any other vector $|n\rangle$ such that $\langle n|v\rangle \neq 0$. By the nature of our Hamiltonian there are several vectors that satisfy that condition since $|v\rangle = u_1|m_1\rangle + u_2|m_2\rangle + \cdots + u_s|v_s\rangle$ for some s and one must consider whenever $|m\rangle = |m_i\rangle$. Instead of trying the product one by one, we should be able to completely determine the vectors that as a non zero result and save the time that product may consume too. A very suitable way to achieve this is to assign a unique tag to each basis vector and then choose a searching method to localize it within the basis and that is exactly how we will do. Following [32] we assign the next tag to each vector A_v of the basis with

$$T(A_v) = \sum_{i=1}^{M} (\sqrt{100i+3}) A_{vi} \tag{1.68}$$

where A_{vi} is the $i-th$ element of vector A_v and we have chosen the numbers of the form $\sqrt{100i+3}$ to assure (approximately) a unique irrational linear combination.

Now all the tags of B are saved maintaining their order in a list named *Tags* and proceed to sort this new list to create a pair of lists *OTags* and *PTags*, the first one is the sorted list, and the second one contains parallelly the position of each tag in *OTag* has in *Tags*. We choose to work with Binary Search (BS) method to find the position of the vector's tag in *OTag* and then consult in *PTag* for its position in the original basis list. With this lists, we write the final process as

1. Compute $H_{\text{BH}}|n\rangle = u_1|m_1\rangle + \cdots + u_s|m_s\rangle$
2. For each $i = 1, \ldots, s$ define $T_i = T(|m_i\rangle)$
3. B.S. of T_i in $OTags$ throws op_i such that $T_i = OTags(op_i)$
4. The position of $|m_i\rangle$ in B is $p_i = PTags(op_i)$
5. Matrx element $H_{m_i n} = H_{p_i n} = u_i$

and do this for each basis element $|n\rangle$. Any other matrix element is zero. This yields finally to the creation of a sparse matrix H and an eigensolver function for the matrix must be applied to it to request either a specific subset of eigenvectors (e. g. ground state) or eigenvalues (energy spectrum) using your preferred numerical method. For the present work the code was written in C++ employing the package Armadillo [35], [36].

1.3.2 Properties and Observables.

Simple Observables.

The aim of this subsection is to display a few results for simple observable quantities obtained using our code that may help us gain a better insight of the SF-MI main differences, and by default, this will constitute a check for the basic code we will further extend to reach the objectives of this work.

We begin by introducing the eigenenergies $E^{(\nu)}$ that arise from the diagonalization (labeled by ν) and the corresponding eigenvectors $C^{(\nu)}$ that stands for the linear combination

$$|\Psi_\nu\rangle = \sum_{l=1}^{D} C_l^{(\nu)} |\{n_1, ..., n_M\}_l\rangle \tag{1.69}$$

for $|\{n_1, ..., n_M\}\rangle_l$ the possible configurations of the system or, more formally, the different Fock states. The ν label is supposed to be in order respect to the value of the energy, being the case $\nu = 0$ the ground state.

The simplest observable is the average particle number per site (labeled i) given by

$$\bar{n}_i = \langle \Psi_0 | \hat{n}_i | \Psi_0 \rangle \tag{1.70}$$

but more interesting should be the fluctuation of this quantity since it gives access to the structure of the basic states within the hole state and is given by

$$\sigma_i = \sqrt{\langle \Psi_0 | \hat{n}_i^2 | \Psi_0 \rangle - \langle \Psi_0 | \hat{n}_i | \Psi_0 \rangle^2}. \tag{1.71}$$

Since the state of the system is a superposition of many possible configurations, the possible filling of each site may vary and thus the fluctuations will increase when $|\Psi_\nu\rangle$ is a spread combination of several states that correspond to the SF phase, in contrast to when the linear combination has a reduced number of importantly participating basis states which is the case of an MI, and consequently, the fluctuations reduces considerably.

Complementing this quantity, we may wish to now the module of the maximal coefficient C_l^ν given for the ground state by

$$|C_{\max}|^2 = \max\{|C_l|^2\} \tag{1.72}$$

and motivated by two important situations: if it is close to 0 it indicates there should be a large number of non-zero coefficients that finally mean an important contribution of a big number of states. On the other hand, if it is near 1 then this participation of any other coefficient is little enough to think the state is mainly represented by almost one Fock state.

Another quantity enclosing relevant information is the energy gap between the ground and the first excited state defined by

$$E_{\text{gap}} = E^{(1)} - E^{(0)}. \tag{1.73}$$

The superfluidity of the system is intimately related to the capacity of the particles to access more energetic states. A more excited state includes necessarily states with more than one particle per site increasing the chances for hoping from one site to other, if the gap is thin this state is accessible for the system then the superfluid phase will

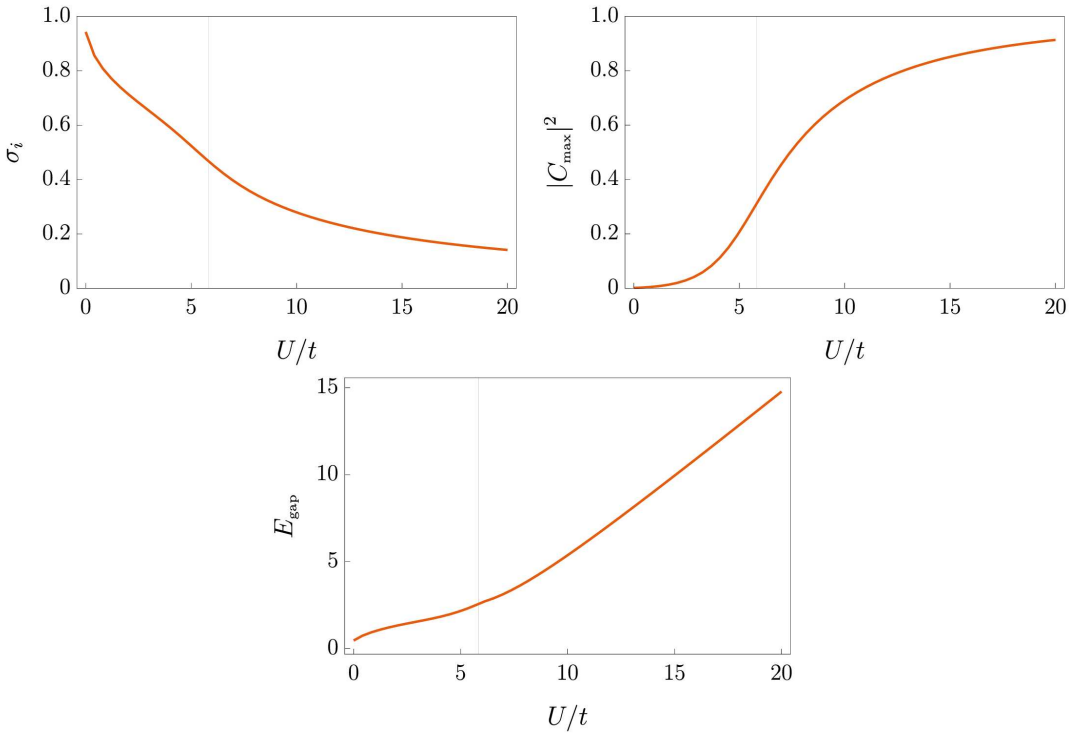

Figure (1.3) Plot of the fluctuations per site σ_i (a), the maximum coefficient C (b), and the energy gap (c) for a system of $N = M = 9$ particles as a function of U/t. The grey vertical line correponds to the critical value $U/t \approx 5.83$ from MF decouling. These results are a reproduction of those in [33].

take place. Contrarily, a big gap prevents particles from occupy more than one site at a time, meaning the Mott-Insulator is favored.

To show the above quantities we also put attention to the difference between the number of particles and sites for an integer filling $N/M = 1$ to see any dependence on the size of the system. The graphics in figure 1.3 refers to the three definitions discussed above. The fluctuations per site (1.3(a)) shows an initial value of 1 as expected but its behavior, while interaction strength grows, does not have a significative signature near the critical value $U_c/t_c \approx 4.65$ where we expected the MI (a result for the thermodynamic limit: $M \to \infty$ while $N/M = 1$ is fixed, using Monte Carlo simulations, [37]). Nothing special happens in the citical value and that has a reason: there is no transition in 1D and we are considering a relatively small number of sites. In fact, the decreasing ratio of the fluctuations is now even lower than before, and apparently, there is no tendency to zero as expected revealing the fluctuations are present even in the insulating phases. It is important to note there is not a matter of the size of the systems since the curves do not differ too much. This quantity does not bring any information about the phase transition.

Continuing with the maximum coefficient $|C_{\max}|^2$, plotted in Fig. 1.3(b), it comes from a nearly zero value in the ground state for a the SF phase that indicates a very spread distribution of the probability of being in any of the basis states. When increasing the ratio U/t the maximum starts getting close to 1 but it is never reached meaning the MI is not a pure Fock state.

The energy gap as in Fig. 1.3(c) starts with the minimum of its value in the regime

for the superfluid phase promoting the participation of states with more than one particle in some sites in the ground state expression. It increases with the ratio of the interaction-kinetic parameter finding finally a linear dependence on it for $U/t \geq 10$. This could be explained from the fact that states with a hole (and thus an extra particle somewhere) are now a more representative subset of Fuck states in the ground state, establishing a new signature of the insulating phase that has been explored experimentally in [29] as well as theoretically in [38] and [39].

Condensate fraction.

In contrast to the Gross Pitaevskii equation, the BHH does not assume the system is a BEC, and neither its presence is obvious from the Fock states form. To measure it, we have to adopt the Penrose and Onsager [40] definition that the condensate is present when one of the so-called natural orbitals is macroscopically occupied, which are nothing less than the eigenvalues of the reduced one-body density matrix,

$$\rho_{ij}^{(1)} = \langle \Psi_0 | \hat{a}_i^\dagger \hat{a}_j | \Psi_0 \rangle, \tag{1.74}$$

meaning the number of particles there N_c is almost N and thus the condensate fraction defined as $f_c = N_c/N$ should remain finite and near 1, even in the thermodynamic limit. Since $\mathrm{Tr}\rho_{ij}^{(1)} = N$ by normalization, the sum of its (positive) eigenvalues should be N, implying that there should be an eigenvalue larger or equal to N/M (because there are only M eigenvalues) but also the maximum eigenvalue can not be less than 1 and thus, $f_c \nleq 1/M$.

Following [41], we have that the BEC is intimate linked to nonvanishing off-diagonal terms of the matrix in question and it is often associated with its presence in the system. Mathematically we have

$$\rho_{ij}^{(1)} \nrightarrow 0 \text{ for } |i-j| \to \infty, \tag{1.75}$$

that makes this object capable of encoding the presence of the condensate in the system. Figure 1.4 is about the condensate fraction, which in this case was obtained by diagonalizing $\rho_{ij}^{(1)}$ and take its greater eigenvalue to calculate f_c. As expected, if the system is in a superfluid state then it is also completely in a BEC state. When interactions become larger, the fraction decreases, and non-condensate states grow in population.

After carefully analyzing the above calculations that do not exhibit a critical point in the same sense of the MFT, we have to remark that the fluctuations per site are still above $\sigma_i \approx 0.3$ and $|C_{\max}|^2$ is not 1 around the critical point, which means that the ground state is definitely not a pure Fock state. The MF decoupling ends up neglecting this fluctuations and this is the origin of the discrepancy, due to dimensionality. Since exact diagonalization takes into account all the couplings between Fock states and the MI phase is experimentally achievable, the conclusion should be that the MI can still be a superposition of some of them, arriving to a pure Fock state only in the limit $U/t \to \infty$ where σ_i vanishes.

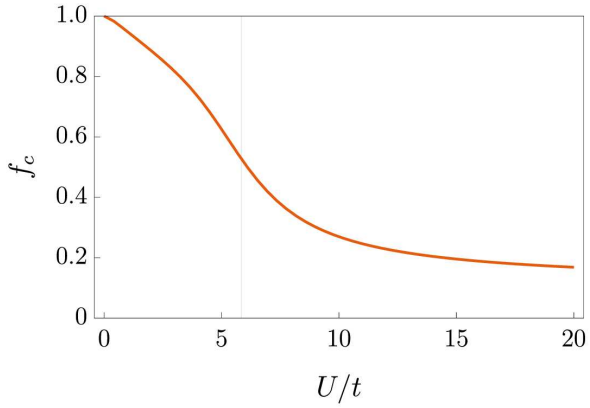

Figure (1.4) Plot of the condensate fraction f_c for a system of $N = M = 9$ particles as a function of U/t. The grey vertical line corresponds to the critical value $U/t \approx 5.83$ from MF decoupling. This result are a reproduction of those in [33].

1.4 Adiabatical reduction of the Fock basis.

From the past sections we learned many aspects of the SF and MI phases in the system through taking a deeper look into the structure of the ground state and the first excited states too, understanding the dynamics linked to the Fock states population and whether there is a BEC hosted in the lattice. One of the highlights concerns the fact that the superfluid phase is widely populated by most of the basic states, contrasting with its counterpart, the MI ground state is built in a more selective fashion. The physical situation contained in the results may also be interpreted in terms of a competition between two dynamics: the first one, driven by the interactions term forces the system to be in the more homogenous configuration that minimizes the energy costs (because of the $U > 0$ weighting it), and the second, a kinetical term promoting hopings from site to site that also (in this case, $-t < 0$). Summing up, the interaction term prefers widespread density states (which is often viewed as a repulsive interaction) and the kinetical term wants to keep the particles in an intense moving state.

Following this insight and the fact that the dimension D of the basis diverges rapidly for a slowly increasing N, a natural idea is to think that for big U/t the calculations may not need to take into account most of the possible configurations of the system, reducing space memory and processing capacity required. The proposal will be, then, to perform a cut-off on the basis of leaving out the more energetic states in this regime, that correspond to those having at least one site with a number occupation above a given integer R. This process is a simple form for an adiabatical elimination process since we are restricting the possibilities to only a subspace and at the same time, we are neglecting some thermal fluctuations.

If we perform a cut-off on the basis of R, then the result will be a set of all the possible configurations in which we can save N balls in M boxes restricted to a maximum of R balls per site. The resulting number of possible configurations is

$$D_R = \sum_{i=0}^{\lfloor \frac{N}{R+1} \rfloor} (-1)^i \binom{M}{i} \binom{N + M - 1 - i(K+1)}{M-1} \tag{1.76}$$

where $\lfloor \cdot \rfloor$ means the floor function and parenthesis are binomial coefficients. This reduction of the basis is very significant for computation efficiency and pushing a little bit further the maximum size of an approachable system. For our case, we can reduce the basis of $N = M = 9$ whose dimension is 24310 to 19855 if we keep only the states with occupations less than $R = 4$. The basis for $N = M = 11$ may see a change from 352716 to 265233 if the same cut off is applied.

At this point, we have focused only on the transition SF-MI that implies an integer filling $n = N/M = 1, 2, ...$ in order for the MI phase to appear. For the case where it is not an integer, the number of particles will be enough to completely fill the lattice an integer number of times plus an excedent number of particles N_e. After taking the limit $U/t \to \infty$ we will never find an MI phase but a different configuration with all of its sites uniformly filled but leaving the extra particles in a perpetual hoping state above this block of particles, that finally minimizes the ground state energy. The repulsive interaction in this limit is so intense that it is improbable that two or more excedent particles occupy the same site, becoming an effective Pauli exclusion for fermions based on the felt by the N_e bosons. These particles are also understood as bosons with a hard shell that makes them behave like fermions called hard-core bosons. The Hamiltonian for the fermionic system consists only of the kinetical part of the BHH:

$$H_f = -t \sum_{\langle i,j \rangle} \hat{f}_i \hat{f}_j. \tag{1.77}$$

To quantify this effect we propose the definition of a quantity that compares the ground-state structure of the BHH for a non-integer filling and the ground state of the analogous fermion system. If the bosonic system has $N = nM + N_e$ particles, then the analogous system should consist of only N_e fermions. The new spectrum will be the same for both fermionic and bosonic cases, despite of the commutation rules; as we see in the next chapters, the hard-core bosons Hamiltonian is proportional to the fermionic Hamiltonian and only shifted by a diagonal term. We call the *ideal basis* to that of the fermionic system. Having computed the ground states of both systems $|G_0\rangle$ and $|G^f\rangle$ (bosonic and fermionic respectively), and in order to compare them, we establish relations between similar states from both the ideal and bosonic basis where the excedent particle configuration is the same as in the fermionic case, identifying, for example, states of the form

$$|1, 0, \ldots, 0\rangle \leftrightarrow |n+1, n, \ldots, n\rangle \tag{1.78}$$

and so on. Guided by this relations we now build an *idealized state* from $|G^f\rangle$ given by

$$|G_I\rangle = (0, \ldots, 0, C_{I_1}, 0, \ldots, 0, C_{I_2}, 0, \ldots, 0, C_{I_{\bar{D}}}, 0, \ldots, 0), \tag{1.79}$$

of the same size as $|G_0\rangle$, where $\bar{D}$ is the dimension of the ideal basis, and the C_{I_i} is the coefficient of the I_i-th fermionic state in $|G^f\rangle$ but located in the entrance belonging to its pair given by 1.78. Fidelity can be now defined as

$$F_G = |\langle G|G_I\rangle|^2. \tag{1.80}$$

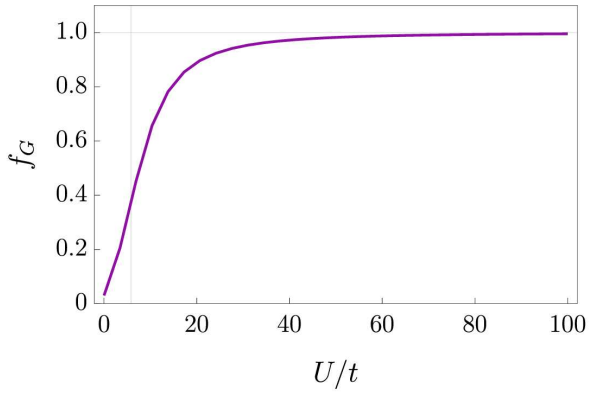

Figure (1.5) Graphic of the fidelity F_G between ground states of a bosonic system of 7 bosons in 6 sites and that of a single fermion system as a function of U/t. The grey horizontal line is the limit value for maximum agreement in their structures $F_G = 1$.

Values of $F_G \approx 1$ indicate both states have almost the same contribution from the related states and may exhibit similar properties.

To illustrate the hard-core boson limit we study a 2D bosonic system with $N = M + 1$ particles with $M = 6$ expecting the ground state structure to look much like the ground state of a single fermion in the same lattice for the limit $U/t \to \infty$. The result is displayed in Fig. 1.5 where the limit is practically reached for $U/t \approx 100$, providing good evidence to suggest that the study of the fermionic system may be accessed through the bosonic system in the hard-core bosons regime where ground states share their structures. This is an important result that will support many of the statements presented in the following and fifth chapters.

Chapter 2: Quantum Simulation of the Harper Model and Topological Features.

This chapter is divided in two sections. The first is the study of the effects of a magnetic field over one particle constrained to a 2D lattice and the typical way in which we model it through the Harper's Model and the possibility of the BHH to mimic these effects. The second part is an introduction to the topological phenomena hosted by this model, being the Berry phase the link in between. It has been a very useful tool and in many cases the first step to the study of important topological phenomena. By now, we will only explore some important quantities such as topological invariants through Streda's Formula. Specifically, this outline is designed to introduce the feasible Quantum Simulation (QS) of the Harper Model via ultracold neutral atoms with artificial magnetic phases [42] as a way to explore its topological properties and to survey extended scenarios for different fillings or sizes of the system, and the possibility of adding new interactions or changes in the nature of particles (bosons or fermions). We understand QS as the fact a quantum system can host analogous physical conditions, properties or nature of another quantum system [43], typically, the simulator target is to model a more complex system or one that is not so easy to access experimentally. In our case, the state-of-the-art of ultracold atoms bring us a high control level over all the parameters and constrains of the BHH, making it a strong candidate for a quantum simulator.

2.1 Hofstadter approach to the Harper Model.

The original Harper Model [44] consists of a single Bloch band crystal electron in a 2D lattice subject to a magnetic field. In his article, Douglas Hofstadter [47] addresses the situation by taking one Bloch band as the Hamiltonian of the system guided by the Luttinger theorem [48] which states that the system may have a solution in the Bloch basis of the case without the magnetic field, even when it is turned on.

Take the Bloch band function given by

$$W(\vec{k}) = 2t[\cos(k_x a) + \cos(k_y a)], \tag{2.1}$$

for a square lattice with spacing a and $t > 0$. Following the reasoning of the author, we

now promote momentum variables to momentum operators and then assume the Peierls substitution: $\hbar\hat{\mathbf{k}} \rightarrow -i\hbar\hat{\mathbf{p}} - (e/c)\hat{\mathbf{A}}(\vec{x})$ where $\hat{\mathbf{A}}$ is the magnetic vectorial potential operator [49] (motivated in turn by the changes of the canonic momentum due to the presence of a magnetic field $\vec{A}$ in a classical Hamiltonian), leaving

$$\hat{H} = 2t\cos\left[\left(\hat{p}_x - \frac{e}{c}\hat{A}_x\right)\frac{a}{\hbar}\right] + 2t\cos\left[\left(\hat{p}_y - \frac{e}{c}\hat{A}_y\right)\frac{a}{\hbar}\right]. \tag{2.2}$$

Expanding the cosen in a potents series we identify the exponentials and write

$$\hat{H} = t[e^{\frac{i}{\hbar}(\hat{p}_x - \frac{e}{c}\hat{A}_x)a} + e^{-\frac{i}{\hbar}(\hat{p}_x - \frac{e}{c}\hat{A}_x)a}] + t[e^{\frac{i}{\hbar}(\hat{p}_y - \frac{e}{c}\hat{A}_y)a} + e^{-\frac{i}{\hbar}(\hat{p}_y - \frac{e}{c}\hat{A}_y)a}] \tag{2.3}$$

Now, if we consider a magnetic field orthogonal to the 2D lattice then it shuold be of the form $\vec{B} = (0,0,1)B$ with B its intensity. The simplest vectorial potential is for a Landau potential of the form $\hat{\vec{A}} = (0, B\hat{x}, 0)$ with $\hat{x}$ the position operator in the x-direction. Since this implies that $[p_j, A_j] = 0$ the Baker-Campbell-Hausdorff theorem applies, producing translation operators $\exp(ap_{x,y}/\hbar)$, arriving to the next energy equation for a bidimensional wave function $\psi(x,y)$

$$t[\psi(x+a,y) + \psi(x-a,y) + e^{-i\frac{Bea^2}{c\hbar}x}\psi(x,y+a) + e^{-i\frac{Bea^2}{c\hbar}}\psi(x,y-a)] = E\psi(x,y). \tag{2.4}$$

which is known as the Harper equation [47], [44]. Note that the energy of the state now depends on the wave function centered at the neighbors sites weighted by a new phase produced by the only presence of the magnetic field. Since the lattice spacing is a, then for a square lattice each site is of the form $(ma, na) = (x, y)$. Considering the Luttinger theorem [48], we take the Bloch ansatz given by $\psi(x,y) = e^{i\nu n}g(ma)$ obtaining the following

$$\begin{pmatrix} g(m+1) \\ g(m) \end{pmatrix} = \begin{pmatrix} \epsilon - \cos(2\pi m\alpha - \nu) & -1 \\ 1 & 0 \end{pmatrix}\begin{pmatrix} g(m) \\ g(m-1) \end{pmatrix}, \tag{2.5}$$

where we named $\alpha = Bea^2/ch = Ba^2/2\pi(\hbar c/e)$: the phase arising from the magnetic field presence, which is in fact the ratio between the magnetic flux in a cell of the lattice and a quantum flux. We call M_n to the matrix of the system for an integer in the argument of the cosine. The previous equation relate $g(m)$ with $g(m+1)$, so it is possible to compose this recursive equation to connect $(g(m+1g(m))$ to $(g(1), g(0))$ through a product of matrices M. Now, we must impose on g the physical condition of being bounded, which translates into the requirement of the product of the matrices to be bounded. Suppose from the cosine that the matrces M_n are periodic in n for some period q which leads to the fact that the product of those matrices are composed of periodic bloques of the form

$$Q = M_q M_{q-1} \cdots M_1 \tag{2.6}$$

then the condition for this periodicity should be

$$2\pi m\alpha - \nu = 2\pi(m+q)\alpha + 2\pi p - \nu \tag{2.7}$$

for some integer p. Solving for α we find that

$$\alpha = \frac{p}{q} \tag{2.8}$$

and this last result shows the equivalence of being periodic and the rationality of the magnetic flux per plaquette α.

Since $\det(M_n) = 1$ for all n then $\det Q = 1$ which means that the product of its eigenvalues is such that $\lambda_1\lambda_2 = 1$, so they should be of the form $e^{\pm i\theta}$ since they are complex conjugates and hence

$$|\mathrm{Tr}(Q)| = |\sum_i \lambda_i| \leq 2. \tag{2.9}$$

Since Q includes a product of the form $\prod_{k=1}^{q}(\epsilon - \cos(2\pi k\alpha - \nu))$ in its first element then the trace should be a polynomial in ϵ of order q. From eq. (2.9), the geometrical interpretation is that the allowed energies of the system are those lying in a neighbourhood of any of the q roots of the trace and it happens for each $\alpha = p/q$.

To deal with the phase ν we can always pick a block Q inside a product and displace it by some arbitrary m_0 just to see that

$$\mathrm{Tr}(Q) = \mathrm{Tr}(\prod_{i=1}^{q} M_i) = \mathrm{Tr}(\prod_{i=m_0}^{q+m_0 \mod q} M_i) \tag{2.10}$$

Since the trace is the same after changing $2\pi m\alpha - \nu$ by $2\pi m\alpha - (\nu - 2\pi m_0\alpha)$ or equivalently changing ν by $-2\pi m_0\alpha = (2\pi/q)(-m_0 p)$ we may propose that the trace is periodical in ν by $2\pi/q$, allowing the usage of a Fourier transform with period $T = 2\pi/q$. The coefficients fo this expansion

$$a_k = \frac{2}{T}\int_{-\frac{T}{2}}^{\frac{T}{2}} f(\nu)\cos(kq\nu)d\nu \quad b_k = \frac{2}{T}\int_{-\frac{T}{2}}^{\frac{T}{2}} f(\nu)\sin(kq\nu)d\nu \tag{2.11}$$

will be non-zero only for $k = -1,\ 0,\ 1$. The term $\cos(q\nu)$ in $f(\nu)$ is independent of ϵ so the term that includes ϵ explicitly is $k = 0$, a constant respect ν. With this separation we may write

$$\mathrm{Tr}(Q(\epsilon,\nu)) = \mathrm{Tr}(Q(\epsilon,\nu_0)) + f(\nu) \tag{2.12}$$

where $f(\nu)$ has a coefficient $\frac{q}{\pi}\int_{-\frac{\pi}{q}}^{\frac{\pi}{q}}\cos^2(q\nu)d\nu = 1$ and it happens for $k = -1$ too, giving a total of $f(\nu) = 2\cos(q\nu)$. Taking ν_0 as a convenient constant $\pi/2q$ that reduce many terms in the equation to zero, the final inequality will be

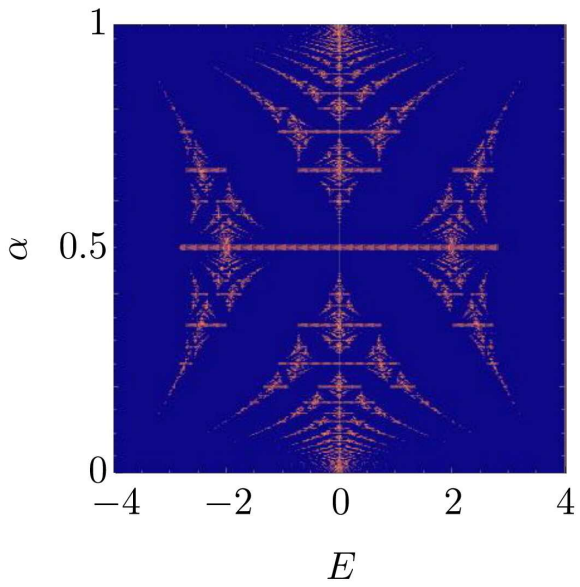

Figure (2.1) Numerical calculation of the allowed energies for a given magnetic flux in the eq. (2.13). This graph is composed of horizontal layers with q line segments according to the corresponding value of $\alpha = p/q$. This is a reproduction of the famous Hofstadter's result [47].

$$|Tr(Q(\epsilon))| \leq 4. \tag{2.13}$$

In figure (2.1) we can see a plot of a numerical calculation of all the energies that satisfy (2.13) for a rational value of α between 0 and 1. This interesting spectrum is conformed by line segments in each value of the magnetic field; for each non reductible value of $\alpha = p/q$ there are q segments, i.e. the energy breaks into q Bloch bands with a well studied structure [47]. When we get close to $\alpha = 0, 1$ we will find infinite segments which is the origin of its fractal behavior. In the same reference, it is shown from a topological point of view that when α is irrational the spectrum is a set of energy points with a structure homeomorphic to a Cantor set, something that also explains the weird sense of non-compatibility when we pick two close rationals one with a bigger number of bands than the other. Due to its peculiar form, the spectrum is known as the Hofstadter Butterfly.

Since the intensity of the magnetic field changes the band structure of the system abruptly, it is a natural question to ask more about the topological nature of this changes, a question that we will be reviewing in part during the rest of this work.

2.2 Gauge symmetry of the Many-Body Hamiltonian.

Suppose a homogenous magnetic field present in the optical lattice directed parallel to its orthogonal surface vector. We impose the following: it would be considered to be a classic field, implying zero quantum fluctuations and it does not depend on a dynamical variable, and we will neglect any back influence from the induced field.

2.2.1 Gauge invariance of non-Abelian gauge fields: continuum case.

The Many-Body Hamiltonian including the magnetic field (leaving out the confinement potentials) reads

$$\hat{H} = \frac{1}{2m}\int d^3x\hat{\psi}^\dagger(\mathbf{x})(-i\hbar\nabla - \frac{e}{c}\hat{A}(\mathbf{x}))^2\hat{\psi}(\mathbf{x}) + g\int d^3x\hat{\psi}^\dagger(\mathrm{x})\hat{\psi}^\dagger(\mathbf{x})\hat{\psi}(\mathbf{x})\hat{\psi}(\mathbf{x}) \quad (2.14)$$

where the term $-i\hbar\nabla - \frac{e}{c}\hat{A}(\mathbf{x})$ is the result of the Peierls substitution. Now, after applying a U(1) gauge transformation as

$$\hat{\psi}(\mathbf{x}) \to e^{i\phi(\mathbf{x})}\hat{\psi}(\mathbf{x}) \quad (2.15)$$

and

$$\hat{A}(\mathbf{x}) \to \hat{A}(\mathbf{x}) + \frac{e}{c}\nabla\phi(\mathbf{x}) \quad (2.16)$$

we will find for the interaction term that after rearranging the operators using the commutation rules that

$$\hat{\psi}^\dagger(\mathbf{x})\hat{\psi}(\mathbf{x}) \to \hat{\psi}^\dagger(\mathbf{x})e^{-i\phi(\mathbf{x})}e^{i\phi(\mathbf{x})}\hat{\psi}(\mathbf{x}) = \hat{\psi}^\dagger(\mathbf{x})\hat{\psi}(\mathbf{x}), \quad (2.17)$$

and in the kinetical term we should make explicit that

$$\left(-i\hbar\nabla - \frac{e}{c}A(\mathbf{x})\right) - \hbar\nabla\phi(\mathbf{x}))e^{i\phi(\mathbf{x})}\psi(\mathbf{x}) = e^{i\phi(\mathbf{x})}\left(-i\hbar\nabla - \frac{e}{c}A(\mathbf{x})\right)\psi(\mathbf{x}). \quad (2.18)$$

Analogously, using the hermiticity of the operators,

$$\psi^\dagger(\mathbf{x})e^{-i\phi(\mathbf{x})}\left(-i\hbar\nabla - \frac{e}{c}A(\mathbf{x})\right) - \hbar\nabla\phi(\mathbf{x}) = \psi^\dagger(\mathbf{x})\left(-i\hbar\nabla - \frac{e}{c}A(\mathbf{x})\right)e^{-i\phi(\mathbf{x})} \quad (2.19)$$

leading to the invariance of the hole Hamiltonian. In this context, the $\mathbf{B} = \nabla \times \mathbf{A}$ defines a U(1) gauge-invariant field. The confinement potentials would not change anything in this calculation if included.

2.3 Simulation of electrons in 2D crystal lattice: the Hofstadter-Harper Model.

Given the similarity of the electron in the crystal lattice and atoms in an optical lattice we could expect similar physical effects in both systems. In this section we attempt to capture the physics of a Bloch electron in the Harper Model through the BHH.

Both systems are tight-binding models and both should include the effects of the magnetic field. Since the particles of the BHH and also the FHM are neutral we must direct the look deeper in the magnetic field nature. From a quantum point of view, the Aharonov-Bohm phase acquired by the wave function of a particle crossing a magnetic field in a closed path is one of its most profound signatures, it captures the magnetic flux meaning the complete action of the magnetic field on the system.

Observing the Harper equation (ec. 2.4) the phase acquired by the displaced wave function is also the phase that one particle acquires by Aharonov-Bohm effect if it moves from one lattice elementary square plaquette (the minimum closed path). From a classical point of view, the AB phase attached to a Bloch electron should be

$$\Phi_{AB} = \frac{e}{c\hbar} \oint_{\square} \mathbf{A} \cdot d\mathbf{l}. \tag{2.20}$$

The Landau gauge we selected, parallel to two of the sides of the square and orthogonal to the others, leaves

$$\Phi_{AB} = \frac{e}{c\hbar} \left[\int_1^2 (0, Bma, 0) \cdot \hat{y} dy + \int_3^4 (0, B(m+1)a, 0) \cdot (-\hat{y}) dy \right] = \frac{Bea^2}{c\hbar} = 2\pi\alpha. \tag{2.21}$$

with the numbers indicating a counterclockwise labeling of the sites in the corners. The geometrical arange of the square suggests that the phase acquired by the neutral atoms in the optical lattice should be of the form

$$\theta_{ij} = \begin{cases} 2\pi\alpha m & \text{for displacements to the right in the row } m \\ -2\pi\alpha m & \text{for displacements to the left in the row } m \\ 0 & \text{otherwise} \end{cases}, \tag{2.22}$$

in order to imprint the same magnetic flux to every elementary plaquette. The proposed Hamiltonian that simulates the electron dynamycs in the optical lattice looks like

$$H_{\text{HHM}} = -t \sum_{\langle i,j \rangle} e^{i\theta_{ij}} \hat{f}_i \hat{f}_j, \tag{2.23}$$

also known as the Hofstadter-Harper Model [51]. The system equiped with the phases create an artifitial magnetic field for neutral atoms. The Hamiltonian in qe. 2.23 can be exactly solved with the same exact diagonalization technique. Solving the for the energies of the system, we may build the graphic in Fig. 2.2 taking into account the density of states given by [52]:

$$\rho(E) = -\frac{1}{\pi N_x N_y} \sum_n \Im \frac{1}{E - \epsilon_n + i\eta} \tag{2.24}$$

where N_x y N_y are the dimensions of the lattice and η is an adjusting parameter. There are minor differences with the Hofstadter butterfly since that is the case of a continuum

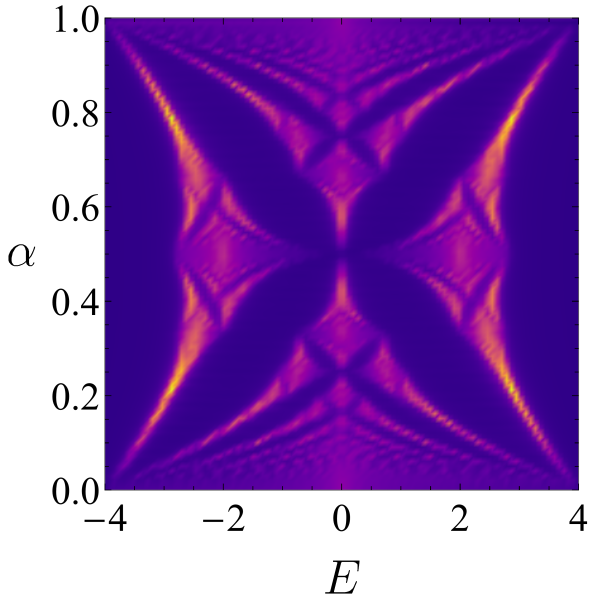

Figure (2.2) Density of states of the Hofstadter-Harper model energy spectrum as a function of the magnetic flux α, obtained by exact diagonalization. The size of the optical lattice is 40x40. We used $\eta \approx 0.01$.

variable of energy. Exact diagonalization provides as many energy dots as the size of the basis, which means that a more defined spectrum requires of a big number of sites.

Asuming the phases carry all the physics of the magnetic field, the natural proposal for the Hamiltonian for bosons with artificial magnetic field is

$$\hat{H} = -t \sum_{\langle i,j \rangle} [e^{i\theta_{ij}} \hat{b}_i^\dagger \hat{b}_j] + \frac{U}{2} \sum_i \hat{n}_i(\hat{n}_i - 1), \tag{2.25}$$

without considering any source of magnetic effects from the sites with one or more bosons [45].

2.3.1 Gauge invariance of Abelian gauge fields: the lattice case.

The concept of gauge invariance can be extended to the case of a discrete space as the lattice as it has been done for Lattice Gauge Theories [45]. There, the transformation is defined for on-site field operators ad for the case of a $U(1)$ it is defined as

$$\hat{b}_j \to e^{i\phi_j} \hat{b}_j. \tag{2.26}$$

After applying it to the kinetic operators as an on-site $U(1)$ gauge transformation we will find

$$\theta_{ij} \to \theta_{ij} - \phi_i + \phi_j = i\theta_{ij} + \Delta\phi \tag{2.27}$$

that is a discretized form of equation (2.16). Taking the circulation of the plaquette so that the vertices 1,2,3 and 4 are in order, the total acquired phase that express the Aharonov-Bohm effect, transforms as

$$\begin{aligned}\theta'_{12}+\theta'_{23}+\theta'_{34}+\theta'_{41} &= \theta_{12}+\phi_1-\phi_2+\theta_{23}+\phi_2-\phi_3+\theta_{34}+\phi_3-\phi_4+\theta_{41}+\phi_4-\phi_1 \\ &= \theta_{12}+\theta_{23}+\theta_{34}+\theta_{41},\end{aligned} \tag{2.28}$$

which means it is an invariant and is often called the Wilson Loop [45]. Given a set of Wilson Loops in the lattice (or fluxes) denoted as $\{W(\square_i)\}$, there are many families of transformation phases $\{\phi_i\}$ that lead to the same physics produced by the Wilson Loops when open boundary conditions are taken (a torus geometry).

2.4 Berry Phase.

A more powerful concept that generalizes the AB phase is that of the Berry phase, or as M. Berry originally called it [55], the *geometric phase* since it arises from the adiabatic evolution of the state of the system driven by continuum changes in the parameter space of the system in time. The geometry of the followed path is highly related to the physics of the system, specially the closed paths, suggesting the presence of a more powerful and not so obvious topological structure that is itself a new interesting and fertil area of study [46], [51]. We will define the Berry phase from [55] and later make the connection to the topological side which follows closely [57].

2.4.1 General formula for the phase factor.

For a general Hamiltonian $\hat{H}(\mathbf{R})$ that depends on a set of real parameters $\mathbf{R}=(X,Y,...)$ we may propose an evolution path in the parameters space given by $\mathbf{R}(t)$ that satisfies $\mathbf{R}(T)=\mathbf{R}(0)$, being a closed curve C. the state of the system $|\psi(t)\rangle$ must satisfy for every t the Schrödinger equation

$$\hat{H}(\mathbf{R}(t))|\psi(t)\rangle = i\hbar|\dot{\psi}(t)\rangle. \tag{2.29}$$

At any instant, the parameters configuration has a corresponding eigenbasis consisting of the family of states $\{n(\mathbf{R})\}$ that is assumed discrete. They must satisfy

$$\hat{H}(\mathbf{R}(t))|n(\mathbf{R}(t))\rangle = E_n(\mathbf{R}(t))|n(\mathbf{R}(t))\rangle \tag{2.30}$$

with E_n the energies. If the system evolves adiabatically, the state $|n(\mathbf{R}(t))\rangle$ will evolve with $\hat{H}$ leaving only one freedom level to change in time: a new phase could be added to the state still satisfying the eigenenergy equation. The adiabatic evolution of the state that solves the eq. 2.29 reads

$$|\psi(t)\rangle = e^{\frac{-i}{\hbar}\int_0^t E_n(\mathbf{R}(t'))dt'}e^{i\gamma_n(t)}|n(\mathbf{R}(t))\rangle. \tag{2.31}$$

where the first phase is the dynamical phase factor and the second arises from the adiabatic evolution of the system. Inserting eq. (2.31) in eq. (2.29) and multiplying it in the left by $\langle n(\mathbf{R}(t))|$ yields

$$\dot{\gamma}_n(t) = i\langle n(\mathbf{R}(t))|\frac{\partial}{\partial \mathbf{R}}|n(\mathbf{R}(t))\rangle \cdot \dot{\mathbf{R}}(t). \tag{2.32}$$

whose solution for the closed path C is given by integration over time and changing variable to find

$$\gamma_n = i \oint_C \langle n(\mathbf{R}(t))|\frac{\partial}{\partial \mathbf{R}}|n(\mathbf{R}(t))\rangle \cdot d\mathbf{R} \tag{2.33}$$

We should advertise from here that γ_n will not be easy to expressed as a explicit function of $\mathbf{R}$. We must note that there is no guarantee neither that the condition $\gamma_n(T) = \gamma_n(0)$ holds, in fact this function is in most of the cases not single valued. The quantity γ_n is known as the Berry phase or geometric phase. From the fact that $\partial_{\mathbf{R}}|n(\mathbf{R}(t)) = 0$ it is easy to check that $\langle n(\mathbf{R}(t))|\partial_{\mathbf{R}}|n(\mathbf{R}(t))\rangle$ is a real number, so the Berry phase is completely complex.

It is useful to define the quantity $\mathcal{A}_n = i\langle n(\mathbf{R}(t))|\partial_{\mathbf{R}}|n(\mathbf{R}(t))\rangle$ often called the Berry connection or the Berry vector potential. Making a gauge transformation on the states taken as

$$|n(\mathbf{R}(t))\rangle \to e^{\chi(\mathbf{R}(\mathbf{t}))}|n(\mathbf{R}(t))\rangle \tag{2.34}$$

then it is only a step away that

$$\mathcal{A}_n \to \mathcal{A}_n - \frac{\partial}{\partial \mathbf{R}}\chi(\mathbf{R}(t)) \tag{2.35}$$

consequently, the integral for γ_n will be change by

$$\gamma_n \to \gamma_n + [\chi(\mathbf{R}(0)) - \chi(\mathbf{R}(T))] \tag{2.36}$$

In 1924, V. Fock claimed that we can always find a transformation capable of cancel the geometric phase via this new summand [56], [57]. It was until 1984 that M. Berry challenged this statement to find that that is not the case of a closed path. Given the nature of the gauge transformation it is required that

$$\chi(\mathbf{R}(0)) = \chi(\mathbf{R}(0)) + 2\pi m \tag{2.37}$$

for some $m \in \mathbb{Z}$. This means that γ_n can only be changed by an integer multiple of 2π for any of the gauge transformations, making it impossible to cancel the complete phase.

Lastly, we can see that the Berry phase of a closed path defined as

$$\gamma_n = i \oint_C \mathcal{A}_n \cdot d\mathbf{R} \tag{2.38}$$

depends only on the shape of the path $\mathbf{R}$, not on the time it takes to complete it, so it can be dropped from now.

2.4.2 Berry curvature.

There is a quantity built from the Berry vector potential that is defined as the gauge-field tensor

$$\Omega^n_{\mu\nu}(\mathbf{R}) = \frac{\partial}{\partial R^\mu}\mathcal{A}^n_\nu(\mathbf{R}) - \frac{\partial}{\partial R^\nu}\mathcal{A}^n_\mu(\mathbf{R}) = i\left[\left\langle \frac{\partial n(\mathbf{R})}{\partial R^\mu}\middle|\frac{\partial n(\mathbf{R})}{\partial R^\nu}\right\rangle - \left\langle \frac{\partial n(\mathbf{R})}{\partial R^\nu}\middle|\frac{\partial n(\mathbf{R})}{\partial R^\mu}\right\rangle\right] \tag{2.39}$$

(by analogy with electrodynamics). The name of this field is the Berry curvature. If we consider a three dimensional parameter space then we are able to rearange the elements of the field to find

$$\gamma_n = \int_S \mathbf{\Omega}_n(\mathbf{R}) \cdot d\mathbf{S} \tag{2.40}$$

$$\mathbf{\Omega}_n(\mathbf{R}) = \boldsymbol{\nabla}_\mathbf{R} \times \mathcal{A}_n(\mathbf{R}) \tag{2.41}$$

where the Berry curvature is related to the vector $\mathbf{\Omega}$ by $\mathbf{\Omega}_n(\mathbf{R}) = \epsilon_{\mu\nu\xi}(\mathbf{\Omega}_n)_\xi$ with $\epsilon_{\mu\nu\epsilon}$ the Levi-Civita tensor. An intuitive interpretation of the Berry curvature in this space comes from eq. (2.41): is a sort of magnetic field in the parameter space. Its main feature is that is a gauge invariant and thus observable, also it is a local quantity that provides a local description of the geometry of the parameter space in contrast with the Berry phase that needs a closed path, otherwise it is not a gauge-invariant with a physical significance.

2.4.3 Berry phase in the Bloch bands and the optical lattice.

Considering a general Hamiltonian for which the Bloch theoreom applies, it would look like

$$\hat{H} = \frac{\hat{p}}{2m} + V(\mathbf{r}) \tag{2.42}$$

with the periodical condition $V(\mathbf{r}+\mathbf{a}) = V(\mathbf{r})$, so the eigenstates satisfy $\psi_{n\mathbf{q}}(\mathbf{r}+\mathbf{a}) = e^{i\mathbf{q}\cdot\mathbf{a}}\psi_{n\mathbf{q}}(\mathbf{r})$ for $\mathbf{q}$ the crystal momentum of the lattice, a member of the Birllouin Zone (BZ). After applying a unitary transformation to the Hamiltonian to find

$$H(\boldsymbol{q}) = e^{-i\boldsymbol{q}\cdot\boldsymbol{r}} H e^{i\boldsymbol{q}\cdot\boldsymbol{r}} + V(\boldsymbol{r}) \tag{2.43}$$

and the transformed eigenstates are $u_{n\mathbf{q}} = e^{-i\mathbf{q}\cdot\mathbf{r}}$ that now satisfy the condition $u_{n\mathbf{q}}(\mathbf{r}+\mathbf{a}) = u_{n\mathbf{q}}(\mathbf{r})$. This boundary condition implies that the eigenstates are in the same Hilbert space characterized by a parameter $\mathbf{q}$ confined to the BZ, defining the parameter space of the $H(\mathbf{q})$. Taking the states in the reciprocal space, we define the Berry phase as

$$\gamma_n = \oint_C \langle u_n(\boldsymbol{q})|i\frac{\partial}{\partial \boldsymbol{q}}|u_n(\boldsymbol{q})\rangle \cdot d\boldsymbol{q} \tag{2.44}$$

and the Berry curvature for a three dimensional case should be

$$\boldsymbol{\Omega}_n(\boldsymbol{q}) = \boldsymbol{\nabla}_{\boldsymbol{q}} \times \langle u_n(\boldsymbol{q})|i\frac{\partial}{\partial \boldsymbol{q}}|u_n(\boldsymbol{q})\rangle. \tag{2.45}$$

One way to produce a closed path in the momentum space of such a system is to impose a magnetic field that produces cyclic trajectories. This way, the Berry phase manifest in several effects [58–60].

When adding this new effect as in the case of artificial magnetic fields, we are imposing a linear variation in $\mathbf{q}$. In that case a closed path is realized when $\mathbf{q}$ sweeps the entire BZ since whenever a path reaches the edge of the BZ, the path automatically closes [61]. The explanation is as follows. Given that the topology of the BZ is that of a torus, there are two points $\mathbf{q}$ and $\mathbf{q}+\mathbf{G}$ (with $\mathbf{G}$ being the reciprocal lattice vector) that can be understood as equal. The Bloch boundary conditions let us conclude that the states $|\psi_n(\boldsymbol{q})\rangle$ and $|\psi_n(\boldsymbol{q}+\boldsymbol{G})\rangle$ may differ only by a phase and it can by selected in order to satisfy the torus geometrical condition $|\psi_n(\boldsymbol{q})\rangle = |\psi_n(\boldsymbol{q}+\boldsymbol{G})\rangle$, which has as a consequence that

$$u_{n\boldsymbol{q}}(\boldsymbol{r}) = e^{i\boldsymbol{G}\cdot\boldsymbol{r}} u_{n\boldsymbol{q}+\boldsymbol{G}}(\boldsymbol{r}). \tag{2.46}$$

The Berry phase that crosses the BZ is known as the Zak's phase:

$$\gamma_n = \int_{\mathrm{BZ}} \langle u_n(\boldsymbol{q})|i\frac{\partial}{\partial \boldsymbol{q}}|u_n(\boldsymbol{q})\rangle \cdot d\boldsymbol{q}. \tag{2.47}$$

It is remarkable that the Zak phase comes from the torus topology of the BZ. In the one dimensional case is the only closed path in the system, and as Zak showed, if the system has inversion symmetry then this phase is either 0 or π, but when it is broken then it may acquires any value [61].

2.4.4 Adiabatic current and the Quantized adiabatic particle transport.

Now consider a one-dimensional periodical Hamiltonian $H(t)$ subjected to a slowly varying time-dependent perturbation (such as a time dependent magnetic vecor potential). The period of the Hamiltonian is T. Since the translational symmetry of the crystal is preserved through all the evolution, the instantaneous basis has a Bloch hform $e^{iqx}|u_n(q,t)\rangle$ with a time dependance, and it will be useful to pick this basis.

The objective is to study the current induced by the variation in external portentials. After expanding the state $|\psi_n(q,t)\rangle$ in terms of the eigenbasis $u_n(q,t)$, evolve with time-dependent coefficients following [57], imposing the condition of parallel transport $\langle u_n(q,t)|\partial_t|u_n(q,t)\rangle$ and performing a first-order approximation, one is able to obtain

$$|\psi(t)\rangle = e^{-\frac{i}{\hbar}\int_0^t dt' \epsilon_n(t')} \left\{ |u_n(q,t)\rangle - \sum_{n'\neq n} |u_{n'}(q,t)\rangle \frac{\langle u_{n'}(q,t)|\partial/\partial t|u_{n'}(q,t)\rangle}{\epsilon_n - \epsilon_{n'}} \right\}. \quad (2.48)$$

where the ϵ are the corresponding energies. The velocity operator is defined by $\boldsymbol{v} \equiv \dot{\boldsymbol{r}} = (i/\hbar)[H, \boldsymbol{r}]$, then after the unitary transformation it becomes $\boldsymbol{v}(\boldsymbol{q}) = e^{-i\boldsymbol{q}\cdot\boldsymbol{r}}[\boldsymbol{r}, H]e^{i\boldsymbol{q}\cdot\boldsymbol{r}} = \partial H(\boldsymbol{q},\boldsymbol{t})/\partial(\hbar\boldsymbol{q})$. Taking its average value $\langle \boldsymbol{v}(\boldsymbol{q})\rangle \equiv v_n(\boldsymbol{q})$ leads to

$$v_n(q) = \frac{\partial \epsilon_n(q)}{\hbar \partial q} - i \sum_{n'\neq n} \left\{ \frac{\langle u_n(q,t)|\partial H/\partial q|u_{n'}(q,t)\rangle\langle u_n(q,t)|\partial/\partial t|u_{n'}(q,t)\rangle}{\epsilon_n - \epsilon_{n'}} - \text{c.c.} \right\}, \quad (2.49)$$

where c. c. means complex conjugate. Now, if we calculate for $\langle u_n|\partial H/\partial q u_{n'}\rangle = (\epsilon_n - \epsilon_{n'})\langle \partial u_n/\partial t|u_{n'}\rangle$, we can instert this result in 2.49 and use the identity $\sum_n |u_n\rangle\langle u_n| = 1$ to obtain

$$v_n(q) = \frac{\epsilon_n(q)}{\hbar \partial q} - i \left[\left\langle \frac{\partial u_n}{\partial q} \middle| \frac{\partial u_n}{\partial t} \right\rangle - \left\langle \frac{\partial u_n}{\partial t} \middle| \frac{\partial u_n}{\partial q} \right\rangle \right]. \quad (2.50)$$

Then we can identify the second term as the Berry curvature $\Omega^n_{\nu\mu}$ for a parameter space (q,t). That allow us to write

$$v_n(q) = \frac{\partial \epsilon_n(q)}{\hbar \partial q} - \Omega^n_{qt}. \quad (2.51)$$

Finally, the induced adiabatic current is obtained by integration of the velocity over all the Brillouin Zone. The first term will vanish since $\epsilon_n(q)$ is preiodical in the closed path, the only term that contribute is the Berry curvature, leaving

$$j = -\sum_n \int_{\text{BZ}} \frac{dq}{2\pi} \Omega^n_{qt} \quad (2.52)$$

which is the adiabatical current induced by a time-dependent perturbation in a band, that is equal, thus, to the q integral of the Berry curvature [62].

2.4.5 Anomalous velocity.

Consider the same problem as the Harper model but instead of a magnetic field, there is a weak electric field $\boldsymbol{E}$ that we include as part of the Peierls substitution including a time dependence in the vector potential. In the $\boldsymbol{q}$-space that Hamiltonian is

$$H(\boldsymbol{q},t) = H\left(\boldsymbol{q} + \frac{e}{\hbar}\boldsymbol{A}(t)\right) \tag{2.53}$$

and we introduce the gauge-invariant crystal momentum $\boldsymbol{k} = \boldsymbol{q} + \frac{e}{\hbar}\boldsymbol{A}(t)$. Since $\boldsymbol{A}(t)$ preserves the translational symmetry, $\boldsymbol{q}$ is a constant of motion. It follows that

$$\dot{\boldsymbol{k}} = -\frac{e}{\hbar}\boldsymbol{E}. \tag{2.54}$$

Starting from the generalization of eq. 2.51 up to three dimensions, and the fact that under this new variable introduction then $\partial/\partial q_\alpha = \partial/\partial k_\alpha$ and $\partial/\partial t = -(e/\hbar)E_\alpha \partial/\partial k_\alpha$, we arrive to

$$\boldsymbol{v}_n(\boldsymbol{k}) = \frac{\partial \epsilon_n(\boldsymbol{k})}{\hbar \partial \boldsymbol{k}} - \frac{e}{\hbar}\boldsymbol{E} \times \boldsymbol{\Omega}_n(\boldsymbol{k}), \tag{2.55}$$

where $\boldsymbol{\Omega}_n(\boldsymbol{k}) = i\langle \boldsymbol{\nabla}_{\boldsymbol{k}} u_n(\boldsymbol{k})| \times |\boldsymbol{\nabla}_{\boldsymbol{k}} u_n(\boldsymbol{k})\rangle$ is the Berry curvature of the nth band.

In equation 2.55, the first term refers to the already known dispersion relation that do no includes the dynamics imprinted on the electrons by the action of the electric field. The second term is accounts for that effects and it is interesting that they are a manifestation of the Berry curvature. This term is the reason why eq. 2.55 is known as the anomalous velocity. The new velocity is transverse to the electric field, which will give rise to a Hall current.

2.4.6 The quantum Hall effect.

As it is well known, the classical Hall effect in an almost two dimensional (xy) rectangular conductor occurs after the appliance of a uniform magnetic field $B\mathbf{z}$, when a current I flows through it. The Lorentz force initially discriminates between the two type of charge carriers: holes and ions, leading to the accumulation of each type of carrier in opposite sides of the conductor. It creates two opposite charge plates that establishes a new potential between them (V_H). The arising electric field increases until both opposite forces (electric and magnetic) acting on the carriers cancel. The resulting expresion for V_H in the equilibrium is

$$V_H = \frac{IB}{ned} \tag{2.56}$$

where n is the charge carriers density and d is the thickness of the conductor. The Hall resistance is given by

$$R_{xy} = \frac{V_H}{I}, \tag{2.57}$$

and thus the Hall conductance is

$$\sigma_{xy} = \frac{Ne}{B}. \tag{2.58}$$

where N is the carrier concentration.

In contrast, the quantum Hall effect first observed in 1980 by Klitzing et. al. [63], was the name given to the fact that the Hall resistance (and thus the Hall conductance) is exactly quantized in units of e^2/h when the magnetic field is in the range in the tens of Teslas. A new explanation of this phenomenon requires the Landau quantization of motion [63]. The number of states N_L within each Landau level is

$$N_L = \frac{eB}{h}. \tag{2.59}$$

When the Landau levels are fully occupied $N = N_L\nu$ with $\nu \in \mathbb{Z}$. Combining equations 2.58 and 2.59 yields

$$\sigma_{xy} = \frac{e^2}{h}\nu \tag{2.60}$$

Now, recovering the developed formalism of the Berry curvature, we may take equations 2.52 and 2.55 to find that the Hall conductance in a 2D lattice in the momentum space (k_x, k_y) can be written as

$$\sigma_{xy} = \frac{e^2}{\hbar}\int_{BZ}\frac{d^2k}{(2\pi)^2}\Omega_{k_xk_y}. \tag{2.61}$$

The integral is equal to an integer times 2π [57], and thus, the quantization of the Hall conductance can be explained through this formalism.

2.5 Streda's Formula.

The quantization of the Hall conductance can also be approached by the study of the electron transport in the same Harper Model directly in terms of the general conductance tensor $\boldsymbol{\sigma}$ in the general Ohm law $\mathbf{I} = \boldsymbol{\sigma}\boldsymbol{E}$ that links linearly the electric field $\mathbf{E}$ and the electric current $\mathbf{I}$ [64,65] and linking it to the density of states in the spectrum by the formula:

$$\sigma_H = \frac{e^2}{\hbar}\frac{\partial N_\psi(E)}{\partial\psi} \tag{2.62}$$

where σ_H is the Hall conductance (σ_{xy}) and $N_\psi(E)$ is defined as the numer of states whose energy is below certain E in the spectrum. This formula is known as the Streda's formula and it operates in the spectrum (ϵ, α), as the Butterfly. From there, we can see that the number $N_\psi(E)$ should be of the form $z \in \mathbb{Z}$ since q is the total number of accesible states for that magnetic field. To see this we write

$$\sigma_H = \frac{e^2}{\hbar}\frac{N_{\psi_2}(E) - N_{\psi_1}(E)}{\psi_2 - \psi_1} = \frac{z_2 - z_1}{q}\frac{q}{1}\frac{e^2}{\hbar} = (z_2 - z_1)\frac{e^2}{\hbar} \tag{2.63}$$

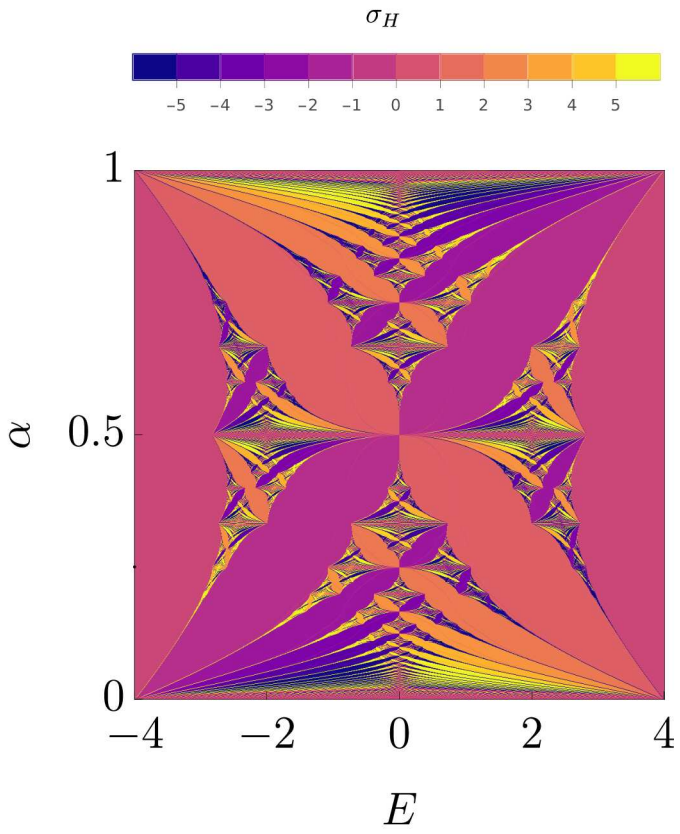

Figure (2.3) The Butterfly topological numbers calculated following Streda's formula. Near $E = \pm 2$ the extremer values of the field display the so called Landau levels [66]. This figure was reproduced by the author and agrees with results in [67].

which means that the Hall conductance in a region of the Butterfly is equal difference between the number of states with energy below E for the value ψ_1 of the magnetic flux and the next ψ_2, which is an integer.

In the Hofstadter Model we can find the Hall conductances in the energy spectrum applying this formula. Computationally, we can think of a discrete set of energies E_i and for each discrete value of the field ψ_j we count the number of states whose energies are lower than that energy to finally apply 2.63. In Figure 2.3 we can find the values of the Hall conductances for different sectors of the Butterfly, which agrees with [68].

Chapter 3: Strong interactions, Order, and Topological Properties of the Cavity-Harper-Hofstadter-Mott model.

In this chapter we introduce a new interaction within the system that consist of an environment created by a pumping haze of photons to the system which will be now enclosed by two parallel high reflectance mirrors that impose new confinement conditions on the captured light inside it. The new cavity maintains one or more photon modes that couple to the geometry of the lattice following an interference pattern created by the pump laser and the haze captured by the mirrors. We will review some of the interesting novel phenomena that arises when a system described by the Bose-Hubbard Hamiltonian and photon mediated interactions, this leads to self-organization and the emergence of Density Wave phase [80].

We also discuss the effect on the system when a measurment based on light detection is performed. In this situation, the system can be considered as on with photon dissipation and, thus, as an open quantum system. The problem is addressed using the quantum trajectories method and we explore the changes in the pre existing MI and SF, and DCM phases after performing a γ weighted measurement, paying attention to some other effects as the long-range tunnelling and Zeno effect [78].

3.1 High-Q Cavity dynamics.

Inside the cavity, the photons are absorbed and emitted by the atoms and in many cases they promote kinetic and on-site interactions and incorporate them in the Hamiltonian is quite complicated [80]. Following Caballero-Benitez, et al., we may focus on the effective light-matter interaction where the quantum fluctuations can be neglected in the same manner that in mean-field theory regarding the bond order. We consider a single pump and cavity beam making an arbitray angle. The cavity light-induced matter interactions is usually encoded in the effective Hamiltonian [80]

$$\hat{H}_{\text{eff}} = \hat{H}^{BH} + \frac{g_{\text{eff}}}{N_s}[J_B^2\hat{B}_-^2 + J_D^2\hat{D}_-^2 + J_D J_B(\hat{B}_-\hat{D}_- + \hat{D}_-\hat{B}_-)] \tag{3.1}$$

where $\hat{H}_{\text{BH}}$ is the Bose-Hubbard Hamiltonian and we have

$$\hat{B}_- = \sum_{\langle i,j\rangle \in \text{OL}} (J_{ij}\hat{b}_i^\dagger \hat{b}_j + h.c.) \tag{3.2}$$

$$\hat{D}_- = \sum_{i \in \text{OL}} J_{ii}\hat{n}_i \tag{3.3}$$

where the J_{ij} factors are light structure parameters attached to the bonds $\hat{B}$ and densities $\hat{D}$. In the particular case of a 90 degree angle between the two beams, they acquire the values $J_{ii} = (-1)^{\|\vec{r}_i\|_1}$ both, where $\vec{r}_i = (m_i, n_i)$ are the integer coordinates of the site i and $\|\vec{r}_i\|_1 = m_i + n_i$ is the norm-1. The coupling parameters for bond J_B and densities J_D. From here we will focus only on the $J_B = 0$, $J_D = 1$ case corresponding to a lattice with deep enough wells at its sites, then

$$\hat{H}_{\text{eff}} = \hat{H}_{\text{BH}} + \frac{g_{\text{eff}}}{N_s^2}\hat{D}_-^2 \tag{3.4}$$

To see the new dynamics offered by the cavity term it is useful to explore the ground state in the limit where the Hamiltonian is composed only by it. For a negative g_{eff}, the Hamiltonian is diagonal in the number basis, so it is easy to see that the states with a maximum ocupation in odd sites only (or the symmetric case, the even sites) minimze the energy of the state, so we expect a linear combination of those states to mainly participate in the ground state. Spacially this means a checkerboard density distribution, a self-organized phase known as the Density Wave (DW) phase. Naturally, when the tunneling and on-site interactions are turned up, a competition starts between all the three dynamics and one may ask for a transition point. In figure 3.1 the diagram for the presence of the DW in the system through the parameter

$$\mathcal{O}_{\text{MW}}^2 = \frac{\langle \hat{D}_-^2 \rangle}{M^2}, \tag{3.5}$$

and a simple panel for the density distibution of the system. The diagram shows the presence of DW phase near the MI regime for g_{eff} below the critical value $g_{\text{eff}} = -0.5U$, which start decreasing when the tunneling is strong in the system. This competence takes place in fact near the Mott lobes zones we explored in previous chapters. The tunneling term is still strong for t/U above the critical value t_c/U_c. At the same time, the panels shows the corresponding density distribution, the MI and SF phases have a uniform distribution but it is not the defining feature. When the DW take place, the bosons in the lattice undergo a self organization phase in the form of a checkerboard. The results coincide with reference [80].

3.2 The Cavity-Harper-Hofstadter-Mott Model. (New Results).

After the previous introduction of the BHH model, its extension to the quantum simulation of the Harper Model through added Berry phases, and the rich physics provided

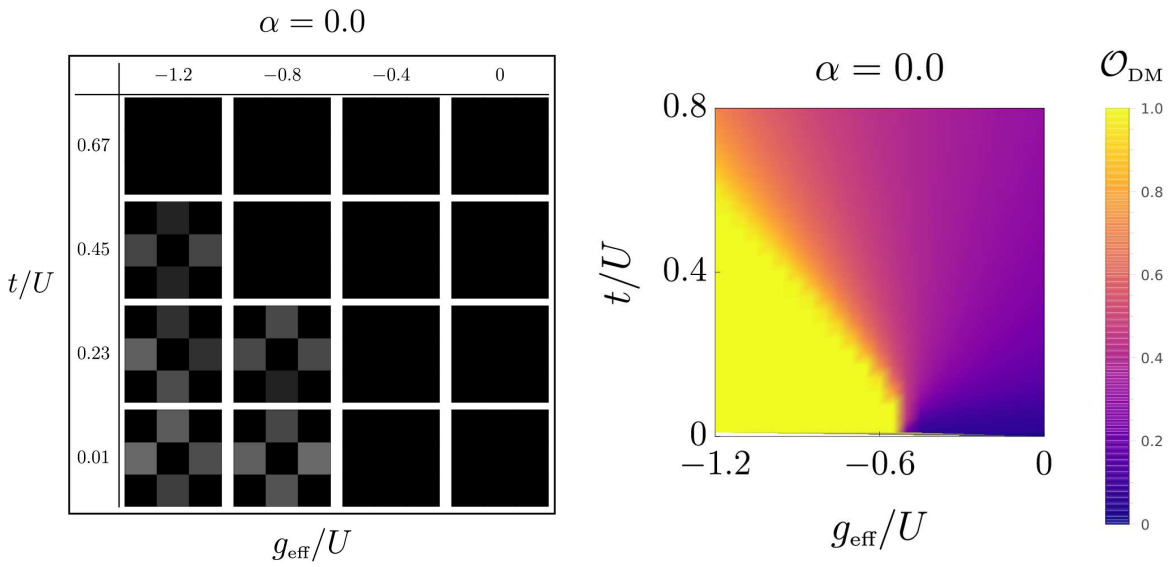

Figure (3.1) Left figure. A panel arrange with the density profiles of a system with 10 particles in a 3x3 lattice. The left down zone corresonding to the SF-MI are homogeneous while the rest of the panels have the checkerboard distribution. Right figure is the diagram that shows the presence of the DW phase in the system in the $(g_{\text{eff}}/U, t_0/U)$ dominion.

by cavity-mediated interaction, we are ready to put all these elements together. The physical situation that we have in mind now consists of ultracold neutral atoms in the presence of an artificial magnetic field, loaded in a periodical 2D optical lattice inside a high-Q cavity (the QOL presented in the previous chapter). As we assumed in the past, the wells of the QOL are considered to be too deep that the only interaction mediated by the light is the on-site interaction. The final Hamiltonian is given by

$$\hat{H} = -t \sum_{\langle i,j \rangle} e^{\theta_{ij}} \hat{b}_i^\dagger \hat{b}_j + \frac{U}{2} \sum_i \hat{n}_i \left(\hat{n}_i - 1\right) + \frac{g_{\text{eff}}}{M} \hat{D}_-^2 \tag{3.6}$$

$$\theta_{ij} = \begin{cases} \pm 2\pi \mathbf{i} \alpha n & \text{for } i \text{ and } j \text{ lying in the row } n \\ 0 & \text{otherwise} \end{cases} \tag{3.7}$$

$$\hat{D}_- = \sum_i (-1)^{\|\mathbf{r}_i\|_1} \hat{n}_i \tag{3.8}$$

where we have the three competing terms of kinetic energy with translation symmetry breaking Berry phase, the on-site interaction, and the cavity mediated on-site interaction. The $\pm$ sign in the phase corresponds to the two opposite directions of the hopping. This is our new Cavity-Harper-Hofstadter-Mott Hamiltonian. Mixing these elements and the artificial gauge field leads to changes in the pre-existing self-organized phase diagram, directly related to the action of magnetic effects on the kinetical term and will be discussed in the following sections.

On the other hand, we are also searching for changes in the self-organized phase originated by the magnetic field for the system filled with neutral bosons, and later we simulate the fermionic case through hard-core bosons limit to check the robustness

of the topological number, the Hall current when the system is altered by the cavity mediated on-site interactions.

We find it useful to first introduce the computational argument of the previously revised hard-core bosons limit. Even when this limit is not always the case in the following calculations, the visualization of this limit is itself an argument supporting that for some values of U/t we may cut-off the basis and leave the more energetic basis vectors out of the diagonalization, independently of the presence of an artificial magnetic field or the cavity.

3.3 Hard-core bosons limit.

3.3.1 The fidelity.

The fidelity $F_G(\alpha, g_{\text{eff}}, U, t)$ as defined in Chapter 1, is roughly speaking a measurement of how big is the participation of an arbitrary subset of the basis in the ground state. Particularly, we proposed the *ideal basis* mainly conformed by states with minimal occupation (fermionic number states for a density $n < 1$) in each of the sites, and in figure 1.5 have been shown that the ground state structure is mostly composed by these states. Now we explore the fidelity for several values of the parameters α, g_{eff} for the fidelity when the magnetic field and the cavity are present; the graphics are displayed in figure 3.2.

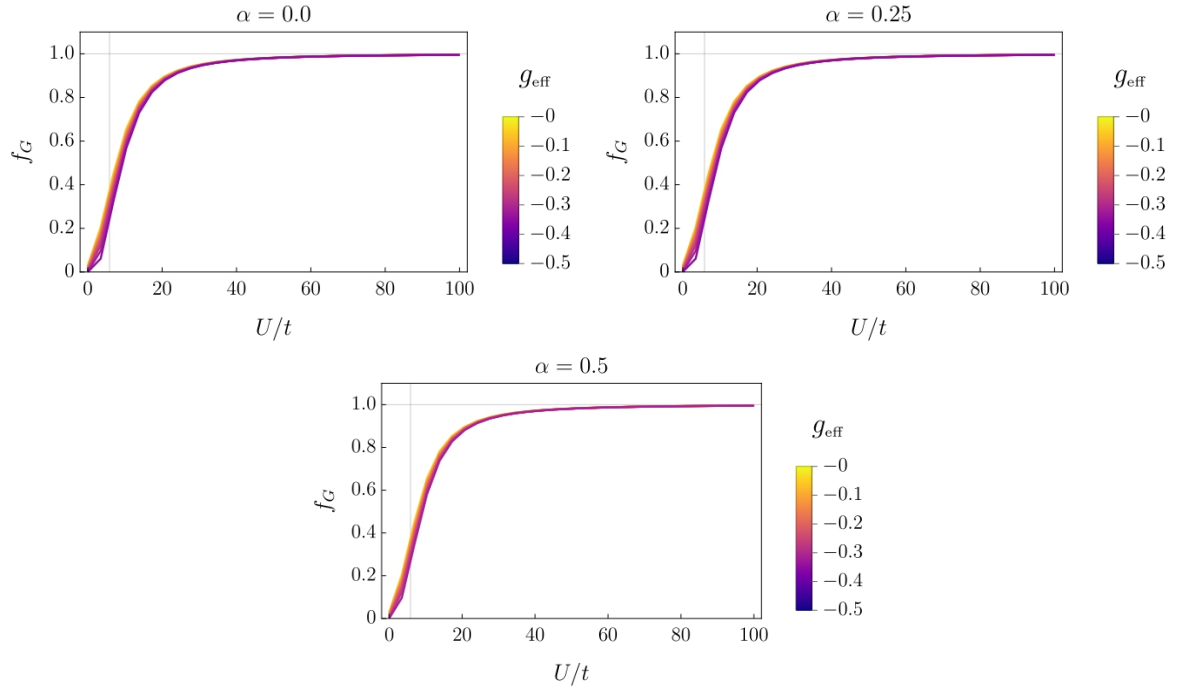

Figure (3.2) Fidelity $F_G(\alpha, g_{\text{eff}}, U, t)$ for different magnetic field and cavity parameters. It is a comparison between a 2x3 lattice filled with 7 bosons, and a single fermion basis. Gray line is the limit constant value 1.

The first thing we note is the fidelity goes to 1 for $U/t \to \infty$ including the cases where the artificial magnetic field and the cavity effects are present, finding the last value plotted in the graphics above 0.994 for all the cases (but still growing), as expected,

which allows us to perform a cut-off on the basis leaving out the most energetic states when studying the ground state, for values of $U/t \gtrsim 10$. Moreover, the limit $\lim_{U/t\to\infty}$ in all the cases makes the particle behave as hard-core bosons in the ideal basis, opening the door to explore fermionic dynamics through hard-core bosons, since the Hamiltonian will carry essentially the same physics as we will see in the next chapter from a more mathematical point of view. It is important to remark from now that this will be true as long as we work with nearest neighbor hopping, otherwise, the Jordan-Wigner transformation for the commutation rules would not be so simple [73], [74].

In the case with zero magnetic field (up and left in Fig. (3.2)), the fidelity starts growing since $U/t > 0$, which gives us an idea of how strong is the restriction that interactions impose on the ground state structure. Note that there is a regime where this restriction loses strength and goes to 0 for a present magnetic field and cavity effects. It is not the cavity on-site interaction or the magnetic field separately that causes this restriction to lose strength and delays the increase of the fidelity to $U/t \approx U_c/t_c$, but the combination of both effects. For $\alpha = 0.25$, 0.5 when the cavity field is more intense $g_{\text{eff}} = -0.5$ the *ideal basis* still has null participation in the ground state meaning the superfluid phase we expect from the BHH alone seems favored under these conditions. Physically, the artificial magnetic field establishes a preferred direction of movement given by the artificial Lorenz force, and hence, kinetical dynamics is still intense but density distribution changed as explained in Chapter 2, and the basic states required to describe it are not those of the *ideal basis*. At the same time, operator $\hat{D}^2_-$ tries to constrain the particles in even or odd sites only, and such configurations are not taken into account for this fidelity.

3.4 Stabilization of the Self-organized phase. (New Results.)

The self-organized phase produced by the density coupling through cavity-mediated interactions acquires a checkerboard distribution over the 2D lattice. DW order also breaks this symmetry and signals a new $\mathbb{Z}_2$ symmetry between even and odd states that corresponds to phases $\pm$ in the operator $\hat{D}_-$ competing too with MI phases creating this peculiar density distribution. A ground state with this density wave order deserves special attention after the incorporation of the magnetic field since it produces changes in the structure of the ground state by the translational symmetry breaking of the lattice as we saw in the previous subsection. To measure the DM order we use the structure factor

$$\mathcal{O}^2_{\text{MW}} = \frac{\langle \hat{D}^2_- \rangle}{M^2}. \tag{3.9}$$

as stated in [80], [81], to create the DW order parameter. We calculate using exact diagonalization the order $\mathcal{O}^2_{\text{MW}}$ for a domain $(t/U, g_{\text{eff}}/U)$ and for different intensities of the magnetic field finding the diagrams in Fig. 3.3. The first diagram shows the already known [80] and experimentally verified self-organization phase [76], in colors red and yellow. Increasing the magnetic field parameter to $\alpha = 0.25$, where the kinetic term is a pure complex operator we find there is an expansion of the region where the self-organization occurs, confirming a stabilization of this pre-existing phase. For

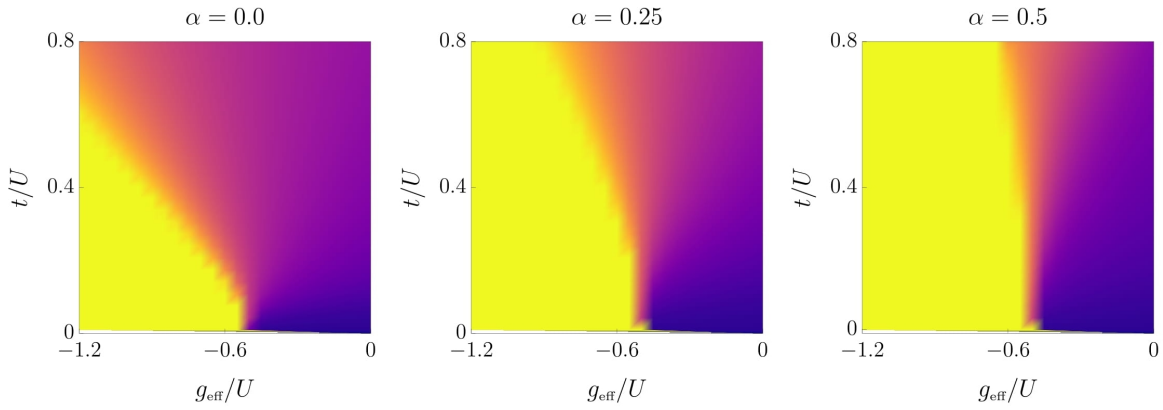

Figure (3.3) Diagrams of the DW order $\mathcal{O}^2_{\text{MW}}$ for different intensities of the magnetic field in α and competing parameters t, U and g_{eff}. The lattice size is 3x3 for 9 bosons and a cut-off of the basis for occupancy numbers above $R = 6$.

$\alpha = 0.5$ we find the maximum expression of the stabilization, where the system takes advantage of the increasing kinetical dynamics prompted by the gauge field.

3.5 Particle-Hole symmetry in the Hard-core bosons limit.

In this section, we will review some calculations to mathematically support the idea presented in the construction of the fidelity. Along the following two sections we will be working with the complete model in eq. (3.6) but assuming the limit of the hard-core bosons, something that may be expressed as

$$\hat{H}_{\text{CHHM}} = -t \sum_{\langle i,j \rangle} e^{\theta_{ij}} \hat{b}_i^\dagger \hat{b}_j + \lim_{U \to \infty} \frac{U}{2} \sum_i \hat{n}_i \left(\hat{n}_i - 1 \right) + \frac{g_{\text{eff}}}{M^2} \hat{D}_-^2 \tag{3.10}$$

where the two terms correspond to the so-called Harper-Hofstadter-Mott model (HHMm) [82] and the C in label CHHM stands for the modes adding the high-Q cavity term.

As we know, the ground state $|G\rangle$ is composed mainly of states with n particles per site except one with $n+1$ particles, as predicted by the previously fidelity calculation. In this regime we can restrict our analysis to (and define) an effective basis $(+)_n$: $\{|n+1, n, \ldots, n\rangle \equiv |1\rangle, \ldots, |n, n, \ldots, n+1\rangle \equiv |M\rangle\}$. We denote the matrix representation of the Hamiltonian in this basis as $H_n^{n+1} = -tK_n^{+1} + 0.5UI_n^{+1} + g_{\text{eff}} D_n^{+1}$ for the matrix representations of the Kinetic, Interaction and Cavity operators respectively, which is a special case of the interpretation of " $+1$ particles in a homogeneous filling of n particles per site". The only non-vanishing terms belonging to the kinetic term are those arising from applying that operator to states with $n+1$ particles in sites $(i+1, j)$ or $(i, j+1)$:

$$e^{-i\bar{\alpha}_j} \hat{b}_{(i,j)}^\dagger \hat{b}_{(i+1,j)} | \ldots, n, n+1, \ldots \rangle_{=b} = e^{-i\bar{\alpha}_j} (n+1) | \ldots, n+1, n, \ldots \rangle_{=a} \tag{3.11}$$

$$\hat{b}_{(i,j)}^\dagger \hat{b}_{(i,j+1)} | \ldots, n, \ldots, n+1, \ldots \rangle_{=b} = (n+1) | \ldots, n+1, \ldots, n, \ldots \rangle_{=c} \tag{3.12}$$

Comparing these matrix elements with those of the Hamiltonian with $n = 0$ (single fermion) then we will find that

$$K_n^{+1} = (n+1)K_0^1 \tag{3.13}$$

Now, consider a similar effective basis consisting of states $(-)_n$: $\{|n-1, n, \ldots, n\rangle, \ldots, |n, n \ldots, n-1\rangle\}$ with same labels. This corresponds to a system with an extra hole module M instead of an extra fermion. By analogy, the matrx operators for this situation will be denoted as $H_n^{-1} = -tK_n^{-1} + 0.5UI_n^{-1} + g_{\text{eff}}D_n^{-1}$, interpreting the notation as "an extra hole (-1) in a homogenous filling of n". The analogous non-vanishing situations for the same pair of states (in the h.c. part of the Hamiltonian) are:

$$e^{i\bar{\alpha}_j}\hat{b}^\dagger_{(i+1,j)}\hat{b}_{(i,j)}|\ldots, n, n-1, \ldots\rangle_{=b} = e^{i\bar{\alpha}_j}(n)|\ldots, n-1, n, \ldots\rangle_{=a} \tag{3.14}$$

$$\hat{b}^\dagger_{(i,j+1)}\hat{b}_{(i,j)}|\ldots, n, \ldots, n-1, \ldots\rangle_{=b} = (n)|\ldots, n-1, \ldots, n, \ldots\rangle_{=c}. \tag{3.15}$$

Again, if we compare with the case $n = 1$, which represents a hole in a system of nM particles in M sites ($nM - 1$ particles in M sites physically) then we will find that

$$K_n^{-1} = nK_1^0 \tag{3.16}$$

and it is easy to see from the equations (9) and (10) taking $n = 0$ and equation (12) and (13) taking $n = 1$ that

$$K_0^1 = \left(K_1^0\right)^* \tag{3.17}$$

From relations (3.13), (3.16) and (3.17) we can derive that

$$K_n^{-1} = n\left(K_0^1\right)^* \tag{3.18}$$

$$K_n^{+1} = \left(K_n^{-1}\right)^* \tag{3.19}$$

$$K_n^{+1} = \frac{n+1}{n}K_n^{-1} \tag{3.20}$$

Recall that for every Hermitian matrix its eigenvalues and those of its conjugate are the same. Expression (3.20) may be understood as a special particle-hole symmetry that makes easier all our calculations and also it offers more accessible experimental conditions.

The interaction term with this two basis only adds a the same contribution to all diagonal elements which is a constant $U_{n(\pm)} = (1/2)(M-1)(n)(n-1) + c_\pm$ with $c_{n\pm} = (n+1)n$ or $(n-1)(n-2)$ for basis $(+)$ and $(-)$ respectively. In order to find the eigenvalues of total Hamiltonian without interactions ($U = 0$) we must find the roots of $\text{Det}[H_{kin} - \lambda\text{Id}] = \text{Pol}(\lambda)$ polinomial. To solve the case with interactions ($U > 0$) we determine the roots of $\text{Det}[H_{kin} + U_{n(\pm)}\text{Id} - \lambda\text{Id}] = \text{Det}[H_{kin} - \bar{\lambda}\text{Id}] = \text{Pol}(\bar{\lambda})$

which is the same polinomial, thus the eigenvalues $\lambda_m = \bar{\lambda}_m + U_{n(\pm)}$ will be shifted by the constant $U_{n(\pm)}$.

For the cavity term we will find that

$$D_n^{+1} = \mathbb{I} \begin{cases} (n+1)^2 & \text{for odd M} \\ 1 & \text{for even M} \end{cases} \tag{3.21}$$

$$D_{n+1}^{-1} = \mathbb{I} \begin{cases} n^2 & \text{for odd M} \\ 1 & \text{for even M} \end{cases} \tag{3.22}$$

where $\mathbb{I}$ is the identity matrix. Again, the spectrum will be shifted by a constant. All the expressions above have been verified numerically.

3.5.1 Several hard-core bosons in the lattice.

Extending the analysis to two non overlapping bosons, we may find for the Kinetical term that writing eqs. 3.11, 3.12, 3.14, and 3.15 the same effect from the one particle case occur to each of the matrix elements, which causes again a particle symmetry between a system with 2 particles and $N-2$ particles. In fact, it is easy to see from there that P particles produce the complex conjugate Hamiltonian of the one produced by $N-P$ particles in the lattice, which comletes the analogue fermionic particle-hole symmetry over all the possible fillings of the lattice. The Interaction term remains unchanged for any of the basis states too.

For the Cavity term the situation is not the same. When there are 2 or more extra hard-core bosons in the system, the cavity-mediated on-site interactions has various possible eigenvalues and many configuration can lead to one of them. For example, when $M > 4$, any configuration of a 2 particles state after been applyed $\hat{D}_-$, may throw only -2,0 or 2 as a possible eigenvalue for any and an extra term equal $\pm n$ or 0 depending on wether the number of sites is even, or odd with an extra negative or positive number operator, as in eq. (3.22). The case for 3 particles and $M > 6$, has as possible eigenvalues -3, -1, 1, and 3. Using this, we find that the general eigenvalue for $\hat{D}_-^2$ is

$$D_n^{+P} = \mathbb{I} \begin{cases} (n+E_P)^2 & \text{for odd M} \\ E_P^2 & \text{for even M} \end{cases} \tag{3.23}$$

$$D_{n+1}^{-P} = \mathbb{I} \begin{cases} (n+E_P)^2 & \text{for odd M} \\ E_P^2 & \text{for even M} \end{cases} \tag{3.24}$$

where the values that E_P can take are

$$E_P = \begin{cases} -P, -P+2, \cdots, P-2, P & \text{for } 0 \leq P \leq \left\lceil \frac{M}{2} \right\rceil \\ E_{M-P} & \text{for } M \geq P > \left\lceil \frac{M}{2} \right\rceil . \end{cases} \tag{3.25}$$

which tell us that for a large g_{eff} the spectrum reduces to the set of eigenvalues $\{P^2, (P-2)^2, \cdots, 1(0)\}$ (the last value depends on whether P is even or odd). Note that for a fixed g_{eff} the biggest contribution of this term is for the half filling in the extra hard-core bosons or extra holes. The fact that the contribution of the cavity is not a diagonal term and produces a change in the spectrum provides a glue to look for changes (or robustness) in the topological numbers of the system, that is the subject of the next section.

3.6 Density distribution of the bosonic case.

Searching for more physical insight of the dynamics of the system, we noted that the distribution of the bosons is sensible to the presence of the magnetic field as well as to the cavity induced interactions. Also, it is notable that the particle-hole symmetry produce a symmetric distribution effect as well. We first consider the system of 9 particles in 9 sites (3x3 lattice) inside the cavity and in the presence of the magnetic field.

Figure 3.4 shows three values for the magnetic field producing interesting distributions. In the absence of magnetic field (subfigure 3.4.a)) the transition between the phases MI/SF to the self-organised phase take place as expected in the phase diagram of Fig. 3.3, we can see the checkerboard distribution in the ordered phase region. Increasing the intensity of the magnetic field but without the cavity (final column in subfigure 3.4.a)), the particles start feeling its effects and tend to localize in the "upper" part of the lattice scheme. To explain this, first let's notice that there is a region in the lattice where the magnetic flux that can be achieved per plaquette is $\pm\alpha$ depending on whether the particle is undergoing a clockwise or anticlockwise trajectory, respectively. The other region is the one composed by the plaquettes between the first row and the last one (only possible for pbc). Since they assign the phases 0 and $\mp\alpha(n-1)$ for $n-1$ rows (clockwise and anticlockwise respectively). The change in the sign of the magnetic flux creates a magnetic barrier in the periodic boundary conditions between the first and the last row for the same type of circulation. On the other hand, if the particle is moving in such a trajectory picking up a positive (negative) magnetic flux then there will be a Lorentz force directed to the left (right) of the motion of the bosons, directing all the particles upward accumulating right before the magnetic barrier. When we take into account the cavity interactions then we will see a competition between the corresponding two distribution and the presence of the checkerboard in the stabilized zone.

When $\alpha = 0.5$ the maximum effect of the magnetic field appears and the striped phase appears. Mathematically, the complex phases in the kinetic part for this case are 1 and -1 for even and odd rows, which implies a higher energy cost for the states whose particles are moving in the even rows, leading to the appearance of these density strips [75]. We can see how the presence of the self-organised phase is broader as expected too.

In figures 3.5, 3.6, and 3.7 we compare the fillings 8/9 and 10/9, where we do not have an MI phase, as argued in past sections. In general, we can find for the filling 10/9 the same dynamics as in the case 9/9 but is notable that in these figures we can observe the particle-hole symmetry, expected for low values of t/U. The panels in Fig 3.6 show

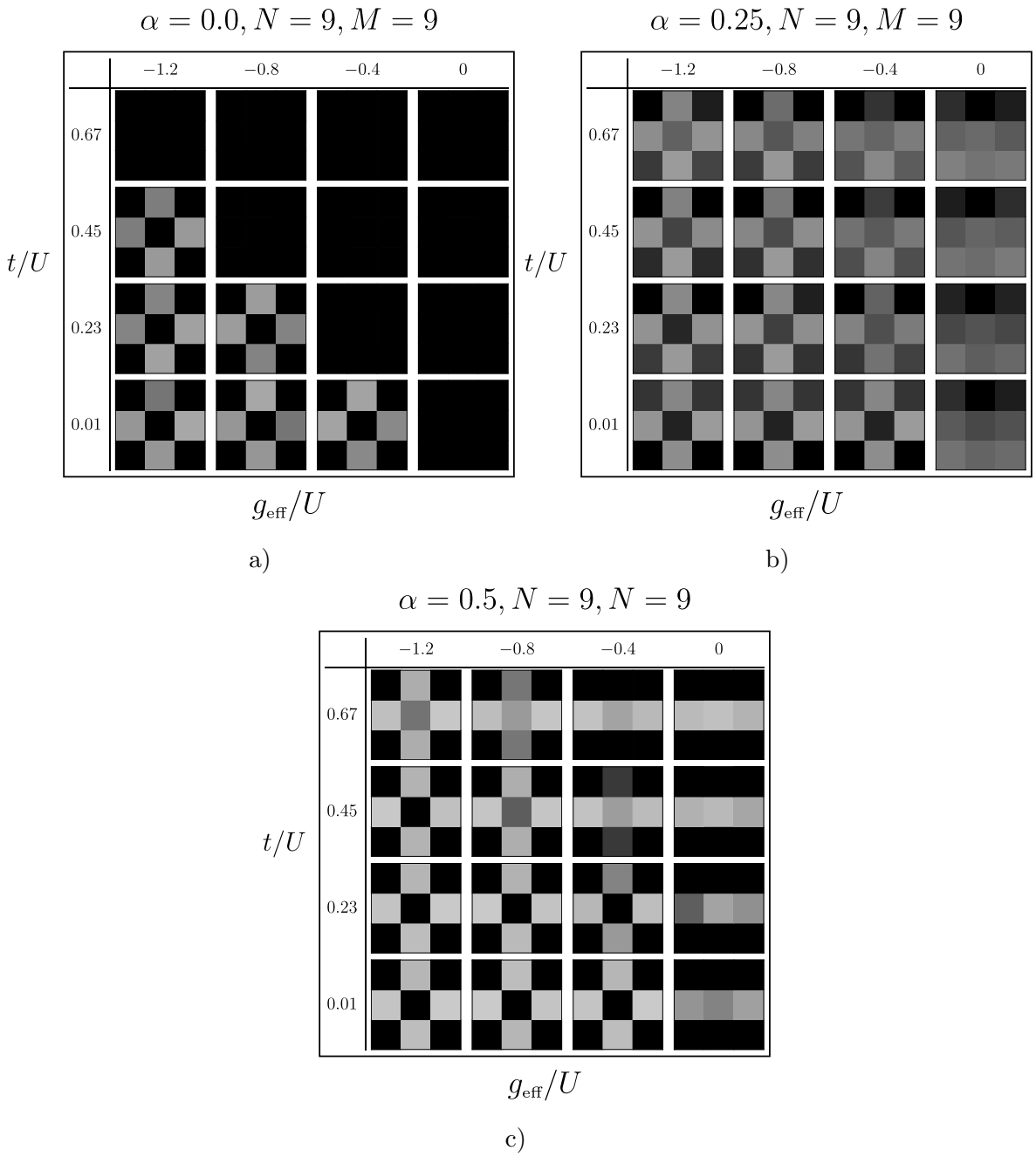

Figure (3.4) Panels for the density distribution of the system inside the cavity without the Magnetic Field ($\alpha = 0.0$) acting on it. On the left, we find the case for 8 particles in 9 sites, and on the right, the case for 10 particles in 9 sites.

how the particles in the 10/9 case feel the Lorentz force toward the same direction as the case 9/9 and for the case 8/9 we have that the particles accumulate in the "lower" part of the lattice. Since for this case we have a hole in the lattice, we can consider it as a moving particle that picks up a phase with sign opposite to the 9/9 and 10/9, that is the holes feel the Lorentz force as if they had "opposite charge" (remember that they are electrically neutral). Note that the symmetry is lost when the values of t/U start growing. In that limit, we expected this since the particles will not longer be considered hard-core bosons.

The situations in Fig. 3.7 let us confirm a symmetry even in the Striped phase that

is originated by the same change of sign in the phase that holes acquire while moving within the lattice. In this case, the phases run as -1 and 1 for even and odd rows, making more probable the states with more particles in the odd rows. Again this symmetry is lost out of the hard-core bosons limit.

All of the cases have the same effects as in 9/9 when the cavity-induced interactions become larger, but now there are sections near the boundary of the self-organised phase where the orders compete.

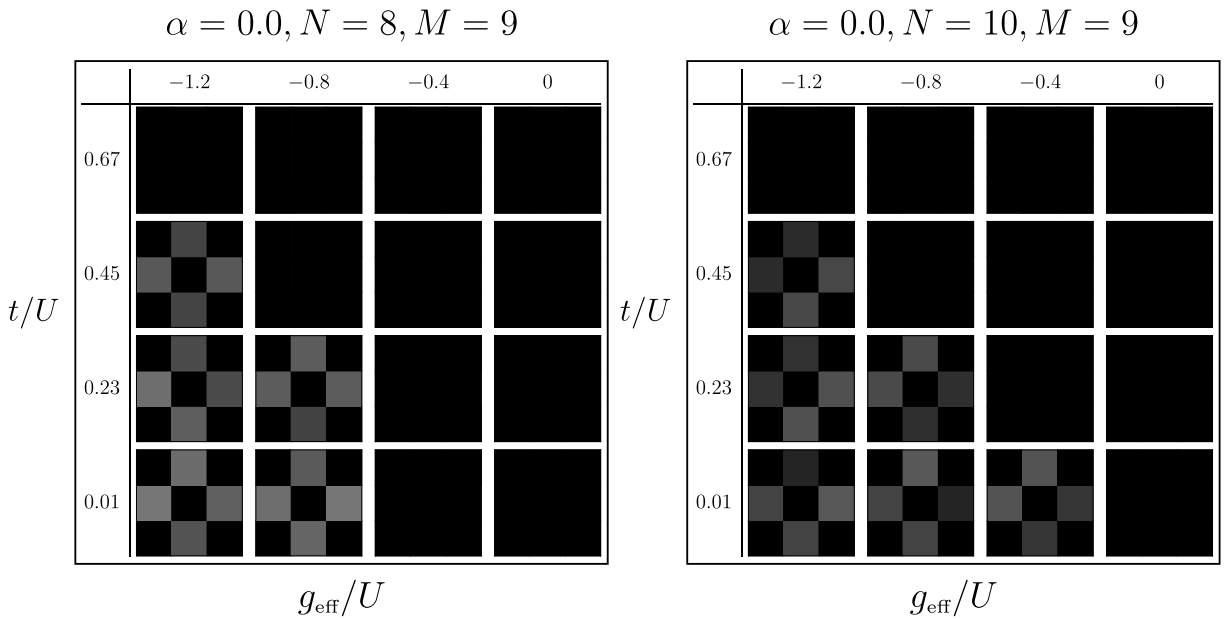

Figure (3.5) Panels for the density distribution of the system inside the cavity without the Magnetic Field ($\alpha = 0.0$) acting on it. To the left, we find the case for 8 particles in 9 sites, and to the right, the case for 10 particles in 9 sites.

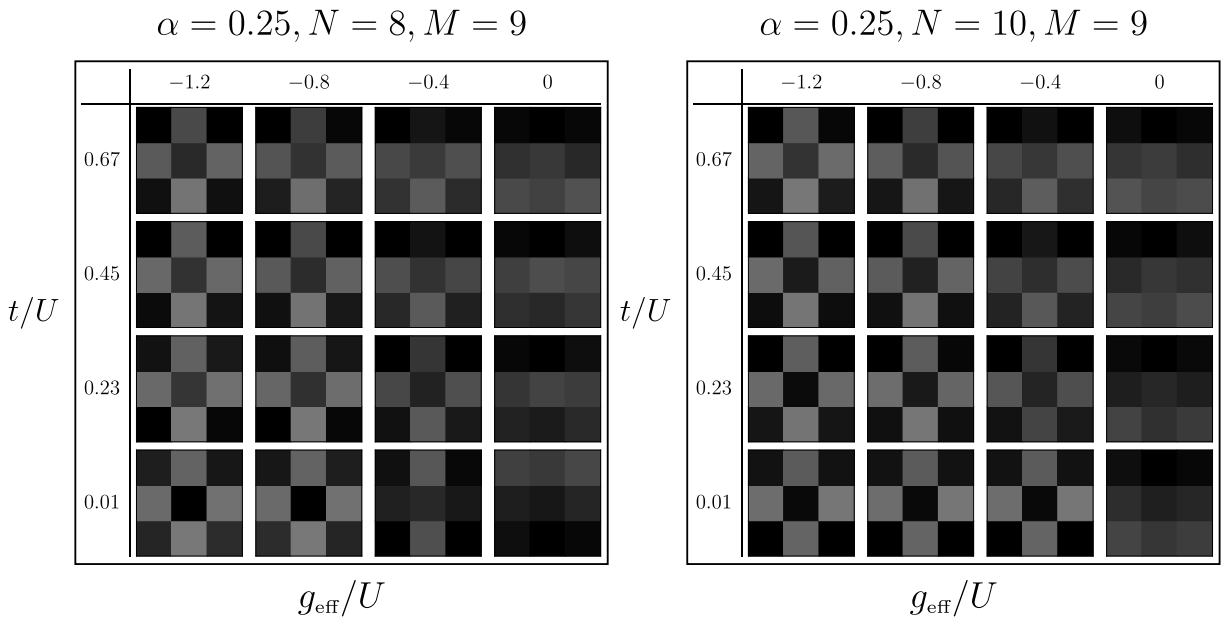

Figure (3.6) Panels for the density distribution of the system inside the cavity without the Magnetic Field ($\alpha = 0.0$) acting on it. To the left, we find the case for 8 particles in 9 sites, and to the right, the case for 10 particles in 9 sites.

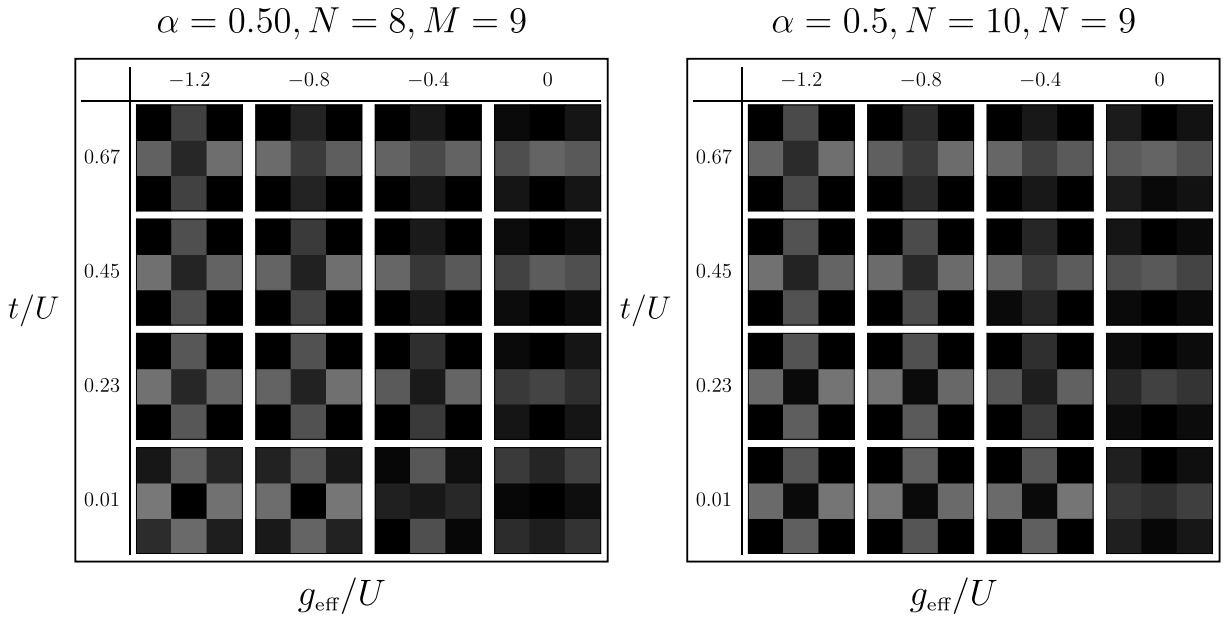

Figure (3.7) Panels for the density distribution of the system inside the cavity without the Magnetic Field ($\alpha = 0.0$) acting on it. To the left, we find the case for 8 particles in 9 sites, and to the right, the case for 10 particles in 9 sites.

3.7 Scales of Energy.

Given all of the dynamics having part in the model, it is important to show that such an experiment is feasible under the state-of-the-art conditions. In this section we provide a short review on what is possible to do in the lab and how can it be combined to physically create our system. Specifically, we aim to show that the scales of energy that all of the ingredients manage can coexist without interfering: the lasers

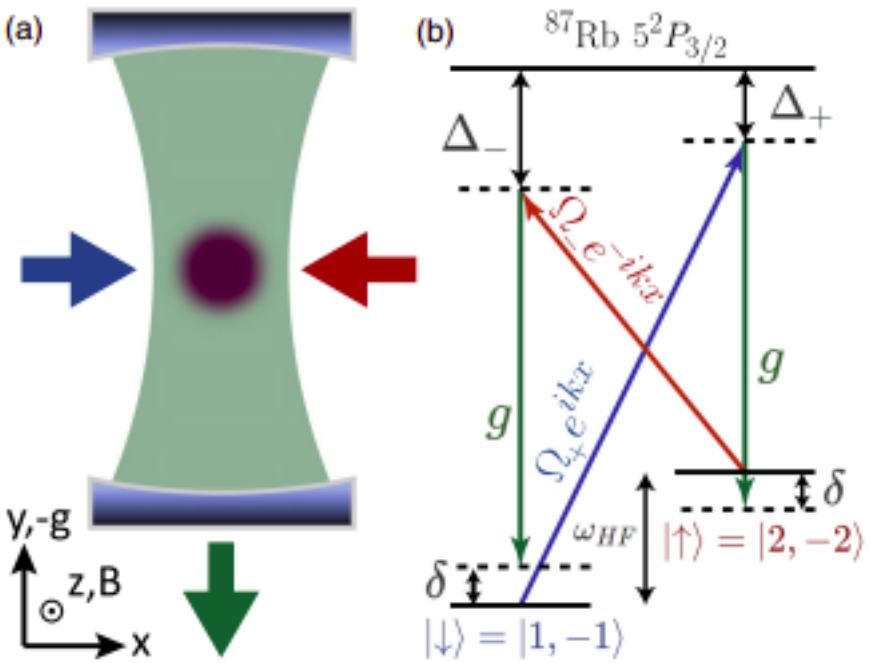

Figure (3.8) (a) Schematic of the experiment. Two Raman pump beams (red and blue arrows), polarized along the cavity axis, counterpropagate through a BEC of Rb (purple) inside a high-Q cavity. The cavity emission (green arrow) is detected by a singlephoton counter. (b) Level diagram illustrating the cavity-assisted Raman coupling between two hyperfine levels of ^{87}Rb acting as the spin states. Figure taken from [8].

required to create the lattice, the Rabi transitions involved in the interactions and the creation of the artificial magnetic field, the detunings with resonance modes of the cavity and atoms and the orders of magnitudes of the potential depth and other thresholds involved in the transitions of the matter; which is what we understand as the scales of energy of the processes.

Our proposal assumes a quantum gas of ^{87}Rb loaded in a 2D optical lattice inside a high-Q cavity, which defines the Quantum Optical Lattice (QOL). We take advantage of two experimental techniques: the first one regarding the creation of artificial magnetic phases via Spin Orbit Coupling and the second one is to take as a plot the already successful setups that allows to create spin textures in a QOL. Now we discus the details and the compatibility between them.

In order to create artificial magnetic phases, there had appeared several and successful attempts exploiting the Spin Orbit Coupling (SOC), being the the one in [8] (a dynamical SOC) the one who captured our attention. In these two experiments, the main idea is to link jumps between a couple of atomic inner states of the atom to imprints of momentum arising from recoil after photons emission, resulting in a change of the state of the photon (acquiring a space dependent phase in the process that can follow the one needed in our system) after it moves in a specific direction. Following this idea, and taking advantage of the presence of the cavity, we take as a good possible setup for our desired system the one achieved by Benjamin Lev's group [8], which utilises a specific cavity mode macroscopically populated (involving a superradiant Dicke-like phase) to create the dynamical SOC.

Briefly, the experiment considers the ultracold atoms inside the cavity and there are two cunterpropagating laser pumps perpendicular to the cavity axis. This lasers will couple the jumps between states $|F, m_F\rangle = |1, -1\rangle \equiv |\downarrow\rangle$ and $|2, -2\rangle \equiv |\uparrow\rangle$ of ^{87}Rb, their wavelengths are selected in such a way that the probability of Rabi transitions between inner states is favored, and such that the spinor effective Hamiltonian is given by

$$\hat{H}_{\text{SOC}} = \begin{bmatrix} \frac{(\hat{\mathbf{p}}+\hbar k_r/2\mathbf{e}_x)^2}{2m} + \hat{\mathbf{D}}_+ - \hbar\tilde{\delta} & \hbar\hat{\mathbf{\Omega}}_{\text{SOC}} \cos k_r y \\ \text{H. c.} & \frac{(\hat{\mathbf{p}}-\hbar k_r/2\mathbf{e}_x)^2}{2m} + \hat{\mathbf{D}}_- \end{bmatrix} \tag{3.26}$$

where k_r is the recoil momentum after photon emission and $\tilde{\delta}$ is the effective two-level spin splitting set by the Raman detuning δ minus a small ac light shift. We have that $\mathbf{D}_\pm = (g^2(x,z)/\Delta_\pm)\cos^2(k_r y)\hat{a}^\dagger\hat{a}$ is the dispersive shift and the dynamical Raman coupling strength is

$$\hat{\Omega}_{\text{SOC}} = \frac{g(x,z)\mathbf{\Omega}_+}{8\sqrt{2}\Delta_+}\hat{a}^\dagger + \frac{g(x,z)\mathbf{\Omega}_-}{8\sqrt{2}\Delta_-}\hat{a} \tag{3.27}$$

where g(x,z) is a given function, and from Figure 3.8 where these parameters are pictured, we can see that the laser amplitudes are $\mathbf{\Omega}_\pm$. For experimental purposes the important quantities here are the detunings between lasers and the atomic resonance ω_a, related by $\Delta_+ = \Delta_- + \omega_{\text{HF}}$ and $\Delta_- \approx 112.2$ GHz, $\omega_{\text{HF}} \approx 6.829$ GHz. In order to produce the massive photon emission via the superradiant state, the pumps must be such that a threshold $\eta_D \equiv \sqrt{N}g(x,z)\Omega_+/8\sqrt{2}\Delta_+ = \sqrt{N}g(x,z)\Omega_-/8\sqrt{2}\Delta_-$ is overcome. This value is around $\eta_D = 128(4)$kHz. such is the energy scale for the SOC to occur and achieve the desired artificial phases required to create the gauge in the system. The Raman coupling strength rises from zero to $\langle\hat{\Omega}_{\text{SOC}}\rangle = 2.2(1)E_r$ for E_r the recoil energy for this transition, $E_r \approx h \times 3.7kHz$ [69]. After getting a recoil momentum, the atoms will gather in spacial regions depending on their spin projection.

Since this experiment considers manipulation of spin states, we consider in parallel successful experiments to create spin textures as the second technique we mentioned before. To build a bridge between these two ideas, we follow the proposal in [70] based on the existent parameters for the experiments in ETH Zurich [71], [72] that have demonstrated the feasibility of these spin textures and control on the gap between both spin bands, having by default a recoil momentum during the Rabi transitions that can be exploited as the one in [8]. Their setup consists of the same QOL, a laser pump, and additionally an external magnetic field. A model for the coupled spin states with light that contemplate all of the parameters in this experiment is given in [70] as

$$\hat{H}^{\text{ab}} = \hbar g \sum_i \left(\frac{\mathbf{J}_z \mathbf{\Omega}_{z,p}\psi_{z,i}}{\Delta_a}\hat{a}^\dagger + \frac{\mathbf{J}_z^* \mathbf{\Omega}_{z,p}^* \psi_{z,i}^*}{\Delta_a}\hat{a} \right) \hat{S}_{z,i} \tag{3.28}$$

taking the sum over all of the sites, $\mathbf{\Omega}_{z,p}(\vec{B})$ the Rabi frequency dependent on the applied magnetic field $\vec{B} = B\hat{z}$. The parameter J_z stands for the amplitude of the cavity light in the z direction and $\phi_{z,i}$ encodes the structure of the light over the lattice

(it can be particularized to the case of a pumping angle of 90 degrees). $\Delta_a = \omega_c - \omega_a$ is the detuning between the light and the atomic resonance. the operator $\hat{S}_{z,i}$ is the spin projection in the z direction on each site. Comparing to Hamiltonian 3.26, the term in parenthesis of the last equation is equivalent to 3.27 relating the detunings Δ_a to $\Delta_\pm$, the laser amplitudes $\mathbf{J}_z$ to $\mathbf{\Omega}_\pm$, and considering function $g(x,z)$ to be equal to light structure factors $\phi_{z,i}$. In table 3.1 we can see the comparison between the order of magnitude of the relevant experimental parameters.

	$\Delta_\pm$, Δ_a	Δ_c	E_r	Spin Bandgap
Lev's Group	$110 - 120GHz$	$10MHz$	$h \times 3.7kHz$	$2.2E_r$
Esslinger's Group	$10 - 100GHz$	$\approx MHz$	$h \times 4kHz$	$2 - 10E_r$

Table (3.1) Comparison between orders of the experimental parameters in Lev's and Esslinger's experiments [8], [71], [72], [70]

From the comparison of models 3.26 and 3.28 build for experiments in Lev and Esslinger Groups respectively and Table 3.1 we aim to give a light on the experimental possibility of using any of the setups to integrate the others capabilities to create a final setup that couples spin states and produce artificial magnetic phases that may lead to physical observations of the effects predicted in this theoretical work.

Chapter 4: High-Q Cavity and Measurement Back-Action.

4.1 Measurement Backaction.

In general, when adding an extra term to the Hamiltonian, by mere intuition from perturbation theory, one expects a competition between ground states of each part of the Hamiltonian and vice-verse. When dealing with measurement the reality is beyond this idea since the competition comes from the measurement itself. In the following we will study what happens when a scattered photon is detected out of the system [78]. The photons come from an intense interaction with the system that actually couples them, when a photon is annihilated by the detector, the system should "notice" this absence enough to change its internal state.

Physically, we are placing the bosons system inside a cavity which has an optical axis along the two mirrors. It is in this direction that the detected photons travel. By now we are not considering the effects of such a cavity, it is only to collect the photons. The photon is detected if and only if it came out of one of the mirrors. There is a pumping beam that introduces the light in the system and also inside the cavity a new beam is created by default (see fig. 4.1). Both beams stablish an interference pattern that finally enlight in a different way the lattice spaces, associating thus certain phases to the particles and their interactions, something that is refered to as the light structure.

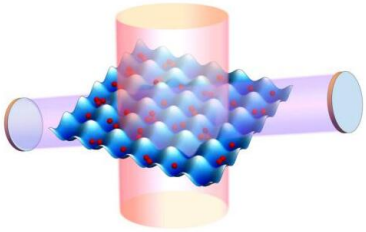

Figure (4.1) Scheme of the physical situation of the BHH system inside a cavity. There is a pump beam coming from the outside and an beam inside the cavity that creates the lght structure. The image is taken from [78].

4.1.1 Quantum Trajectories.

Now, the method we will use is called *quantum trajectories* [77] (this is an alternative numerical approach to arrive to the results that the Master equation of this open system should give us). The method proposes an ensemble composed by many evolution processes from a starting state of the system involving measurment processes. We define the operator $\hat{c} = \sqrt{2\kappa}\hat{a}$ to represent the photon detection (and anihilation) with κ the photon decay rate. The proposed Hamiltonian that accounts the leakeage of photons by measurment is given in [78] as

$$H_{\text{eff}} = H_{\text{BHH}} - i\frac{\hbar}{2}\hat{c}^\dagger\hat{c} = H_{\text{BHH}} - i\hbar\kappa\hat{a}^\dagger\hat{a}, \tag{4.1}$$

where $\hat{a}^{(\dagger)}$ is the photon annihilation (creation) operator. Since one photon is coupled to the rest of the system and also it mediates interactions, it is possible to derive an identity between the interaction operators and the photon detection:

$$\hat{a} \cong C(\hat{B} + \hat{D}) \tag{4.2}$$

where

$$\hat{B} = \sum_{\langle j,i\rangle} J_{ij}\hat{b}_i^\dagger\hat{b}_j \tag{4.3}$$

$$\hat{D} = \sum_{i=1}^{L} J_{jj}\hat{n}_j \tag{4.4}$$

for J_{ij} complex scalars standing for the phases acquired due to the light strutcure mediation, the number operator is $n_j = b_j^\dagger b_j$ which are proportional to on-site interactions. The constant C is the Rayleigh scattering constant

$$C = \frac{i\Omega_{10}a_0}{i\Delta_p - \kappa} \tag{4.5}$$

where $\Delta_p = \omega_p - \omega_a$ is the detuning frecuanty, the difference between the pumpin frecuency and the atom resonance frecuency, and $\Omega_{10} = g_1 g_0/\delta_a$ involves the atom-light coupling constants g_i, for the pump beam and the scattered light. These are experimental parameters that we are not going to deal with directly, instead we will resume their relationship in the parameter

$$\gamma = |C|^2\kappa, \tag{4.6}$$

so

$$H_{\text{eff}} = H_{\text{BHH}} - i\hbar\gamma(\hat{B} + \hat{D})^2. \tag{4.7}$$

The light structure is taking into account in the coefficients J_{ij}. We focus on the physical content and will consider only two possible configurations. The first one is when the beam inside the cavity and the pumping beam have such an angle that the

nodes of the pattern match with the even sites of the lattice and light have a phase 1 in the other sites. In that point the light does not produce any scattered photons and the coefficients are $J_{even} = 0$ and $J_{odd} = 1$. On the other hand, if we take the two beams forming a 90 degrees angle, we are able to find a moment when even and odd sites have opposite polarization, obtaining $J_{jj} = (-1)^j$. In general we can consider several configurations arising from the form of the operator $\hat{D} = \sum_{i=1}^{N} e^{2\pi l/R}\hat{n}_l$ where $2\pi l = (\vec{k}_{in} - \vec{k}_{out}) \cdot r_l$ for the direction of the pumping and cavity beam and the l position of the lattice.

Recalling the supposition we made earlier for the lattice sites to be deep enough to allow only on-site photon mediated interactions then the kinetic part $\hat{B}$ does not contribute and consequently $\hat{a} \propto \hat{D}$, the Hamiltonian would reduce to

$$H_{\text{eff}} = H_{\text{BHH}} - i\hbar\gamma\hat{D}^2 \tag{4.8}$$

and we now take units convention $\hbar = 1$.

4.1.2 Numerical method for the quantum trajectories.

The method with which we model the evolution of the system is as follows [77], [78]:

- Define a non hermitian Hamiltonian taking into account that the photon detection-annihilation process by the operator $i\hbar\hat{c}^\dagger\hat{c}/2$ and assume that the state of the system $|\psi(t)\rangle$ evolves obeying the Schrödinger equation for

$$\hat{H}_{\text{eff}} = \hat{H}_{BH} - i\hbar\hat{c}^\dagger\hat{c}/2 \tag{4.9}$$

- Define a random variable $r \in (0, 1)$ representing the unkown moment when of the photon detection
- Define the unitary evolution operator

$$\hat{U}(t) = e^{-i\hat{H}_{\text{eff}}t/\hbar} \tag{4.10}$$

- Stop the evolution in t_j, when happens $\langle\psi(t_0)|\psi(t_j)\rangle = r$
- Assume the previous step as the detection moment and apply the corresponding operator $\hat{c}$ to the state and renormalize to starte the proces again

$$|\psi(t_j)\rangle \to \frac{\hat{c}|\psi(t_j)\rangle}{\sqrt{\langle\psi(t_j)|\hat{c}^\dagger\hat{c}|\psi(t_j)\rangle}}. \tag{4.11}$$

Understanding the evolution operator

$$\begin{aligned}\hat{U}(t, t_0) &= \exp\left(-iH_{eff}(t - t_0)/\hbar\right) \\ &= \exp\left(-iH_{\text{BHH}} - \gamma\hat{D}^2\right)\end{aligned} \tag{4.12}$$

we interpret the measurement term wieghted by γ as a dissipation term that will reduce the norm of the state.

When applying the method, we evolve the state in M steps of Δt in time until $t \to \infty$, that means the change in the value of $\langle \sigma_D^2 \rangle$ is not significant anymore. Making this process N times, we keep only the final points of each trajectory to create the ensemble and average all of them. For the operator $\hat{D}$ this is denoted as

$$\langle \hat{D} \rangle_{\text{traj}} \tag{4.13}$$

The fluctuations of this operator are taken to be

$$\langle \sigma_D^2 \rangle_{traj} = \langle \hat{D}^2 \rangle_{\text{traj}} - \langle \hat{D} \rangle_{\text{traj}}^2. \tag{4.14}$$

4.1.3 Numerical process.

Evolution Operator.

We denote the matrix representation of the evolution operator as A. From Linear Algebra is possible to write it as

$$A = SMS^{-1} \tag{4.15}$$

where $S = (V_1, V_2, \ldots, V_n)$ with V_i the i-th eigenvector of A and $M = \text{Diagmat}(v_1, v_2, \ldots, v_n)$ with v_i el i-ésimo eigenvalor. Expanding the Taylor series we find that

$$e^A = Se^M S^{-1} \tag{4.16}$$

with $e^M = \text{Diagmat}(e^{v_1}, e^{v_2}, \ldots, e^{v_n})$.

Calculating one quantum trajectory.

We define $\hat{U}(t - t_0) \equiv$ Evol as a constant and start with the state $G(0)$ in a SF state obtaining the ground state of Bose Hubbard Hamiltonian without interactions. The pseudo code is

- Set initial G
- r = Rand(0,1) (random number)
- for($i = 1$; $i < P$; $i++$) {
- if($\|G\|_2 < r$){G = D*G
- $G = G/\|G\|_2$ and save
- r = Rand(0,1) (new random number) }
- else{
- save $G/\|G\|_2$ }
- G = EvolutionOperator*G }

where P is the number of steps.

4.1.4 Competition between kinetical and on-site interactions, and measurement.

When solving the master equation for a system like this, the uncertainity on the measurement operator is usually big, what makes it difficult to work with it [78]. In the method of quantum trajectories we can access the variance of any operator by analyzing the complete ensemble of trajectories. We can calculate $\langle \sigma_D^2 \rangle$ whose value give us an idea of how different from the ground state of the operator $\hat{D} = \hat{N}_{odd}$ (which is the sum of the particles in odd sites) is the ground state of the complete system. Following this reasoning we are able to calculate the results in fig. 4.2

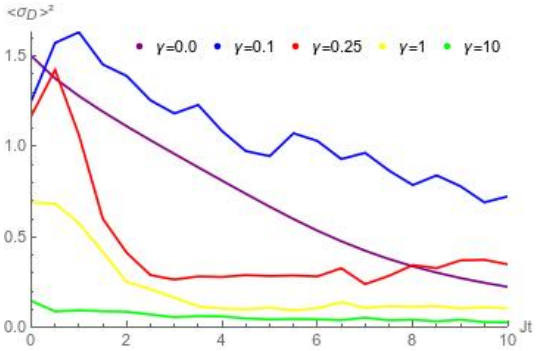

Figure (4.2) Graphic of the variance of the measurement operator as a function of U/J for different measurement strenghts. We used a system of $N = M = 6$ and 1000 trajectories. This result agrees qualitatively with the original calculation from [78].

that coincide qualitatively with the results in [78]. What this image basically tells us is how much the original fluctuations per site function vary after performing a measurement. The value $\gamma = 0$ for the no measurement case agrees with the already function $\langle \sigma_i \rangle$ that shows the SF on small values of U/J and the MI for $U/J \to \infty$. After performing a weak measurement we note that the state is squeezed below the ground state until it reaches its maximum to later fall to the MI phase for bigger values of U/J. When we have a strong measurement, both the superfluid and Mott Insulator are impossible to reach for any value of U/J.

Evolution of a single trajectory.

To get a deeper view of what is happening in the system, we analyze a specific trajectory under weak and strong measurement to see its evolution. We define a cummulative density function for the posibility that the odd sites host N_{odd} number of particle in any configuration as

$$p(N_{odd}) = \sum_{\text{states } i \text{ with } N_{odd} \text{ bosons in odd sites.}} |c_i|^2 \tag{4.17}$$

where the $|c_i|$'s are the participation that the states i have in the ground states of the system. We plot this evolution in fig. 4.3.

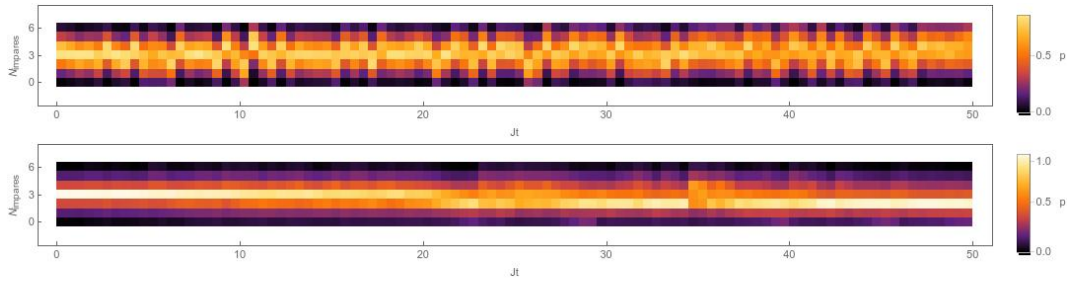

Figure (4.3) Subfigures a) and b) in that order. Time evolution of the probability of an occupation of N_{odd} particule sin the odd sites of a single trajectory. Subfigure a) represent the weak interaction and measurement case $U/J = 0.1$ y $\gamma/J = 0.1$. Subfigure b) corresponds to strong interactions and weak measurement $U/J = 10$. The system has $N = M = 6$. These results qualitatively agree with the original calculation from [78].

Subfigure 4.3.a) that considers the case of weak interaction and measurement regime. Right at the beginning of the trajectory we note there are 3 bosons in the 3 odd sites that corresponds to the SF phase. As the time goes on, the measurement breaks the SF phase moving the bosons out of the odd sites, since the kinetic energy is still important, they do not stay longer in that configuration and start oscilating but staying away from the SF phase. Note that the probability profiles get squeezed as time increase, producing $\langle \sigma_D^2 \rangle$ to get smaller. Subfigure 4.3b) shows the case of strong interactions. We can see the MI from the begining with 3 bosons in 3 odd sites. In contrast with the previous case, the probability profile is very localized, but eventually the measurement breaks the MI phase.

We may interpret from this that the measurement is projecting the state of the system into its own space of eigenstates and it is getting stonger with time, so eventually the SF or MI will be lost.

4.1.5 Long-range tunneling and Zeno Effect.

In addition to the dynamics of of the system it can produce unusual effects in it; effects that are not taken into account by the BH Hamiltonian such as tunneling from one site to other that is not a neighbour and the Zeno effect that mantains the system in such a state the exhibits the same eigenvalue of the measurement operator. In our case, if the measurement strenght is strong enough we may observe these phenomena as it is showed in Fig. 4.4.

The case of subfigure 4.4.a) was designed to see the Zeno effect. A system of 7 bosons and 7 sites under and a measurement operator $\hat{D} = \hat{n}_3 + \hat{n}_4 + \hat{n}_5$. Given the giant value of γ, when the measurement is performed the state will be projected into the state that corresponds to the eigenvalue of 3 in it. What the evolution shows is that the state of the system can change but it has to be in the eigenspace for that value. The space is now divided into three zones, two exterior that preserve the two particles in each one, and the central one that preserves the three particles inside (in the image there is a problem with the initial condition that will be solved). We can say that the number of particles in the three central sites is frozen by the Zeno effect.

In subfigure 4.4.b) the attempt is to show the long-range tunneling. Starting with the configuration $(0, 1, 2, 1, 0)$ and evolving under the light structure $J = (0, 1, 0, 1, 0)$,

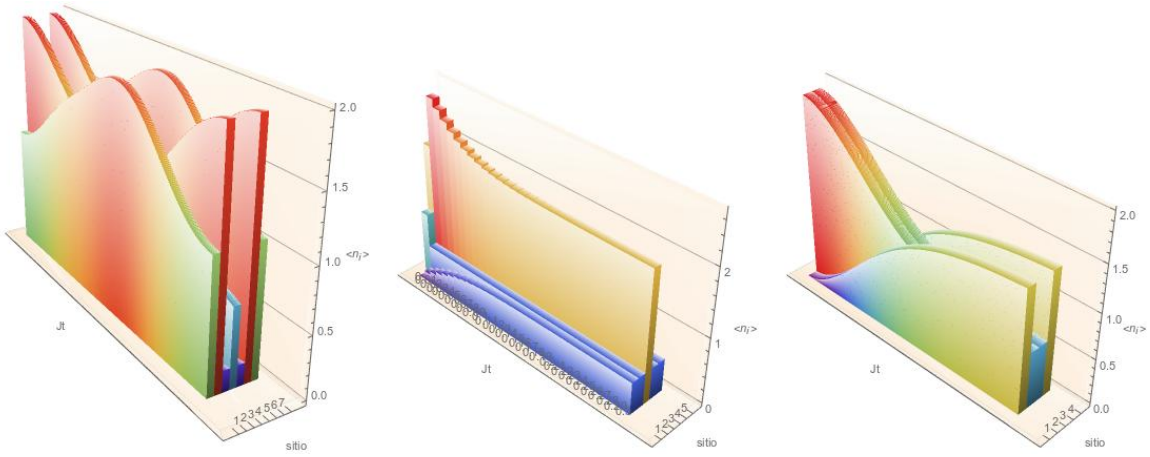

Figure (4.4) Subfigures a), b) y c) in that order. Results for the calculation of density by site over one quantum trajectory for different initial conditions and light structures. In a) the system is has $N = M = 7$, initial state is $|1, 1, 1, 1, 1, 1, 1\langle$ and the phases of the light structure are $J = (0, 0, 1, 1, 1, 0, 0)$, what indicates that only three sites scatter photons. In b) we have $N = 4$, $M = 5$ and a initial state of $(0, 1, 2, 1, 0)$ with light structure of $J = (0, 1, 0, 1, 0)$. Lastly, in c) the system size is $N = M = 4$, initial state is $(0, 2, 2, 0)$ and light structure is $J = (0, -1, 1, 0)$. For all the cases: $\gamma/J = 1000$ y $U/J = 0$. These results qualitatively agree with the original calculation from [78].

we expect by Zeno effect that site one and three preserve the cummulative number of particles frozen which is true. The interesting thing is that the 2 particles in the middle site decrease but the number of particles in the endings increase. Since there was no moment in which the number of particles in sites 1 or 3 was not 1, we can conclude a long-range tunneling induced by the measurement.

Lastly, subfigure 4.4.c) shows what happens for an initial configuration $(0, 2, 2, 0)$ with the phases being $J = (0, -1, 1, 0)$. By Zeno effect the measurement $\hat{D} = \hat{n}_3 - \hat{n_2}$ tries to keep the difference of the particles in sites 1 and 2 (equal to 0) frozen. The system evolve freely tunneling particles from the central zone to the endings but keeping that difference unchanged.

4.2 High-Q Cavity interactions and Back-Action.

In this chapter we incorporate the cavity mediated interactions into the measurement back-action study presented in Chapter 4, in fact we are completing the model: this term was neglected in that section. The new effective Hamiltonian will be

$$H_{\text{eff}} = H_{\text{BHH}} - \frac{g_{\text{eff}}}{M^2}\hat{D}_-^2 - i\hbar\gamma\hat{D}_-^2. \tag{4.18}$$

We follow the calculations of the variance $\langle\sigma_D^2\rangle$ through the quantum trajectories method to compare the changes for weak and strong measurement regimes.

4.3 Measurement back-action enhancement by cavity-mediated interactions (New Results).

After considering the effects of the cavity into the system, we proceed to calculate the variance of the measurement operator using the quantum trajectories method. The results are present in figure 4.5 for weak (left) and strong (right) measurements. We picked a value of $g_{\text{eff}} = -2.5U$ which is well below the installation of the DW phase at least for the plotted values of U/t above 1, after the SF phase. The results are presented in fig. 4.5, where we can see that the cavity effects. In the case of no measurement at all, the change is evident and it is something due to the fact that in this regime the system is mostly in the DW regime, the MI and SF behaviors are not expected. We note also that for weak measurements the new variance decrease with a lower rate to the MI. On the other hand, a strong measurement do not change significantly the dynamics.

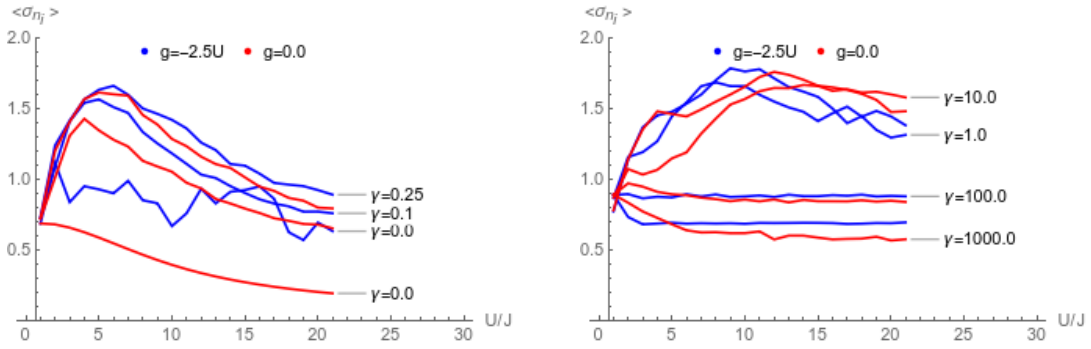

Figure (4.5) Numerical calculation of $\langle \sigma_D^2 \rangle$ for a system with cavity mediated interactions and size $N = M = 4$ for over 10000 trajectories. To the left the weak measurement and to the right, the strong measurement.

Chapter 5: Conclusions.

In this thesis we have reviewed and reproduced most of the required theory to understand the dynamics of ultracold neutral bosons both in the presence of an artificial magnetic field and when they are placed inside a high-Q cavity. Evidence that the hard-core bosons limit impose an alike fermions interaction through the fidelity of the ground state and a more general approach with the energy spectrum reduction have been provided. In particular, the reduction of the spectrum allows us to study the topological properties quantities of the system and the useful symmetry particle-hole was also showed, which offers an easy access to the dynamics of one or two fermions in the lattice by producing one or two holes in it.

The introduction of the artificial magnetic field as calculated here is compatible with already known effects such as the artificial Lorentz force for charge carriers and the stripped phase. When these behavior are combined with the cavity we found an interesting result: the stabilization of the self organized DW phase in the presence of the artificial magnetic field. It has been shown the gauge field affects the movement of the particles having consequences in the superfluid phase making it weaker in competence with the DW phase, something that we referd to as the DW phase stabilization. This is an original result.

Finally, after studying the interesting phenomena that measurement backaction produces on the preexisting phases we encountered an enhancement on the backaction effects such as the destruction of the MI and SF for weak and strong measurements and the inaccessibility to the MI for large values of U/t.

Appendixes.

6.1 Appendix A: Calculations from Chapter 1.

Starting with the Hamiltonian operator 1.14 we apply a transformation to the momentum space of the site operators given by

$$\begin{aligned} \hat{b}_i &= \frac{1}{\sqrt{N_s}} \sum_{\mathbf{k}} \hat{a}_{\mathbf{k}} e^{-i\mathbf{k}\cdot\mathbf{r}_i} \\ \hat{b}_i^\dagger &= \frac{1}{\sqrt{N_s}} \sum_{\mathbf{k}} \hat{a}_{\mathbf{k}}^\dagger e^{i\mathbf{k}\cdot\mathbf{r}_i}, \end{aligned} \tag{6.1}$$

taking only a finite volume V, obtaining discrete values of momenta $\hbar\mathbf{k}$ running over the first Brillouin Zone (BZ). Later, the usual limit for $V \to \infty$ will allow us to change the sums by integrals using the fact that $\sum_i e^{i(\mathbf{k}-\mathbf{k}')\cdot r_i} = M\delta_{\mathbf{k}\mathbf{k}'}$ for M the total number of sites. Calling $H_{(1),(2),(3)}$ each of the sums in 1.14 respectively, we insert the definitions to find

$$H_{(1)} = -t\frac{1}{N_s} \sum_{<i,j>} \sum_{\mathbf{k}} a_{\mathbf{k}}^\dagger e^{i\mathbf{k}\cdot r_i} \sum_{\mathbf{k'}} a_{\mathbf{k'}} e^{-i\mathbf{k'}\cdot r_j} \tag{6.2}$$

$$= -t \sum_{\mathbf{k}} \sum_{\mathbf{k'}} \sum_{<i,j>} a_{\mathbf{k}}^\dagger a_{\mathbf{k'}} e^{i(\mathbf{k}\cdot r_i - \mathbf{k'}\cdot r_j)}$$

$$= -t \sum_{\mathbf{k}} \sum_{\mathbf{k'}} \sum_{<i,j>} a_{\mathbf{k}}^\dagger a_{\mathbf{k'}} e^{i(\mathbf{k}\cdot r_i - \mathbf{k'}\cdot (r_j + r_i - r_i))}$$

$$= -t \sum_{\mathbf{k}} \sum_{\mathbf{k'}} \sum_{<i,j>} a_{\mathbf{k}}^\dagger a_{\mathbf{k'}} e^{i(\mathbf{k}-\mathbf{k'})\cdot r_i} e^{-i\mathbf{k'}\cdot (r_j - r_i)}$$

$$= -t \sum_{\mathbf{k}} \sum_{\mathbf{k'}} \sum_{<i,j>} a_{\mathbf{k}}^\dagger a_{\mathbf{k'}} e^{i(\mathbf{k}-\mathbf{k'})\cdot r_i} e^{-i\mathbf{k'}\cdot (r_j - r_i)}$$

Note that the sum over $\langle i,j\rangle$ involve only the vector $r_j - r_i = (0, ..., a, ..., 0)$ for NN, where a es the lattice spacing, equal for all directions. Each r_i has $2d$ vectors $\bar{a_m}$ (being d the spacial dimension of the lattice). Fixing r_i and moving r_j then

$$\sum_{<i,j>} e^{i(\mathbf{k}-\mathbf{k'})\cdot r_i} e^{-i\mathbf{k'}\cdot(r_j-r_i)}$$

$$= \sum_i e^{i(\mathbf{k}-\mathbf{k'})\cdot r_i}(e^{-i\mathbf{k'}\cdot(a,\ldots,0)} + e^{-i\mathbf{k'}\cdot(-a,\ldots,0)} + \cdots + e^{-i\mathbf{k'}\cdot(0,\ldots,a)} + e^{-i\mathbf{k'}\cdot(0,\ldots,-a)})$$

$$= \sum_i e^{i(\mathbf{k}-\mathbf{k'})\cdot r_i}((e^{ik'_1 a} + e^{-ik'_1 a}) + \cdots + (e^{ik'_d a} + e^{-ik'_d a}))$$

$$= \sum_i e^{i(\mathbf{k}-\mathbf{k'})\cdot r_i}(2\cos(k'_1 a) + 2\cos(k'_2 a) + \cdots + 2\cos(k'_d a))$$

$$= \sum_i e^{i(\mathbf{k}-\mathbf{k'})\cdot r_i}(2\sum_j^d \cos(k'_j a))$$

$$= N_s \delta_{\mathbf{k},\mathbf{k'}}(2\sum_j^d \cos(k'_j a))$$

since r_i acquires again the value r_j, for that case $\bar{a}_m$ is now opposite.
This leaves the first part of the Hamiltonian as

$$H_{(1)} = -t\frac{1}{N_s} N_s \sum_{\mathbf{k}} \sum_{\mathbf{k'}} a^\dagger_{\mathbf{k}} a_{\mathbf{k}}, \delta_{\mathbf{k},\mathbf{k'}}(2\sum_j^d \cos(k'_j a)) \tag{6.3}$$

$$= \sum_{\mathbf{k}} a^\dagger_{\mathbf{k}} a_{\mathbf{k}}(-2t\sum_j^d \cos(k'_j a))$$

$$= \sum_{\mathbf{k}} a^\dagger_{\mathbf{k}} a_{\mathbf{k}}(-\bar{\epsilon}_{\mathbf{k}})$$

with $\bar{\epsilon}_{\mathbf{k}} = 2t\sum_{j=1}^d \cos(k'_j a)$. For the second part of the Hamiltonian we have

$$H_{(2)} = \frac{1}{2}U\sum_i (\frac{1}{\sqrt{N_s}}\sum_{\mathbf{k}} a^\dagger_{\mathbf{k}} e^{i\mathbf{k}\cdot r_i})(\frac{1}{\sqrt{N_s}}\sum_{\mathbf{k'}} a^\dagger_{\mathbf{k}}, e^{i\mathbf{k'}\cdot r_i})(\frac{1}{\sqrt{N_s}}\sum_{\mathbf{k"}} a_{\mathbf{k"}} e^{-i\mathbf{k"}\cdot r_i})(\frac{1}{\sqrt{N_s}}\sum_{\mathbf{k"'}} a_{\mathbf{k"'}}, e^{-i\mathbf{k"'}\cdot r_i}) \tag{6.4}$$

$$= \frac{1}{2}\frac{U}{N_s^2}\sum_{\mathbf{k}}\sum_{\mathbf{k'}}\sum_{\mathbf{k"}}\sum_{\mathbf{k"'}} a^\dagger_{\mathbf{k}} a^\dagger_{\mathbf{k}}, a_{\mathbf{k"}} a_{\mathbf{k"'}}, \sum_i e^{i(\mathbf{k}+\mathbf{k'}-\mathbf{k"}-\mathbf{k"'})}$$

$$= \frac{1}{2}\frac{U}{N_s}\sum_{\mathbf{k}}\sum_{\mathbf{k'}}\sum_{\mathbf{k"}}\sum_{\mathbf{k"'}} a^\dagger_{\mathbf{k}} a^\dagger_{\mathbf{k}}, a_{\mathbf{k"}} a_{\mathbf{k"'}}, \delta_{\mathbf{k}+\mathbf{k'},\mathbf{k"}+\mathbf{k"'}}$$

Lastly, for the third part of the Hamiltonian:

$$H_{(3)} = -\mu \sum_i (\sum_{\mathbf{k}} a^\dagger_{\mathbf{k}} e^{i\mathbf{k}\cdot r_i})(\sum_{\mathbf{k'}} a_{\mathbf{k'}} e^{-i\mathbf{k'}\cdot r_i}) \tag{6.5}$$

$$= -\mu \frac{1}{N_s} \sum_i \sum_{\mathbf{k}} \sum_{\mathbf{k'}} a^\dagger_{\mathbf{k}} a_{\mathbf{k'}} e^{i(\mathbf{k}-\mathbf{k'})\cdot r_i}$$

$$= -\mu \frac{N_s}{N_s} \sum_{\mathbf{k}} \sum_{\mathbf{k'}} a^\dagger_{\mathbf{k}} a_{\mathbf{k'}} \delta_{\mathbf{k},\mathbf{k'}}$$

$$= -\mu \sum_{\mathbf{k}} a^\dagger_{\mathbf{k}} a_{\mathbf{k}}$$

Being the total Hamiltonian $H = H_{(1)} + H_{(2)} + H_{(3)}$, its final expression is as

$$H = \sum_{\mathbf{k}} (-\bar{\epsilon}_{\mathbf{k}} - \mu) a^\dagger_{\mathbf{k}} a_{\mathbf{k}} + \frac{1}{2} \frac{U}{N_s} \sum_{\mathbf{k}} \sum_{\mathbf{k'}} \sum_{\mathbf{k''}} \sum_{\mathbf{k'''}} a^\dagger_{\mathbf{k}} a^\dagger_{\mathbf{k}}, a_{\mathbf{k''}} a_{\mathbf{k'''}}, \delta_{\mathbf{k}+\mathbf{k'},\mathbf{k''}+\mathbf{k'''}} \tag{6.6}$$

In a BEC the average number of atoms in the system N_0 (in the least energetical state) is much greater than 1, so if $N_0 = \langle a^\dagger_0 a_0 \rangle$ and $\langle a_0 a^\dagger_0 \rangle - \langle a_0 a^\dagger_0 \rangle = 1$, then $\langle a_0 a^\dagger_0 \rangle \approx \langle a^\dagger_0 a_0 \rangle$ and this allow us to see the agreement with a commutation of both operators and conclude $N_0 = \langle a^\dagger_0 \rangle \langle a_0 \rangle$. Since $\langle a_0 \rangle$ and $\langle a^\dagger_0 \rangle$ are complex conjugates then $\langle a_0 \rangle = \langle a^\dagger_0 \rangle = \sqrt{N_0}$.

The heart of Bogoliubov approach is that the creation and anihilation operators now shall be replaced by its average value plus a fluctuation

$$\begin{aligned} a^\dagger_0 &\to \sqrt{N_0} + a^\dagger_0 \\ a_0 &\to \sqrt{N_0} + a_0. \end{aligned} \tag{6.7}$$

Each time $\mathbf{k} = 0$ this sustitution applies then. There are many combinations in the sums so this must be done carefully by parts. NWhenever the fluctiation terms multiply the product is effectively zero. To find the terms with only one operator note that in the sum for $a^\dagger_{\mathbf{k}} a^\dagger_{\mathbf{k}}$ when $\mathbf{k} = 0$ there will be terms of first order. Let's consider only this term:

$$(-\bar{\epsilon}_0 - \mu)(\sqrt{N_0} + a^\dagger_0)(\sqrt{N_0} + a_0) + \frac{1}{2} \frac{U}{N_s} (\sqrt{N_0} + a^\dagger_0)(\sqrt{N_0} + a^\dagger_0)(\sqrt{N_0} + a_0)(\sqrt{N_0} + a_0)$$

Doing only the products for terms including only one operator we will have that

$$H^{(1)} = (-\bar{\epsilon}_0 - \mu)(\sqrt{N_0}(a^\dagger_0 + a_0)) + \frac{1}{2} \frac{U}{N_s} (a^\dagger_0 (\sqrt{N_0})^3) + a^\dagger_0 (\sqrt{N_0})^3) + a_0 (\sqrt{N_0})^3) + a_0 (\sqrt{N_0})^3) \tag{6.8}$$

$$= (-\bar{\epsilon}_0 - \mu)(\sqrt{N_0}(a_0^\dagger + a_0)) + \frac{1}{2}\frac{U}{N_s}(2a_0^\dagger(\sqrt{N_0})^3) + 2a_0(\sqrt{N_0})^3)$$

$$= (-\bar{\epsilon}_0 - \mu)(\sqrt{N_0}(a_0^\dagger + a_0)) + \frac{U}{N_s}(a_0^\dagger(\sqrt{N_0})^3) + a_0(\sqrt{N_0})^3)$$

$$= (-\bar{\epsilon}_0 - \mu + \frac{U}{N_s}N_0)(\sqrt{N_0}(a_0^\dagger + a_0))$$

Since this term must be 0 for each $a_0^\dagger$ and a_0 then:

$$-\bar{\epsilon}_0 - \mu + \frac{U}{N_s}N_0 = 0$$

Given that $\bar{\epsilon}_0 = 2t\sum_j^d \cos(k_j a)$ with $\mathbf{k} = \bar{0}$ then $\bar{\epsilon}_0 = 2t\sum_{j=1}^d 1 = 2td$ and so

$$-2td - \mu + \frac{U}{N_s}N_0 = 0$$

and

$$\mu = Un_0 - zt$$

where $n_0 = \frac{N_0}{N_s}$ y $z = 2d$.

Continuing with the approximation to find zero and second order terms that form part of the effective Hamiltonian $\hat{H}^i_{\text{eff}}$ substitute all operators with $\sqrt{N_0}$ because in this case there is no operator in any of addends. Then

$$H^{(0)} = (-\bar{\epsilon}_0 - \mu)N_0 + \frac{1}{2}\frac{U}{N_s}N_0N_0 \tag{6.9}$$

$$= (-\bar{\epsilon}_0 - \mu + \frac{1}{2}Un_0)N_0$$

$$= (-2td - \mu + \frac{1}{2}Un_0)N_0$$

For the terms of second order, we will only keep the terms with two operators labeled with $\mathbf{k} = 0$, otherwise the resulting terms will be dropped. Terms including three operators for $\mathbf{k}$ being 0 have been already counted by second order terms or will be part of third order terms. Selecting the term using these rules the result is

$$\frac{1}{2}\frac{U}{N_s}(\sum_{\mathbf{k"}}\sum_{\mathbf{k"'}}\sqrt{N_0}\sqrt{N_0}a_{\mathbf{k"}},a_{\mathbf{k"'}},\delta_{0,\mathbf{k"}+\mathbf{k"'}}, + \sum_{\mathbf{k'}}\sum_{\mathbf{k"'}}\sqrt{N_0}a^\dagger_{\mathbf{k'}},\sqrt{N_0}a_{\mathbf{k"'}},\delta_{\mathbf{k'},\mathbf{k"}} +$$

$$\sum_{\mathbf{k'}}\sum_{\mathbf{k''}}\sqrt{N_0}a^{\dagger}_{\mathbf{k'}},a_{\mathbf{k''}}\sqrt{N_0}\delta_{\mathbf{k'},\mathbf{k''}}+\sum_{\mathbf{k}}\sum_{\mathbf{k'''}}a^{\dagger}_{\mathbf{k}}\sqrt{N_0}\sqrt{N_0}a_{\mathbf{k'''}},\delta_{\mathbf{k},\mathbf{k'''}},$$
$$+\sum_{\mathbf{k}}\sum_{\mathbf{k''}}a^{\dagger}_{\mathbf{k}}\sqrt{N_0}a_{\mathbf{k''}}\sqrt{N_0}\delta_{\mathbf{k},\mathbf{k''}}+\sum_{\mathbf{k}}\sum_{\mathbf{k'''}}a^{\dagger}_{\mathbf{k}}a^{\dagger}_{\mathbf{k}},\sqrt{N_0}\sqrt{N_0}\delta_{\mathbf{k}+\mathbf{k'},0})$$

$$=\frac{1}{2}\frac{U}{N_s}N_0(\sum_{\mathbf{k}}a_{\mathbf{k}}a_{\text{-}\mathbf{k}}+\sum_{\mathbf{k}}a^{\dagger}_{\mathbf{k}}a_{\mathbf{k}}+\sum_{\mathbf{k}}a^{\dagger}_{\mathbf{k}}a_{\mathbf{k}}+\sum_{\mathbf{k}}a^{\dagger}_{\mathbf{k}}a_{\mathbf{k}}+\sum_{\mathbf{k}}a^{\dagger}_{\text{-}\mathbf{k}}a^{\dagger}_{\mathbf{k}}$$

$$=\frac{1}{2}Un_0(\sum_{\mathbf{k}}a_{\mathbf{k}}a_{\text{-}\mathbf{k}}+\sum_{\mathbf{k}}4a^{\dagger}_{\mathbf{k}}a_{\mathbf{k}}+\sum_{\mathbf{k}}a^{\dagger}_{\mathbf{k}}a^{\dagger}_{\text{-}\mathbf{k}}).$$

with $n_0 = N_0/N_s$. Finally the effective hamiltonion acquires the next form

$$H^i_{\text{eff}}=(-2td-\mu+\frac{1}{2}Un_0)N_0+\sum_{\mathbf{k}}(-\bar{\epsilon}_{\mathbf{k}}-\mu)a^{\dagger}_{\mathbf{k}}a_{\mathbf{k}}+\frac{1}{2}Un_0(\sum_{\mathbf{k}}a_{\mathbf{k}}a_{\text{-}\mathbf{k}}+\sum_{\mathbf{k}}4a^{\dagger}_{\mathbf{k}}a_{\mathbf{k}}+\sum_{\mathbf{k}}a^{\dagger}_{\mathbf{k}}a^{\dagger}_{\text{-}\mathbf{k}}) \tag{6.10}$$

$$=(-2td-(Un_0-2td)+\frac{1}{2}Un_0)N_0+\sum_{\mathbf{k}}(-\bar{\epsilon}_{\mathbf{k}}-\mu+2Un_0)a^{\dagger}_{\mathbf{k}}a_{\mathbf{k}}+\frac{1}{2}Un_0(\sum_{\mathbf{k}}a_{\mathbf{k}}a_{\text{-}\mathbf{k}}+a^{\dagger}_{\text{-}\mathbf{k}}a^{\dagger}_{\mathbf{k}})$$

$$=-\frac{1}{2}Un_0)N_0+\sum_{\mathbf{k}}(-\bar{\epsilon}_{\mathbf{k}}-Un_0+2dt+2Un_0)a^{\dagger}_{\mathbf{k}}a_{\mathbf{k}}+\frac{1}{2}Un_0(\sum_{\mathbf{k}}a_{\mathbf{k}}a_{\text{-}\mathbf{k}}+a^{\dagger}_{\text{-}\mathbf{k}}a^{\dagger}_{\mathbf{k}})$$

Defining $\epsilon_{\mathbf{k}} = zt - \bar{\epsilon}_{\mathbf{k}}$:

$$=-\frac{1}{2}Un_0N_0+\sum_{\mathbf{k}}(\epsilon_{\mathbf{k}}+Un_0)a^{\dagger}_{\mathbf{k}}a_{\mathbf{k}}+\frac{1}{2}Un_0(\sum_{\mathbf{k}}a_{\mathbf{k}}a_{\text{-}\mathbf{k}}+a^{\dagger}_{\text{-}\mathbf{k}}a^{\dagger}_{\mathbf{k}})$$

$$=-\frac{1}{2}Un_0N_0+\frac{1}{2}\sum_{\mathbf{k}}(\epsilon_{\mathbf{k}}+Un_0)a^{\dagger}_{\mathbf{k}}a_{\mathbf{k}}+\frac{1}{2}\sum_{\mathbf{k}}(\epsilon_{\mathbf{k}}+Un_0)a^{\dagger}_{\mathbf{k}}a_{\mathbf{k}}+\frac{1}{2}Un_0(\sum_{\mathbf{k}}a_{\mathbf{k}}a_{\text{-}\mathbf{k}}+a^{\dagger}_{\text{-}\mathbf{k}}a^{\dagger}_{\mathbf{k}})$$

$$=-\frac{1}{2}Un_0N_0+\frac{1}{2}\sum_{\mathbf{k}}(\epsilon_{\mathbf{k}}+Un_0)(a_{\mathbf{k}}a^{\dagger}_{\mathbf{k}}-1)+\frac{1}{2}\sum_{\mathbf{k}}(\epsilon_{\mathbf{k}}+Un_0)a^{\dagger}_{\mathbf{k}}a_{\mathbf{k}}+\frac{1}{2}Un_0(\sum_{\mathbf{k}}a_{\mathbf{k}}a_{\text{-}\mathbf{k}}+a^{\dagger}_{\text{-}\mathbf{k}}a^{\dagger}_{\mathbf{k}})$$

$$=-\frac{1}{2}Un_0N_0-\frac{1}{2}\sum_{\mathbf{k}}(\epsilon_{\mathbf{k}}+Un_0)+\frac{1}{2}(\sum_{\mathbf{k}}(\epsilon_{\mathbf{k}}+Un_0)a_{\mathbf{k}}a^{\dagger}_{\mathbf{k}}+\sum_{\mathbf{k}}(\epsilon_{\mathbf{k}}+Un_0)a^{\dagger}_{\mathbf{k}}a_{\mathbf{k}}+Un_0\sum_{\mathbf{k}}(a_{\mathbf{k}}a_{\text{-}\mathbf{k}}+a^{\dagger}_{\text{-}\mathbf{k}}a^{\dagger}_{\mathbf{k}}))$$

$$=-\frac{1}{2}Un_0N_0-\frac{1}{2}\sum_{\mathbf{k}}(\epsilon_{\mathbf{k}}+Un_0)+\frac{1}{2}(\sum_{\mathbf{k}}a_{\mathbf{k}}a^{\dagger}_{\mathbf{k}}(\epsilon_{\mathbf{k}}+Un_0)+a^{\dagger}_{\mathbf{k}}a_{\mathbf{k}}(\epsilon_{\mathbf{k}}+Un_0)+Un_0a_{\text{-}\mathbf{k}}a_{\mathbf{k}}+Un_0a^{\dagger}_{\text{-}\mathbf{k}}a^{\dagger}_{\mathbf{k}})$$

$$= -\frac{1}{2}Un_0N_0 - \frac{1}{2}\sum_{\mathbf{k}}(\epsilon_{\mathbf{k}}+Un_0) + \frac{1}{2}(\sum_{\mathbf{k}} a_{\text{-}\mathbf{k}}a^{\dagger}_{\text{-}\mathbf{k}}(\epsilon_{\mathbf{k}}+Un_0) + a^{\dagger}_{\mathbf{k}}a_{\mathbf{k}}(\epsilon_{\mathbf{k}}+Un_0) + Un_0a_{\text{-}\mathbf{k}}a_{\mathbf{k}} + Un_0a^{\dagger}_{\mathbf{k}}a^{\dagger}_{\text{-}\mathbf{k}})$$

$$= -\frac{1}{2}Un_0N_0 - \frac{1}{2}\sum_{\mathbf{k}}(\epsilon_{\mathbf{k}}+Un_0) + \frac{1}{2}\sum_{\mathbf{k}}(a^{\dagger}_{\mathbf{k}}, a_{\text{-}\mathbf{k}})\cdot((\epsilon_{\mathbf{k}}+Un_0)a_{\mathbf{k}} + Un_0a^{\dagger}_{\text{-}\mathbf{k}}, Un_0a_{\mathbf{k}} + (\epsilon_{\mathbf{k}}+Un_0)a^{\dagger}_{\text{-}\mathbf{k}})$$

$$= -\frac{1}{2}Un_0N_0 - \frac{1}{2}\sum_{\mathbf{k}}(\epsilon_{\mathbf{k}}+Un_0) + \frac{1}{2}\sum_{\mathbf{k}}\begin{pmatrix} a^{\dagger}_{\mathbf{k}} & a_{\text{-}\mathbf{k}} \end{pmatrix}\begin{bmatrix} \epsilon_{\mathbf{k}}+Un_0 & Un_0 \\ Un_0 & \epsilon_{\mathbf{k}}+Un_0 \end{bmatrix}\begin{pmatrix} a_{\mathbf{k}} \\ a^{\dagger}_{\text{-}\mathbf{k}} \end{pmatrix} \tag{6.11}$$

Observe that from 7th to 8th step we used the following facts:

$$\epsilon_{\mathbf{k}} = \sum_{j=1}^{d}\cos(k_ja) = \sum_{j=1}^{d}\cos(-k_ja) = \epsilon_{\text{-}\mathbf{k}} \tag{6.12}$$

$$\sum_{\mathbf{k}} a_{\mathbf{k}}a^{\dagger}_{\mathbf{k}}(\epsilon_{\mathbf{k}}+Un_0) = \sum_{\text{-}\mathbf{k}} a_{\text{-}\mathbf{k}}a^{\dagger}_{\mathbf{k}}(\epsilon_{\mathbf{k}}+Un_0) \tag{6.13}$$

becuase of the last identity and the fact that the sum runs over all possible $\mathbf{k}$ in a symmetric region of the Fourier space, we may change the sign of the label

$$\sum_{\mathbf{k}} Un_0a^{\dagger}_{\text{-}\mathbf{k}}a^{\dagger}_{\mathbf{k}} = \sum_{\mathbf{k}} Un_0a^{\dagger}_{\mathbf{k}}a^{\dagger}_{\text{-}\mathbf{k}} \tag{6.14}$$

We now introduce the new operators $b\dagger_k$ y b_k, for which the Bogoliubov transformation will be applied. The old operators relate with the news through

$$\begin{pmatrix} b_{\mathbf{k}} \\ b^{\dagger}_{\text{-}\mathbf{k}} \end{pmatrix} = \begin{bmatrix} u_{\mathrm{k}} & v_{\mathrm{k}} \\ u^*_{\mathrm{k}} & v^*_{\mathrm{k}} \end{bmatrix}\begin{pmatrix} a_{\mathbf{k}} \\ a^{\dagger}_{\text{-}\mathbf{k}} \end{pmatrix} \tag{6.15}$$

with u's and v's being complex. From there,

$$b_{\mathbf{k}} = u_{\mathbf{k}}a_{\mathbf{k}} + v_{\mathbf{k}}a^{\dagger}_{\text{-}\mathbf{k}}$$

$$b^{\dagger}_{\text{-}\mathbf{k}} = v^*_{\mathbf{k}}a_{\mathbf{k}} + u^*_{\mathbf{k}}a^{\dagger}_{\text{-}\mathbf{k}}$$

and so

$$b_{\text{-}\mathbf{k}} = u_{\text{-}\mathbf{k}}a_{\text{-}\mathbf{k}} + v_{\text{-}\mathbf{k}}a^{\dagger}_{\mathbf{k}}$$

$$b^{\dagger}_{\mathbf{k}} = v^*_{\text{-}\mathbf{k}}a_{\text{-}\mathbf{k}} + u^*_{\text{-}\mathbf{k}}a^{\dagger}_{\mathbf{k}}$$

.

on the other hand

$$b_{\text{-}\mathbf{k}} = (b^{\dagger}_{\text{-}\mathbf{k}})^{\dagger} = (v^{*}_{\mathbf{k}} a_{\mathbf{k}} + u^{*}_{\mathbf{k}} a^{\dagger}_{\text{-}\mathbf{k}})^{\dagger} = v_{\mathbf{k}} a^{\dagger}_{\mathbf{k}} + u_{\mathbf{k}} a_{\text{-}\mathbf{k}}$$

$$b^{\dagger}_{\mathbf{k}} = (u_{\mathbf{k}} a_{\mathbf{k}} + v_{\mathbf{k}} a^{\dagger}_{\text{-}\mathbf{k}})^{\dagger} = u^{*}_{\mathbf{k}} a^{\dagger}_{\mathbf{k}} + v^{*}_{\mathbf{k}} a_{\text{-}\mathbf{k}}$$

Making both expressions equal for operators $b_{\text{-}\mathbf{k}}$ y $b^{\dagger}_{\mathbf{k}}$ it is immediate that $u_{\mathbf{k}} = u_{\text{-}\mathbf{k}}$, $u^{*}_{\mathbf{k}} = u^{*}_{\text{-}\mathbf{k}}$, $v_{\mathbf{k}} = v_{\text{-}\mathbf{k}}$ y $v^{*}_{\mathbf{k}} = v^{*}_{\text{-}\mathbf{k}}$.

In order to assure the new operators obey the bosonic commutation rules:

$$[b_{\mathbf{k}}, b^{\dagger}_{\mathbf{k}}] = b_{\mathbf{k}} b^{\dagger}_{\mathbf{k}} - b^{\dagger}_{\mathbf{k}} b_{\mathbf{k}} = (u_{\mathbf{k}} a_{\mathbf{k}} + v_{\mathbf{k}} a^{\dagger}_{\text{-}\mathbf{k}})(u^{*}_{\mathbf{k}} a^{\dagger}_{\mathbf{k}} + v^{*}_{\mathbf{k}} a_{\text{-}\mathbf{k}}) - (u^{*}_{\mathbf{k}} a^{\dagger}_{\mathbf{k}} + v^{*}_{\mathbf{k}} a_{\text{-}\mathbf{k}})(u_{\mathbf{k}} a_{\mathbf{k}} + v_{\mathbf{k}} a^{\dagger}_{\text{-}\mathbf{k}})$$

$$= |u_{\mathrm{k}}|^2 a_{\mathbf{k}} a^{\dagger}_{\mathbf{k}} + u_{\mathbf{k}} v^{*}_{\mathbf{k}} a_{\mathbf{k}} a_{\text{-}\mathbf{k}} + v_{\mathbf{k}} u^{*}_{\mathbf{k}} a^{\dagger}_{\text{-}\mathbf{k}} a^{\dagger}_{\mathbf{k}} + |v_{\mathbf{k}}|^2 a^{\dagger}_{\text{-}\mathbf{k}} a_{\text{-}\mathbf{k}} - (|u_{\mathrm{k}}|^2 a^{\dagger}_{\mathbf{k}} a_{\mathbf{k}} + u_{\mathbf{k}} v^{*}_{\mathbf{k}} a_{\text{-}\mathbf{k}} a_{\mathbf{k}} + v_{\mathbf{k}} u^{*}_{\mathbf{k}} a^{\dagger}_{\mathbf{k}} a^{\dagger}_{\text{-}\mathbf{k}} + |v_{\mathbf{k}}|^2 a^{\dagger}_{\text{-}\mathbf{k}} a_{\text{-}\mathbf{k}})$$

$$= |u_{\mathbf{k}}|^2 (a_{\mathbf{k}} a^{\dagger}_{\mathbf{k}} - a^{\dagger}_{\mathbf{k}} a_{\mathbf{k}}) + |v_{\mathbf{k}}|^2 (a^{\dagger}_{\text{-}\mathbf{k}} a_{\text{-}\mathbf{k}} - a_{\text{-}\mathbf{k}} a^{\dagger}_{\text{-}\mathbf{k}})$$

$$= |u_{\mathbf{k}}|^2 - |v_{\mathbf{k}}|^2$$

thanks to the commutation rule $[a_{\mathbf{k}}, a^{\dagger}_{\mathbf{s}}] = \delta_{k,s}$. As a result, it must be true that

$$|u_{\mathbf{k}}|^2 - |v_{\mathbf{k}}|^2 = 1, \tag{6.16}$$

and as a consequence, the matrix has inverse and so

$$\begin{pmatrix} a_{\mathbf{k}} & , a^{\dagger}_{\text{-}\mathbf{k}} \end{pmatrix} = \begin{bmatrix} u^{*}_{\mathbf{k}} & -v_{\mathbf{k}} \\ -v^{*}_{\mathbf{k}} & u_{\mathbf{k}} \end{bmatrix} \begin{pmatrix} b_{\mathbf{k}} \\ b^{\dagger}_{\text{-}\mathbf{k}} \end{pmatrix}$$

or equally

$$a_{\mathbf{k}} = u^{*}_{\mathbf{k}} b_{\mathbf{k}} - v_{\mathbf{k}} b^{\dagger}_{\text{-}\mathbf{k}}$$

$$a_{\text{-}\mathbf{k}} = u^{*}_{\mathbf{k}} b_{\text{-}\mathbf{k}} - v_{\mathbf{k}} b^{\dagger}_{\mathbf{k}}$$

$$a^{\dagger}_{\text{-}\mathbf{k}} = -v^{*}_{\mathbf{k}} b_{\mathbf{k}} + u_{\mathbf{k}} b^{\dagger}_{\text{-}\mathbf{k}}$$

$$a^{\dagger}_{\mathbf{k}} = -v^{*}_{\mathbf{k}} b_{\text{-}\mathbf{k}} + u_{\mathbf{k}} b^{\dagger}_{\mathbf{k}}.$$

Inserting 6.15 in 6.11 yields to

$$= -\frac{1}{2}Un_0N_0 - \frac{1}{2}\sum_{\mathbf{k}}(\epsilon_{\mathbf{k}} + Un_0)$$

$$+\frac{1}{2}\sum_{\mathbf{k}}\left(\begin{array}{cc} -v^*_{\mathbf{k}}b_{\text{-}\mathbf{k}} + u_{\mathbf{k}}b^\dagger_{\mathbf{k}} & , u^*_{\mathbf{k}}b_{\text{-}\mathbf{k}} - v_{\mathbf{k}}b^\dagger_{\mathbf{k}} \end{array} \right) \left[\begin{array}{cc} \epsilon_{\mathbf{k}} + Un_0 & Un_0 \\ Un_0 & \epsilon_{\mathbf{k}} + Un_0 \end{array} \right] \left(\begin{array}{c} u^*_{\mathbf{k}}b_{\mathbf{k}} - v_{\mathbf{k}}b^\dagger_{\text{-}\mathbf{k}} \\ -v^*_{\mathbf{k}}b_{\mathbf{k}} + u_{\mathbf{k}}b^\dagger_{\text{-}\mathbf{k}} \end{array} \right)$$

the matrix part is equal to

$$\begin{aligned} &= A[(-v^*_{\mathbf{k}}b_{\text{-}\mathbf{k}} + u_{\mathbf{k}}b^\dagger_{\mathbf{k}})(u^*_{\mathbf{k}}b_{\mathbf{k}} - v_{\mathbf{k}}b^\dagger_{\text{-}\mathbf{k}}) + (u^*_{\mathbf{k}}b_{\text{-}\mathbf{k}} - v_{\mathbf{k}}b^\dagger_{\mathbf{k}})(-v^*_{\mathbf{k}}b_{\mathbf{k}} + u_{\mathbf{k}}b^\dagger_{\text{-}\mathbf{k}})] \\ &+B[(-v^*_{\mathbf{k}}b_{\text{-}\mathbf{k}} + u_{\mathbf{k}}b^\dagger_{\mathbf{k}})(-v^*_{\mathbf{k}}b_{\mathbf{k}} + u_{\mathbf{k}}b^\dagger_{\text{-}\mathbf{k}})] + (u^*_{\mathbf{k}}b_{\text{-}\mathbf{k}} - v_{\mathbf{k}}b^\dagger_{\mathbf{k}})(u^*_{\mathbf{k}}b_{\mathbf{k}} - v_{\mathbf{k}}b^\dagger_{\text{-}\mathbf{k}}) \end{aligned}$$

$$A[-b_{\text{-}\mathbf{k}}b_{\mathbf{k}}v^*_{\mathbf{k}}u^*_{\mathbf{k}}+b_{\text{-}\mathbf{k}}b^\dagger_{\text{-}\mathbf{k}}v^*_{\mathbf{k}}v_{\mathbf{k}}+b^\dagger_{\mathbf{k}}b_{\mathbf{k}}u_{\mathbf{k}}u^*_{\mathbf{k}}-b^\dagger_{\mathbf{k}}b^\dagger_{\text{-}\mathbf{k}}u_{\mathbf{k}}v_{\mathbf{k}}-b_{\text{-}\mathbf{k}}b_{\mathbf{k}}u_{\mathbf{k}}v^*_{\mathbf{k}}+b_{\text{-}\mathbf{k}}b^\dagger_{\text{-}\mathbf{k}}u_{\mathbf{k}}u_{\mathbf{k}}+b^\dagger_{\mathbf{k}}b_{\mathbf{k}}v_{\mathbf{k}}v^*_{\mathbf{k}}-b^\dagger_{\mathbf{k}}b^\dagger_{\text{-}\mathbf{k}}v_{\mathbf{k}}u_{\mathbf{k}}]$$

$$+B[-b_{\text{-}\mathbf{k}}b_{\mathbf{k}}v^*_{\mathbf{k}}v^*_{\mathbf{k}}+b_{\text{-}\mathbf{k}}b^\dagger_{\text{-}\mathbf{k}}v^*_{\mathbf{k}}u_{\mathbf{k}}+b^\dagger_{\mathbf{k}}b_{\mathbf{k}}u_{\mathbf{k}}v^*_{\mathbf{k}}-b^\dagger_{\mathbf{k}}b^\dagger_{\text{-}\mathbf{k}}u_{\mathbf{k}}u_{\mathbf{k}}-b_{\text{-}\mathbf{k}}b_{\mathbf{k}}u^*_{\mathbf{k}}u^*_{\mathbf{k}}+b_{\text{-}\mathbf{k}}b^\dagger_{\text{-}\mathbf{k}}u^*_{\mathbf{k}}v_{\mathbf{k}}+b^\dagger_{\mathbf{k}}b_{\mathbf{k}}v_{\mathbf{k}}u^*_{\mathbf{k}}-b^\dagger_{\mathbf{k}}b^\dagger_{\text{-}\mathbf{k}}v^*_{\mathbf{k}}u^*_{\mathbf{k}}]$$

$$\begin{aligned} &= -b_{\text{-}\mathbf{k}}b_{\mathbf{k}}[-A(v^*_{\mathbf{k}}u^*_{\mathbf{k}}+u^*_{\mathbf{k}}v^*_{\mathbf{k}})+B(v^*_{\mathbf{k}}v^*_{\mathbf{k}}+u^*_{\mathbf{k}}u^*_{\mathbf{k}})]+b^\dagger_{\mathbf{k}}b^\dagger_{\text{-}\mathbf{k}}[-A(u_{\mathbf{k}}v_{\mathbf{k}}+v_{\mathbf{k}}u_{\mathbf{k}})+B(u_{\mathbf{k}}u_{\mathbf{k}}+v_{\mathbf{k}}v_{\mathbf{k}})] \\ &+b^\dagger_{\mathbf{k}}b_{\mathbf{k}}[A(u_{\mathbf{k}}u^*_{\mathbf{k}} + v_{\mathbf{k}}v^*_{\mathbf{k}}) - B(u_{\mathbf{k}}v^*_{\mathbf{k}} + v_{\mathbf{k}}u^*_{\mathbf{k}})] + b_{\text{-}\mathbf{k}}b^\dagger_{\text{-}\mathbf{k}}[A(v^*_{\mathbf{k}}v_{\mathbf{k}} + u^*_{\mathbf{k}}u_{\mathbf{k}}) - B(v^*_{\mathbf{k}}u_{\mathbf{k}}) + u^*_{\mathbf{k}}v_{\mathbf{k}}] \end{aligned}$$

$$\begin{aligned} &= -b_{\text{-}\mathbf{k}}b_{\mathbf{k}}[-A(2u^*_{\mathbf{k}}v^*_{\mathbf{k}}) + B((v^*_{\mathbf{k}})^2 + (u^*_{\mathbf{k}})^2)] + b^\dagger_{\mathbf{k}}b^\dagger_{\text{-}\mathbf{k}}[-A(2u_{\mathbf{k}}v_{\mathbf{k}}) + B((u_{\mathbf{k}})^2 + (v_{\mathbf{k}})^2)] \\ &+b^\dagger_{\mathbf{k}}b_{\mathbf{k}}[A(|u_{\mathbf{k}}|^2 + |v_{\mathbf{k}}|^2) - B(u_{\mathbf{k}}v^*_{\mathbf{k}} + v_{\mathbf{k}}u^*_{\mathbf{k}})] + b_{\text{-}\mathbf{k}}b^\dagger_{\text{-}\mathbf{k}}[A(|v_{\mathbf{k}}|^2 + |u^*_{\mathbf{k}}|^2) - B(u_{\mathbf{k}}v^*_{\mathbf{k}} + v_{\mathbf{k}})u^*_{\mathbf{k}}] \end{aligned}$$

being $A = \epsilon_{\mathbf{k}} + Un_0$ and $B = Un_0$. Introducing the sum

$$\begin{aligned} &= -\frac{1}{2}Un_0N_0 - \frac{1}{2}\sum_{\mathbf{k}}(\epsilon_{\mathbf{k}} + Un_0)+ \\ &\frac{1}{2}\sum_{\mathbf{k}} -b_{\text{-}\mathbf{k}}b_{\mathbf{k}}[-A(2u^*_{\mathbf{k}}v^*_{\mathbf{k}}) + B((v^*_{\mathbf{k}})^2 + (u^*_{\mathbf{k}})^2)] + b^\dagger_{\mathbf{k}}b^\dagger_{\text{-}\mathbf{k}}[-A(2u_{\mathbf{k}}v_{\mathbf{k}}) + B((u_{\mathbf{k}})^2 + (v_{\mathbf{k}})^2)] \\ &+b^\dagger_{\mathbf{k}}b_{\mathbf{k}}[A(|u_{\mathbf{k}}|^2 + |v_{\mathbf{k}}|^2) - B(u_{\mathbf{k}}v^*_{\mathbf{k}} + v_{\mathbf{k}}u^*_{\mathbf{k}})] + b_{\text{-}\mathbf{k}}b^\dagger_{\text{-}\mathbf{k}}[A(|v_{\mathbf{k}}|^2 + |u^*_{\mathbf{k}}|^2) - B(u_{\mathbf{k}}v^*_{\mathbf{k}} + v_{\mathbf{k}})u^*_{\mathbf{k}}] \end{aligned}$$

$$= -\frac{1}{2}Un_0N_0 - \frac{1}{2}\sum_{\mathbf{k}}(\epsilon_{\mathbf{k}} + Un_0) +$$

$$\frac{1}{2}\sum_{\mathbf{k}} -b_{\text{-}\mathbf{k}}b_{\mathbf{k}}[-A(2u^*_{\mathbf{k}}v^*_{\mathbf{k}}) + B((v^*_{\mathbf{k}})^2 + (u^*_{\mathbf{k}})^2)] + b^\dagger_{\mathbf{k}}b^\dagger_{\text{-}\mathbf{k}}[-A(2u_{\mathbf{k}}v_{\mathbf{k}}) + B((u_{\mathbf{k}})^2 + (v_{\mathbf{k}})^2)]$$

$$+b^\dagger_{\mathbf{k}}b_{\mathbf{k}}[A(|u_{\mathbf{k}}|^2 + |v_{\mathbf{k}}|^2) - B(u_{\mathbf{k}}v^*_{\mathbf{k}} + v_{\mathbf{k}}u^*_{\mathbf{k}})] +$$
$$b_{\mathbf{k}}b^\dagger_{\mathbf{k}}[A(|v_{\mathbf{k}}|^2 + |u^*_{\mathbf{k}}|^2) - B(u_{\mathbf{k}}v^*_{\mathbf{k}} + v_{\mathbf{k}})u^*_{\mathbf{k}}]$$

$$= -\frac{1}{2}Un_0N_0 - \frac{1}{2}\sum_{\mathbf{k}}(\epsilon_{\mathbf{k}} + Un_0) +$$

$$\frac{1}{2}\sum_{\mathbf{k}} -b_{\text{-}\mathbf{k}}b_{\mathbf{k}}[-A(2u^*_{\mathbf{k}}v^*_{\mathbf{k}}) + B((v^*_{\mathbf{k}})^2 + (u^*_{\mathbf{k}})^2)] + b^\dagger_{\mathbf{k}}b^\dagger_{\text{-}\mathbf{k}}[-A(2u_{\mathbf{k}}v_{\mathbf{k}}) + B((u_{\mathbf{k}})^2 + (v_{\mathbf{k}})^2)]$$

$$+b^\dagger_{\mathbf{k}}b_{\mathbf{k}}[A(|u_{\mathbf{k}}|^2 + |v_{\mathbf{k}}|^2) - B(u_{\mathbf{k}}v^*_{\mathbf{k}} + v_{\mathbf{k}}u^*_{\mathbf{k}})] +$$
$$(1 + b^\dagger_{\mathbf{k}}b_{\mathbf{k}})[A(|v_{\mathbf{k}}|^2 + |u^*_{\mathbf{k}}|^2) - B(u_{\mathbf{k}}v^*_{\mathbf{k}} + v_{\mathbf{k}})u^*_{\mathbf{k}}]$$

$$= -\frac{1}{2}Un_0N_0 - \frac{1}{2}\sum_{\mathbf{k}}(\epsilon_{\mathbf{k}} + Un_0) +$$

$$\frac{1}{2}\sum_{\mathbf{k}} -b_{\text{-}\mathbf{k}}b_{\mathbf{k}}[-A(2u^*_{\mathbf{k}}v^*_{\mathbf{k}}) + B((v^*_{\mathbf{k}})^2 + (u^*_{\mathbf{k}})^2)] + b^\dagger_{\mathbf{k}}b^\dagger_{\text{-}\mathbf{k}}[-A(2u_{\mathbf{k}}v_{\mathbf{k}}) + B((u_{\mathbf{k}})^2 + (v_{\mathbf{k}})^2)]$$

$$+2b^\dagger_{\mathbf{k}}b_{\mathbf{k}}[A(|u_{\mathbf{k}}|^2 + |v_{\mathbf{k}}|^2) - B(u_{\mathbf{k}}v^*_{\mathbf{k}} + v_{\mathbf{k}}u^*_{\mathbf{k}})]$$
$$+[A(|v_{\mathbf{k}}|^2 + |u^*_{\mathbf{k}}|^2) - B(u_{\mathbf{k}}v^*_{\mathbf{k}} + v_{\mathbf{k}})u^*_{\mathbf{k}}]$$

$$= -\frac{1}{2}Un_0N_0 - \frac{1}{2}\sum_{\mathbf{k}}(\epsilon_{\mathbf{k}} + Un_0) +$$

$$\frac{1}{2}\sum_{\mathbf{k}} -b_{\text{-}\mathbf{k}}b_{\mathbf{k}}[-A(2u^*_{\mathbf{k}}v^*_{\mathbf{k}}) + B((v^*_{\mathbf{k}})^2 + (u^*_{\mathbf{k}})^2)] + b^\dagger_{\mathbf{k}}b^\dagger_{\text{-}\mathbf{k}}[-A(2u_{\mathbf{k}}v_{\mathbf{k}}) + B((u_{\mathbf{k}})^2 + (v_{\mathbf{k}})^2)]$$

$$+[A(|v_{\mathbf{k}}|^2 + |u^*_{\mathbf{k}}|^2) - B(u_{\mathbf{k}}v^*_{\mathbf{k}} + v_{\mathbf{k}})u^*_{\mathbf{k}}] + \sum_{\mathbf{k}} b^\dagger_{\mathbf{k}}b_{\mathbf{k}}[A(|u_{\mathbf{k}}|^2 + |v_{\mathbf{k}}|^2) - B(u_{\mathbf{k}}v^*_{\mathbf{k}} + v_{\mathbf{k}}u^*_{\mathbf{k}})].$$

Requesting this to be equal to

$$-\frac{1}{2}Un_0N_0 - \frac{1}{2}\sum_{\mathbf{k}}[\hbar\omega_{\mathbf{k}} - (\epsilon_{\mathbf{k}} + Un_0)] + \sum_{\mathbf{k}}\hbar\omega_{\mathbf{k}}b^\dagger_{\mathbf{k}}b_{\mathbf{k}} \tag{6.17}$$

is to request the coefficients of each pair of operators to be equal, and is straight that

$$A(-2u^*_{\mathbf{k}}v^*_{\mathbf{k}}) + B((v^*_{\mathbf{k}})^2 + (u^*_{\mathbf{k}})^2) = 0 \tag{6.18}$$

$$A(-2u_{\mathbf{k}}v_{\mathbf{k}}) + B((v_{\mathbf{k}})^2 + (u_{\mathbf{k}})^2) = 0 \tag{6.19}$$

$$A(|u_{\mathbf{k}}|^2 + |v_{\mathbf{k}}|^2) - B(u_{\mathbf{k}}v_{\mathbf{k}}^* + v_{\mathbf{k}}u_{\mathbf{k}}^*) = \hbar\omega_{\mathbf{k}} \tag{6.20}$$

Note that 6.18 and 6.19 are complex conjugates which leaves an equation system for A and B

$$A(-2u_{\mathbf{k}}v_{\mathbf{k}}) + B((v_{\mathbf{k}})^2 + (u_{\mathbf{k}})^2) = 0$$
$$A(2|v_{\mathbf{k}}|^2 + 1) - B(u_{\mathbf{k}}v_{\mathbf{k}}^* + v_{\mathbf{k}}u_{\mathbf{k}}^*) = \hbar\omega_{\mathbf{k}}$$

$$A(-2u_{\mathbf{k}}v_{\mathbf{k}}) + B((v_{\mathbf{k}})^2 + (u_{\mathbf{k}})^2) = 0$$
$$A(2|v_{\mathbf{k}}|^2) - B(u_{\mathbf{k}}v_{\mathbf{k}}^* + v_{\mathbf{k}}u_{\mathbf{k}}^*) = \hbar\omega_{\mathbf{k}} - A$$

substituting A and B

$$(\epsilon_{\mathbf{k}} + Un_0)(-2u_{\mathbf{k}}v_{\mathbf{k}}) + Un_0((v_{\mathbf{k}})^2 + (u_{\mathbf{k}})^2) = 0$$
$$(\epsilon_{\mathbf{k}} + Un_0)(2|v_{\mathbf{k}}|^2) - Un_0(u_{\mathbf{k}}v_{\mathbf{k}}^* + v_{\mathbf{k}}u_{\mathbf{k}}^*) = \hbar\omega_{\mathbf{k}} - (\epsilon_{\mathbf{k}} + Un_0)$$

The determinant of the associated matrix is

$$\Delta = (2u_{\mathbf{k}}v_{\mathbf{k}})(u_{\mathbf{k}}v_{\mathbf{k}}^* + v_{\mathbf{k}}u_{\mathbf{k}}^*) - ((u_{\mathbf{k}})^2 + (v_{\mathbf{k}})^2)(2|v_{\mathbf{k}}|^2)$$
$$= 2(u_{\mathbf{k}})^2|v_{\mathbf{k}}|^2 + 2(v_{\mathbf{k}})^2|u_{\mathbf{k}}|^2 - 2|v_{\mathbf{k}}|^2(u_{\mathbf{k}})^2 - 2|v_{\mathbf{k}}|^2(v_{\mathbf{k}})^2$$
$$= 2(v_{\mathbf{k}})^2(|u_{\mathbf{k}}|^2 - |v_{\mathbf{k}}|^2) = 2(v_{\mathbf{k}})^2$$

and one obtains

$$Un_0 = \frac{(-2u_{\mathbf{k}}v_{\mathbf{k}})(\hbar\omega_{\mathbf{k}} - (\epsilon_{\mathbf{k}} + Un_0)))}{2(v_{\mathbf{k}})^2)} \tag{6.21}$$

so

$$v_{\mathbf{k}} = -\frac{\hbar\omega_{\mathbf{k}} - (\epsilon_{\mathbf{k}} + Un_0)}{Un_0}u_{\mathbf{k}} \tag{6.22}$$

For the other variable we have

$$\epsilon_{\mathbf{k}} + Un_0 = -\frac{((u_{\mathbf{k}})^2 + (v_{\mathbf{k}})^2)(\hbar\omega_{\mathbf{k}} - (\epsilon_{\mathbf{k}} + Un_0))}{2(v_{\mathbf{k}})^2)} \tag{6.23}$$

then

$$-2(v_{\mathbf{k}})^2)(\epsilon_{\mathbf{k}} + Un_0) = ((u_{\mathbf{k}})^2 + (v_{\mathbf{k}})^2)(\hbar\omega_{\mathbf{k}} - (\epsilon_{\mathbf{k}} + Un_0))$$

and

$$0 = (u_{\mathbf{k}})^2(\hbar\omega_{\mathbf{k}} - (\epsilon_{\mathbf{k}} + Un_0)) + (v_{\mathbf{k}})^2(\hbar\omega_{\mathbf{k}} + (\epsilon_{\mathbf{k}} + Un_0))$$

using 6.22,

$$0 = (u_{\mathbf{k}})^2(\hbar\omega_{\mathbf{k}} - (\epsilon_{\mathbf{k}} + Un_0)) + (u_{\mathbf{k}})^2\frac{(\hbar\omega_{\mathbf{k}} - (\epsilon_{\mathbf{k}} + Un_0))^2}{(Un_0)^2}(\hbar\omega_{\mathbf{k}} + (\epsilon_{\mathbf{k}} + Un_0))$$

then

$$0 = (Un_0)^2 + (\hbar\omega_{\mathbf{k}} - (\epsilon_{\mathbf{k}} + Un_0))(\hbar\omega_{\mathbf{k}} + (\epsilon_{\mathbf{k}} + Un_0))$$

Next, we divide by $(\hbar\omega_{\mathbf{k}} - (\epsilon_{\mathbf{k}} + Un_0)) \neq 0$

$$0 = (Un_0)^2 + (\hbar\omega_{\mathbf{k}})^2 - (\epsilon_{\mathbf{k}} + Un_0)^2$$

to find

$$0 = (Un_0)^2 + (\hbar\omega_{\mathbf{k}})^2 + -(\epsilon_{\mathbf{k}})^2 - 2\epsilon_{\mathbf{k}}Un_0 - (Un_0)^2$$

and finally,

$$\hbar\omega_{\mathbf{k}} = \sqrt{\epsilon_{\mathbf{k}}^2 + 2\epsilon_{\mathbf{k}}Un_0} \tag{6.24}$$

Lastly, note that we have the equation

$$(\epsilon_{\mathbf{k}} + Un_0)(2|v_{\mathbf{k}}|^2) - Un_0(u_{\mathbf{k}}v_{\mathbf{k}}^* + v_{\mathbf{k}}u_{\mathbf{k}}^*) = \hbar\omega_{\mathbf{k}} - (\epsilon_{\mathbf{k}} + Un_0)$$

$$= 2(\epsilon_{\mathbf{k}} + Un_0)(|v_{\mathbf{k}}|^2 - 1) + Un_0(u_{\mathbf{k}}u_{\mathbf{k}}^*\frac{(\hbar\omega_{\mathbf{k}} - (\epsilon_{\mathbf{k}} + Un_0))}{Un_0} + u_{\mathbf{k}}^*u_{\mathbf{k}}\frac{(\hbar\omega_{\mathbf{k}} - (\epsilon_{\mathbf{k}} + Un_0))}{Un_0})$$

$$2(\epsilon_{\mathbf{k}} + Un_0)(|u_{\mathbf{k}}|^2 - 1) + 2|u_{\mathbf{k}}|^2(\hbar\omega_{\mathbf{k}} - (\epsilon_{\mathbf{k}} + Un_0)) = \hbar\omega_{\mathbf{k}} - (\epsilon_{\mathbf{k}} + Un_0)$$

$$2|u_{\mathbf{k}}|^2(\hbar\omega_{\mathbf{k}} - (\epsilon_{\mathbf{k}} + Un_0) + (\epsilon_{\mathbf{k}} + Un_0)) - 2(\epsilon_{\mathbf{k}} + Un_0) = \hbar\omega_{\mathbf{k}} - \epsilon_{\mathbf{k}} + Un_0$$

so

$$2|u_{\mathbf{k}}|^2\hbar\omega_{\mathbf{k}} = \hbar\omega_{\mathbf{k}} + \epsilon_{\mathbf{k}} + Un_0$$

thus

$$|u_{\mathbf{k}}|^2 = \frac{1}{2}(1 + \frac{\epsilon_{\mathbf{k}} + Un_0}{\hbar\omega_{\mathbf{k}}})$$

$$|v_{\mathbf{k}}|^2 = |u_{\mathbf{k}}|^2 - 1 = \frac{1}{2}(\frac{\epsilon_{\mathbf{k}} + Un_0}{\hbar\omega_{\mathbf{k}}} - 1)$$

Following with the general calculation, we focus in to know the density of the condensate n_0, which requires to know the total density n in terms of the effective Hamiltonian

$$n = \frac{1}{N_s}\sum_{\mathbf{k}} \left\langle a^\dagger_{\mathbf{k}} a_{\mathbf{k}} \right\rangle_{H^{eff}} \tag{6.25}$$

we separate n_0 since the beginning

$$= n_0 + \frac{1}{N_s}\sum_{\mathbf{k}\neq 0} \left\langle a^\dagger_{\mathbf{k}} a_{\mathbf{k}} \right\rangle_{H^{eff}}$$

and writing this in terms of 6.15 then

$$= n_0 + \frac{1}{N_s}\sum_{\mathbf{k}\neq 0} \left\langle (-v^*_{\mathbf{k}} b_{\text{-}\mathbf{k}} + u_{\mathbf{k}} b^\dagger_{\mathbf{k}})(u^*_{\mathbf{k}} b_{\mathbf{k}} - v_{\mathbf{k}} b^\dagger_{\text{-}\mathbf{k}}) \right\rangle_{H^{eff}}$$

$$= n_0 + \sum_{\mathbf{k}\neq 0} \langle -v^*_{\mathbf{k}} u^*_{\mathbf{k}} b_{\text{-}\mathbf{k}} b_{\mathbf{k}} \rangle_{H^{eff}} + \left\langle v^*_{\mathbf{k}} v_{\mathbf{k}} b_{\text{-}\mathbf{k}} b^\dagger_{\text{-}\mathbf{k}} \right\rangle_{H^{eff}} + \left\langle u_{\mathbf{k}} u^*_{\mathbf{k}} b_{\mathbf{k}} b^\dagger_{\mathbf{k}} \right\rangle_{H^{eff}} + \left\langle u_{\mathbf{k}} v_{\mathbf{k}} b^\dagger_{\mathbf{k}} b^\dagger_{\text{-}\mathbf{k}} \right\rangle_{H^{eff}}$$

where the operatores $b_{\text{-}\mathbf{k}} b_{\mathbf{k}}$ and $b^\dagger_{\mathbf{k}} b^\dagger_{\text{-}\mathbf{k}}$ are always 0, since they lead to products of orthogonal states for all $\mathbf{k} \neq 0$, obtaining then

$$n = n_0 + \sum_{\mathbf{k}\neq 0} \left\langle |v_{\mathbf{k}}|^2 b_{\text{-}\mathbf{k}} b^\dagger_{\text{-}\mathbf{k}} \right\rangle_{H^{eff}} + \left\langle |u_{\mathbf{k}}|^2 b_{\mathbf{k}} b^\dagger_{\mathbf{k}} \right\rangle_{H^{eff}}$$

$$= n_0 + \sum_{\mathbf{k}\neq 0} \left\langle |v_{\mathbf{k}}|^2 b_{\mathbf{k}} b^\dagger_{\mathbf{k}} \right\rangle_{H^{eff}} + \left\langle |u_{\mathbf{k}}|^2 b_{\mathbf{k}} b^\dagger_{\mathbf{k}} \right\rangle_{H^{eff}}$$

$$= n_0 + \sum_{\mathbf{k}\neq 0} |v_{\mathbf{k}}|^2 \left\langle b_{\mathbf{k}} b^\dagger_{\mathbf{k}} \right\rangle_{H^{eff}} + |u_{\mathbf{k}}|^2 \left\langle b_{\mathbf{k}} b^\dagger_{\mathbf{k}} \right\rangle_{H^{eff}}$$

$$= n_0 + \sum_{\mathbf{k}\neq 0} |v_{\mathbf{k}}|^2 \left\langle 1 + b^\dagger_{\mathbf{k}} b_{\mathbf{k}} \right\rangle_{H^{eff}} + |u_{\mathbf{k}}|^2 \left\langle b_{\mathbf{k}} b^\dagger_{\mathbf{k}} \right\rangle_{H^{eff}}$$

and so

$$n = n_0 + \sum_{\mathbf{k}\neq 0} [(|v_{\mathbf{k}}|^2 + |u_{\mathbf{k}}|^2) \left\langle b^\dagger_{\mathbf{k}} b_{\mathbf{k}} \right\rangle_{H^{eff}} + |v_{\mathbf{k}}|^2]$$

inserting the values of $|u_{\mathbf{k}}|^2$ y $|v_{\mathbf{k}}|^2$

$$n = n_0 + \sum_{\mathbf{k}\neq 0}[(\frac{1}{2}\frac{\epsilon_{\mathbf{k}+Un_0}}{\hbar\omega_{\mathbf{k}}} + 1 + \frac{1}{2}\frac{\epsilon_{\mathbf{k}+Un_0}}{\hbar\omega_{\mathbf{k}}} - 1)\left\langle b^\dagger_{\mathbf{k}} b_{\mathbf{k}}\right\rangle_{H^{eff}} + \frac{1}{2}\frac{\epsilon_{\mathbf{k}+Un_0}}{\hbar\omega_{\mathbf{k}}} - 1]$$

and inserting $\left\langle b^\dagger_{\mathbf{k}} b_{\mathbf{k}}\right\rangle_{H^{eff}}$, the Bose distribution evaluated in $\hbar\omega_{\mathbf{k}}$ it follows that

$$n = n_0 + \sum_{\mathbf{k}\neq 0}[(\frac{\epsilon_{\mathbf{k}+Un_0}}{\hbar\omega_{\mathbf{k}}})(\frac{1}{e^{\beta\hbar\omega_{\mathbf{k}}} - 1}) + \frac{\epsilon_{\mathbf{k}+Un_0-\hbar\omega_{\mathbf{k}}}}{2\hbar\omega_{\mathbf{k}}}] \tag{6.26}$$

In the limit where $T = 0$ we have $\beta \to \infty$, therefore $\frac{1}{e^{\beta\hbar\omega_{\mathbf{k}}-1}} \to 0$ for all $\mathbf{k} \neq 0$, finding the density

$$n = n_0 + \sum_{\mathbf{k}\neq 0}[\frac{\epsilon_{\mathbf{k}} + Un_0 - \hbar\omega_{\mathbf{k}}}{2\hbar\omega_{\mathbf{k}}}] \tag{6.27}$$

and for the continuous limit for $\mathbf{k}$ we must do $\sum_{\mathbf{k}} \to V\int_{-\frac{\pi}{a}}^{\frac{\pi}{a}} d\mathbf{k}/(2\pi)^d$, then

$$n = n_0 + V\int_{-\frac{\pi}{a}}^{\frac{\pi}{a}} \frac{\epsilon_{\mathbf{k}} + Un_0 - \hbar\omega_{\mathbf{k}}}{2\hbar\omega_{\mathbf{k}}}\frac{d\mathbf{k}}{(2\pi)^d} \tag{6.28}$$

taking the variable change $\mathbf{k} = \frac{2\pi}{a}\mathbf{q}$ we find for $\bar{\epsilon}_{\mathbf{k}} = 2t\sum_{j=1}^d \cos(k_j a) \to \bar{\epsilon}_{\mathbf{q}} = 2t\sum_{j=1}^d \cos(2\pi q_j)$, hence $\epsilon_{\mathbf{k}} = zt - 2t\sum_{j=1}^d \cos(k_j a) = 2t(d - 2t\sum_{j=1}^d \cos(k_j a)) = 2t\sum_{j=1}^d [1-\cos(k_j a)] \to \epsilon_{\mathbf{q}} = 2t\sum_{j=1}^d [1-\cos(2\pi q_j)]$ and it's clear that $\hbar\omega_{\mathbf{k}} = \sqrt{\epsilon_{\mathbf{k}^2+2\epsilon_{\mathbf{k}}Un_0}} \to \hbar\omega_{\mathbf{q}} = \sqrt{\epsilon_{\mathbf{q}^2+2\epsilon_{\mathbf{q}}Un_0}}$ remains unchanged and the integral is now

$$n = n_0 + V\int_{-\frac{1}{2}}^{\frac{1}{2}} \frac{\epsilon_{\mathbf{q}} + Un_0 - \hbar\omega_{\mathbf{q}}}{2\hbar\omega_{\mathbf{q}}} d\mathbf{q}(\frac{2\pi}{a})^d \frac{1}{(2\pi)^d}$$

modifying the integration limits in such a manner that $k_j = \pm\pi/a$ and then $q_j = \pm 1/2$. Knowing that $N_s = V/(a^d)$ then in the end the density will be

$$n = n_0 + \frac{N_s}{2}\int_{-\frac{1}{2}}^{\frac{1}{2}} (\frac{\epsilon_{\mathbf{q}} + Un_0}{\hbar\omega_{\mathbf{q}}} - 1)d\mathbf{q} \tag{6.29}$$

Given that $\epsilon_{\mathbf{q}} = 2t\sum_{j=1}^d [1 - \cos(2\pi q_j)]$ and, in general, $1 - \cos(x) \leq \frac{x^2}{2}$ then $1 - \cos(2\pi q_j) \leq \frac{4\pi^2 q_j^2}{2}$, and $\epsilon_{\mathbf{q}} \leq 2t\sum_{j=1}^d 4\pi^2 q_j^2 = 4\pi^2 t\sum_{j=1}^d q_j^2 = 4\pi^2|\mathbf{q}|^2 t$.

Now, if we take the limit $U/t \to \infty$ the more weighted terms in $\frac{\epsilon_{\mathbf{q}}+Un_0}{\hbar\omega_{\mathbf{k}}+2\epsilon_{\mathbf{q}}Un_0}$ are those including U so

$$\frac{\epsilon_{\mathbf{q}} + Un_0}{\sqrt{\hbar\omega_{\mathbf{k}} + 2\epsilon_{\mathbf{q}}Un_0}} \to_{\frac{U}{t}\to\infty} \frac{Un_0}{\sqrt{2\epsilon_{\mathbf{q}}Un_0}} = \sqrt{\frac{Un_0}{2\epsilon_{\mathbf{q}}}}$$

and taking into account that

$$\epsilon_{\mathbf{q}} \leq 4\pi^2|\mathbf{q}|^2 t$$

then

$$\sqrt{\frac{1}{4\pi^2|\mathbf{q}|^2 t}} \leq \sqrt{\frac{1}{\epsilon_{\mathbf{q}}}}$$

therfore,

$$\frac{1}{2\pi|\mathbf{q}|}\sqrt{\frac{Un_0}{2t}} \leq \frac{\epsilon_{\mathbf{q}} + Un_0}{\sqrt{\hbar\omega_{\mathbf{k}} + 2\epsilon_{\mathbf{q}} Un_0}}.$$

From this is clear that

$$\frac{1}{2\pi}\sqrt{\frac{Un_0}{2t}} \int_{-\frac{1}{2}}^{\frac{1}{2}} \frac{d\mathbf{q}}{|\mathbf{q}|} \leq \int_{-\frac{1}{2}}^{\frac{1}{2}} \frac{\epsilon_{\mathbf{q}} + Un_0}{\sqrt{\hbar\omega_{\mathbf{k}} + 2\epsilon_{\mathbf{q}} Un_0}} \tag{6.30}$$

for this tendence of U/t. Calling I_d to the result of the integral in the left for d dimensions and considering that $\int_{-1/2}^{1/2} d\mathbf{q} = \prod_{j=1}^{d} \int_{-1/2}^{1/2} dq_j = \prod_{j=1}^{d}(1/2 + 1/2) = 1$ one may arrive to

$$n \approx n_0 + \frac{1}{2}\frac{1}{2\pi}\sqrt{\frac{Un_0}{2t}} I_d - \frac{1}{2} = n_0 + \frac{1}{4\pi}\sqrt{\frac{Un_0}{2t}} I_d - \frac{1}{2} \tag{6.31}$$

which is a quadratic equation for $\sqrt{n_0}$

$$0 = n_0 + \frac{1}{2}\frac{1}{2\pi}\sqrt{\frac{Un_0}{2t}} I_d - \frac{1}{2} - n$$

whose solution is

$$\sqrt{n_0} = \frac{-\frac{1}{4\pi}\sqrt{\frac{U}{2t}} I_d + \sqrt{\frac{1}{16\pi^2}\frac{U}{2t} I_d^2 + 4(\frac{1}{2} + n)}}{2}$$

,

thus,

$$n_0 = \left(\frac{1}{2}\sqrt{\frac{I_d^2}{16\pi^2}\frac{U}{2t} + 4n + 2} - \frac{I_d}{8\pi}\sqrt{\frac{U}{2t}}\right)^2$$

And note that $n_0 \to 0$ if $U/t \to \infty$ which is almost the expected behavior. When this limit is taken it is equivalent to drop the hopping parameter and thus, physically we expect that the condensate fraction n_0/n go to zero for some finite critial value of U/t since Mott Insulator is a real phase, but judging by equation

References

[1] Bloch, I., Dalibard, J. and Nascimbène, S. Quantum simulations with ultracold quantum gases. Nature Phys 8, 267–276 (2012).

[2] Zohar E., Cirac J. I., and Reznik B. Quantum simulations of lattice gauge theories using ultracold atoms in optical lattices. Rep. Prog. Phys. 79 014401 (2016).

[3] Barbarino S., Taddia L., Rossini D., Mazza L., and Fazio R. Synthetic gauge fields in synthetic dimensions: interactions and chiral edge modes. New J. Phys. 18 035010 (2016).

[4] Zohar E., Cirac J. I., and Reznik B. Cold-Atom Quantum Simulator for SU(2) Yang-Mills Lattice Gauge Theory. Phys. Rev. Lett. 110, 125304 (2013).

[5] Miguel A Cazalilla and Ana Maria Rey. Ultracold Fermi gases with emergent SU(N) symmetry. Rep. Prog. Phys. 77 124401. (2014).

[6] Jotzu, G., Messer, M., Desbuquois, R. et al. Experimental realization of the topological Haldane model with ultracold fermions. Nature 515, 237–240 (2014).

[7] Miyake H., Siviloglou G. A., Kennedy C. J., Burton W. C., and Ketterle W. Realizing the Harper Hamiltonian with Laser-Assisted Tunneling in Optical Lattices. Phys. Rev. Lett. 111, 199903. (2013).

[8] Kroeze R. M., Guo Y., and Lev B. L. Dynamical Spin-Orbit Coupling of a Quantum Gas. Phys. Rev. Lett. 123, 160404 (2019).

[9] Aidelsburger, M., Lohse, M., Schweizer, C. et al. Measuring the Chern number of Hofstadter bands with ultracold bosonic atoms. Nature Phys 11, 162–166 (2015).

[10] Ivanov D. A., Ivanova T. Y,Caballero-Benitez S. F., and Mekhov I. B. Feedback-Induced Quantum Phase Transitions Using Weak Measurements. Phys. Rev. Lett. 124, 010603. (2020).

[11] S. F. Caballero-Benítez, G. Mazzucchi, and I. B. Mekhov. Quantum simulators based on the global collective light-matter interactions. Phys. Rev. A 93, 0636632 (2016).

[12] D. Jaksch, C. Bruder, J. I. Cirac, C. W. Gardiner, and P. Zoller. Cold Bosonic Atoms in Optical Lattices. Phys. Rev. Lett. 81, 3108, (1998).

[13] D. van Oosten, P. van der Straten, and H. T. C. Stoof. Quantum phases in an optical lattice. Phys. Rev. A 63, 053601 (2001).

[14] M. Raizen, C. Salomon, and Q. Niu, Phys. New Light on Quantum Transport. Today 50, No. 7, 30 (1997).

[15] S. Friebel et al. CO_2-laser optical lattice with cold rubidium atoms. Phys. Rev. A 57, R20 (1998)

[16] Anthony J. Leggett. Bose-Einstein condensation in the alkali gases: Some fundamental concepts. Rev. Mod. Phys. 73, 307 (2001).

[17] Maksims Arzamasovs and Bo Liu. Tight-binding tunneling amplitude of an optical lattice. Eur. J. Phys. 38 065405 (2017).

[18] Kohn, W. Analytic Properties of Bloch Waves and Wannier Functions. Physical Review, 115(4), 809–821 (1959).

[19] He, L., and D. Vanderbilt.Exponential Decay Properties of Wannier Functions and Related Quantities. Phys. Rev. Lett. 86, 5341 (2001).

[20] H. A. Gersch and G. C. Knollman. Quantum Cell Model for Bosons. Phys. Rev. 129, 959 (1963).

[21] Oliver Morsch and Markus Oberthaler. Dynamics of Bose-Einstein condensates in optical lattices. Rev. Mod. Phys. 78, 179 (2006).

[22] Matthew P. A. Fisher, Peter B. Weichman, G. Grinstein, and Daniel S. Fisher. Boson localization and the superfluid-insulator transition Phys. Rev. B 40, 546 (1989).

[23] Moritz Hiller. Parametric Bose-Hubbard Hamiltonians: Quantum Dissipation, Irreversibility, and Pumping. PhD Thesis Dissertation. Georg-August Universität zur Göttingen (2007).

[24] G. G. Batrouni, V. Rousseau, R. T. Scalettar, M. Rigol, A. Muramatsu, P. J. H. Denteneer, and M. Troyer. Mott Domains of Bosons Confined on Optical Lattices Phys. Rev. Lett. 89, 117203 (2002).

[25] V. A. Kashurnikov, N. V. Prokof'ev, and B. V. Svistunov. Revealing the superfluid–Mott-insulator transition in an optical lattice. Phys. Rev. A 66, 031601(R) (2002).

[26] Stefan Wessel, Fabien Alet, Matthias Troyer, and G. George Batrouni. Quantum Monte Carlo simulations of confined bosonic atoms in optical lattices Phys. Rev. A 70, 053615 (2004).

[27] M. Rigol, R. T. Scalettar, P. Sengupta, and G. G. Batrouni. Time-of-flight observables and the formation of Mott domains of fermions and bosons on optical lattices Phys. Rev. B 73, 121103(R) (2006).

[28] C. Kollath, U. Schollwöck, J. von Delft, and W. Zwerger. Spatial correlations of trapped one-dimensional bosons in an optical lattice Phys. Rev. A 69, 031601(R) (2004).

[29] Greiner M., Mandel O., Esslinger T., Hänsch T. W. and Bloch I. Quantum phase transition from a superfluid to a Mott insulator in a gas of ultracold atoms. Nature 3;415(6867):39-44. (2002).

[30] Immanuel Bloch, Jean Dalibard, and Wilhelm Zwerger. Many-body physics with ultracold gases. Rev. Mod. Phys. 80, 885 (2008).

[31] K. Sheshadri, H. R. Krishnamurthy, R. Pandit and T. V. Ramakrishnan. Superfluid and Insulating Phases in an Interacting-Boson Model: Mean-Field Theory and the RPA. EPL, Volume 22, Number 4 (1993).

[32] Zhang, J. M. and Dong, R. X. Exact diagonalization: the Bose–Hubbard model as an example. Eur. J. Phys. 31 591 (2010).

[33] Robert Roth and Keith Burnett. Phase diagram of bosonic atoms in two-color superlattices Phys. Rev. A 68, 023604 (2003).

[34] Ed S.Coakley, Vladimir Rokhlin. A fast divide-and-conquer algorithm for computing the spectra of real symmetric tridiagonal matrices. Applied and Computational Harmonic Analysis, Volume 34, Issue 3, (2013)

[35] Conrad Sanderson and Ryan Curtin. Armadillo: a template-based C++ library for linear algebra. Journal of Open Source Software, Vol. 1, pp. 26, 2016.

[36] Conrad Sanderson and Ryan Curtin. A User-Friendly Hybrid Sparse Matrix Class in C++. Lecture Notes in Computer Science (LNCS), Vol. 10931, pp. 422-430, 2018.

[37] Batrouni G. G. and Scalettar R. T. World-line quantum Monte Carlo algorithm for a one-dimensional Bose model. Phys. Rev. B 46, 9051. (1992).

[38] Subir Sachdev, K. Sengupta, and S. M. Girvin. Mott insulators in strong electric fields. Phys. Rev. B 66, 075128 (2002).

[39] K. Braun-Munzinger, J. A. Dunningham, and K. Burnett. Excitations of Bose-Einstein condensates in optical lattices. Phys. Rev. A 69, 053613 (2004).

[40] Oliver Penrose and Lars Onsager. Bose-Einstein Condensation and Liquid Helium. Phys. Rev. 104, 576 (1956).

[41] C. N. Yang. Concept of Off-Diagonal Long-Range Order and the Quantum Phases of Liquid He and of Superconductors. Rev. Mod. Phys. 34, 694 (1962).

[42] Miyake H., Siviloglou G. A., Kennedy C. J., Burton W. C, and Ketterle W. Phys. Rev. Lett. 111, 185302. (2013).

[43] Trabesinger, A. Quantum simulation. Nature Phys 8, 263 (2012).

[44] P. G. Harper. Single Band Motion of Conduction Electrons in a Uniform Magnetic Field. Proc. Phys. Soc. A 68 874 (1955).

[45] Maciej Lewenstein, Anna Sanpera, Verónica Ahufinger. *Ultracold Atoms in Optical Lattices. Simulating Quantum Many-Body Systems*, Oxford University Press, 1ra Ed, 2012.

[46] Zhang D. W., Zhu Y. O., Zhao Y. X., Yan H., and Zhu S. L. Topological quantum matter with cold atoms, Advances in Physics, 67:4, 253-402. (2019).

[47] Douglas R. Hofstadter, *Energy levels and wave functions of Bloch electrons in rational and irrational magnetic fields*, Phys. Rev. B 14, 2239 (1976).

[48] J. M. Luttinger *The Effect of a Magnetic Field on Electrons in a Periodic Potential*, Phys. Rev. 84, 814 (1951).

[49] Peierls, R. *On the theory of diamagnetism of conduction electrons.* Z. Phys. 80: 763–791 (1933).

[50] J. M. Zhang, R. X. Dong, *Exact diagonalization: the Bose-Hubbard model as an example* Eur. J. Phys. 31, 591 (2010).

[51] M Aidelsburger. Artificial gauge fields and topology with ultracold atoms in optical lattices. 2018 J. Phys. B: At. Mol. Opt. Phys. 51 193001. (2018).

[52] Katarzyna Czajka, Anna Gorczyca, Maciej M. Maśka, and Marcin Mierzejewski. *Hofstadter butterfly for a finite correlated system* Phys. Rev. B 74, 125116 (2006).

[53] K. Osterloh, M. Baig, L. Santos, P. Zoller, and M. Lewenstein *Cold Atoms in Non-Abelian Gauge Potentials: From the Hofstadter "Moth" to Lattice Gauge Theory.* Phys. Rev. Lett. 95, 010403 (2005).

[54] I. Montvay, G. Münster. *Quantum Fields on a Lattice.*Cambridge University Press, 1ra Ed, 1994.

[55] M. V. Berry. Quantal phase factors accompanying adiabatic changesProc. R. Soc. Lond. A39245–57. (1984).

[56] V. Fock. About the relationship between the integrals of the quantum mechanical equations of motion and Schrödinger's wave equation. Z. Phys. 49, 323 (1928).

[57] Xiao, D., Chang, M.-C. and Niu, Q. Berry phase effects on electronic properties. Rev. Mod. Phys. 82(3) (2010).

[58] Mikitik, G. P., and Y. V. Sharlai. Manifestation of Berry's Phase in Metal Physics. Phys. Rev. Lett. 82, 2147. (1999)

[59] Mikitik, G. P., and Y. V. Sharlai. Berry Phase and de Haas–van Alphen Effect in $LaRhIn_5$. Phys. Rev. Lett. 93, 106403. (2004).

[60] Mikitik, G. P., and Y. V. Sharlai. The phase of the de Haas–van Alphen oscillations, the Berry phase, and band-contact lines in metals. Low Temp. Phys. 33, 439. (2007)

[61] Zak, J. Berry's phase for energy bands in solids. Physical Review Letters, 62(23), 2747–2750. (1989).

[62] Thouless, D. J. Quantization of particle transport. Phys. Rev. B 27, 6083. (1983).

[63] Klitzing, K. v., G. Dorda, and M. Pepper. New Method for High-Accuracy Determination of the Fine-Structure Constant Based on Quantized Hall Resistance. Phys. Rev. Lett. 45, 494. (1980).

[64] P Streda. Theory of quantised Hall conductivity in two dimensions. J. Phys. C: Solid State Phys. 15 L717 (1982).

[65] L Smrcka and P Streda. Transport coefficients in strong magnetic fields. J. Phys. C: Solid State Phys. 10 2153 (1977).

[66] W. Beugeling, N. Goldman, and C. Morais Smith. Topological phases in a two-dimensional lattice: Magnetic field versus spin-orbit coupling. Phys. Rev. B 86, 075118 (2012).

[67] D. Osadchy and J. E. Avron. Hofstadter butterfly as quantum phase diagram. J. Math. Phys. 42, 5665 (2001).

[68] R. O. Umucalılar, Hui Zhai, and M. Ö. Oktel. Trapped Fermi Gases in Rotating Optical Lattices: Realization and Detection of the Topological Hofstadter Insulator. Phys. Rev. Lett. 100, 070402 (2008).

[69] Daniel A. Steck, "Rubidium 87 D Line Data", available online at http://steck.us/alkalidata (revision 2.1.4, 23 December 2010).

[70] Karen Lozano-Méndez, Alejandro H. Cásares and Santiago F. Caballero-Benítez. Spin Entanglement and Magnetic Competition via Long-Range Interactions in Spinor Quantum Optical Lattices. Phys. Rev. Lett. 128, 080601 (2022).

[71] M. Landini, N. Dogra, K. Kroeger, L. Hruby, T. Donner and T. Esslinger. Formation of a Spin Texture in a Quantum Gas Coupled to a Cavity.

[72] P. Zupancic, D. Dreon, X. Li, A. Baumgärtner, A. Morales, W. Zheng, N. R. Cooper, T. Esslinger and T. Donner. P-Band Induced Self-Organization and Dynamics with Repulsively Driven Ultracold Atoms in an Optical Cavity. Phys. Rev. Lett. 123, 233601 (2019).

[73] P. Jordan and E. Wigner. Above the Pauli Exclusion Principle. Z. Phys. 47, 631 (1928).

[74] Fradkin E., Field Theories of Condensed Matter Sytems. Addison-Wesley, Redwood City. (1993).

[75] Dian-Cheng Zhang, Shi-Jie Yang. Stripe phase induced by artificial gauge fields in a three-components bosonic square lattice. Phys. Let. A 433, 128035 (2022).

[76] R. Landig, L. Hruby, N. Dogra, M. Landini, R Mott, T. Donner and T. Esslinger. Quantum phases from competing short- and long-range interactions in an optical lattice. Nature volume 532, pages 476–479 (2016).

[77] Wiseman H. M., Milburn G. J. *Quantum Measurement and Control*. Cambridge University Press. (2010).

[78] Gabriel Mazzucchi, Wojciech Kozlowski, Santiago F. Caballero-Benitez, Thomas J. Elliott, and Igor B. Mekhov. *Quantum measurement-induced dynamics of many-body ultracold bosonic and fermionic systems in optical lattices*, PRA 93, 023632 (2016)

[79] Ameneh Sheikhan, Ferdinand Brennecke, Corinna Kollath. Cavity-induced chiral states of fermionic quantum gases. Phys. Rev. A 93, 043609 (2016)

[80] S. F. Caballero-Benitez and I. B. Mekhov. Bond order via light-induced synthetic many-body interactions of ultracold atoms in optical lattices . New J. Phys. 18 113010 (2016).

[81] G. G. Batrouni, R. T. Scalettar, V. G. Rousseau, and B. Grémaud. Competing Supersolid and Haldane Insulator Phases in the Extended One-Dimensional Bosonic Hubbard Model Phys. Rev. Lett. 110, 265303 (2013).

[82] D. Hügel, H. U. R. Strand, P. Werner, and L. Pollet. Anisotropic Harper-Hofstadter-Mott model: Competition between condensation and magnetic fields. Phys. Rev. B 96, 054431 (2017).